VLÁKNA a TEXTIL

1

VÚTCH

CHEMITEX

TECHNICKÁ UNIVERZITA LIBEREC · FAKULTA TEXTILNÍ ·

VÚCHV

Fakulta chemickej a potravinárskej technológie

Trenčianska univerzita
Fakulta priemyselných technológií v Púchove
Alexandra Dubčeka v Trenčíne

Spoločnosť priemyselnej chémie
ZSVTS

Fibres and Textiles (1) 2015
Vlákna a textil (1) 2015
Marec 2015

Special issue venue 20th International Conference STRUTEX
held on December 1.- 2. 2014 in Liberec, Czech Republic

CONTENT

OBSAH

2

4

EFFECT OF FINISHING PROCESS ON PLIED COMPACT AND CONVENIONAL RING SPUN YARN PROPERTIES

Moaaz Eldeeb[1], Sayed Ibrahim[1], Ismael Rakha[2], Fawkia Fahim[2] and Eman Elshahat[2]

[1]Technical University of Liberec, Faculty of Textile Engineering, Dep. of Textile Technology, Liberec, Czech Republic
[2]Mansoura University, Faculty of Engineering, Dep. of Textile Engineering, Mansoura, Egypt
moaz.ahmed.samy.moustafa.el.deeb@tul.cz; tel.: +420 774 582 387

Abstract: This work deals with the effect of finishing process on the properties of cotton ring and compact triple plied yarns of 9.8 tex (Ne 60) at different levels of single and plied twist. Singing was applied only for conventional ring spun. It was found that the properties of compact yarns have higher mechanical properties before and after applying finishing process even the relative improvement in the conventional ring yarn properties was higher. The hairiness of finished compact yarn (not singed) was better compared to the conventional singed ring spun yarn. A graphical method was used to find the range of single and ply twist to be inserted to fulfill some given properties such as strength, elongation, irregularity and hairiness (feasible region).
Key words: Compact, plied yarn, finishing, twist factor, feasible region.

1   INTRODUCTION

Compact yarns have superior quality particularly in terms of strength and hairiness, this enhances yarn quality and improves post spinning process performance [1-3]. Recently there is an increasing trend to use plied compact yarns making use of its better evenness, strength and hairiness properties. It is known that plying process improves yarn properties. During this process some single yarn twist are altered which improves yarn appearance, stability, snarling and structure [4-5]. A. Barella studied the change of yarn structure after plying and explained how hairiness is affected [6]. A. Coulson et al. concluded that the strongest plied yarn can be achieved by using low single twist and higher ply twist factor [7]. During plied, yarn finishing process compact yarns behave in a different way than conventional ring spun yarns [8]. Yeşilpınar recommend not to singe the compact sewing threads during finishing to reduce sewing threads production cost [9]. Yet there is few information about the effect of finishing on compact plied finished yarn properties. In this study, a comparative study is carried out to find the effect of finishing process on ring and compact plied yarn properties at different levels of single and plied twist.

2   EXPERIMENTAL

Egyptian cotton fibers Giza 86 were used to produce combed conventional and compact yarns of 9.8 tex (Ne 60). The running conditions and machine settings were kept constant during applying different levels of English single twist factor 3 to 5 (α_{tex} 28.7-47.8). Yarns then we replied using different levels of English ply twist factor 3 to 6 (α_{tex} 28.7-57.4). Finishing process including singeing, mercerizing and dyeing were applied for all yarns except Compact yarns were not singed. The results were analyzed applying the stepwise backward regression model. Since yarn quality is a combination of some yarn properties, this necessitates to set some predetermined limits of yarn properties and accordingly changing the level of the factors affecting these parameters. To achieve this target, a graphical method is used by overlaying the contour lines to find the so-called "feasible region". A simple program written in Matlab code was applied in this work.

3   RESULTS AND DISCUSSION

3.1   Yarn Tenacity

Figure 1 shows yarn tenacity before finishing process and Table1 shows the percentage of improvement in yarn parameters after finishing process. It can be observed that after yarn finishing process, tenacity of both compact and conventional yarn has the same trend. For both compact and conventional yarns, as ply twist factor increases, yarn tenacity increases to maximum and consequently decreases. It is evident that tenacity of both compact and conventional yarns are improved with respect to their corresponding plied yarns than before finishing. This is because mercerizing (during finishing) has the effect of swelling fibers converting their bean-like section to circular.

This increases fiber cohesion inside the yarn resulting in higher yarn tenacity. However in the finished plied conventional yarns, the increase in tenacity is higher than that finished compact yarn. This may be due to the higher compactness of compact yarn structure, as compared to conventional yarn structure, which restricts the accessibility of caustic soda liquor to axial fibers. This makes the effect of mercerizing less pronounced for compact than conventional ring yarns. The differences in finished plied yarn tenacity among plying twist factor are dependent on single yarn twist and spinning method. Results showed that ply twist factor has maximum influence on the improvement (%) in yarn tenacity after finishing process.
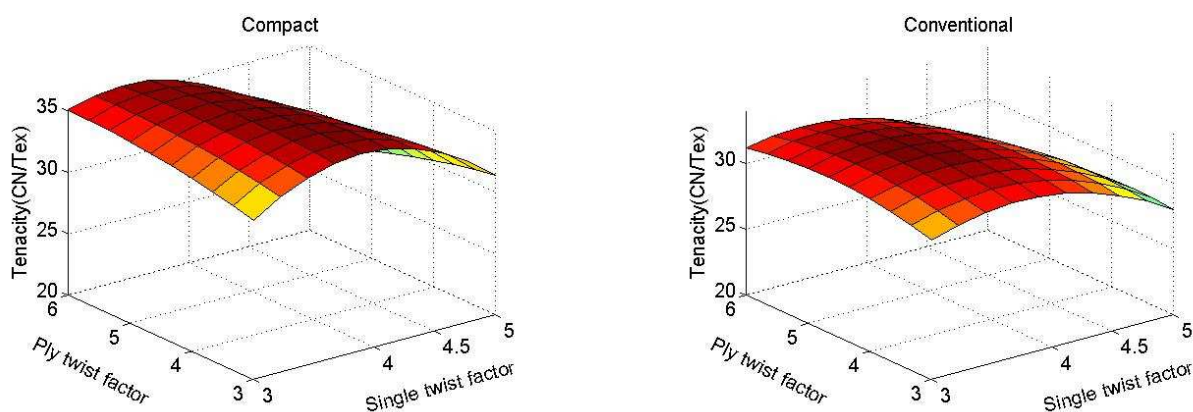
Figure 1 Tenacity of raw yarns at different single and ply twist factor

Table 1 Improvement (%) in Tenacity of finished plied conventional and compact yarn

Single yarn twist factor (α_{es})	Ply yarn twist factor (α_{ep})	Ply / single twist ratio ($\alpha_{ep} / \alpha_{es}$)	Improvement (%) in tenacity of finished plied yarns	
			Conventional yarn	Compact yarn
3	3	1.00	10.0	5.00
	4	1.33	8.0	3.90
	5	1.67	6.0	3.00
	6	2.00	4.0	1.90
4	3	0.75	12.0	6.00
	4	1.00	9.7	4.95
	5	1.25	9.0	4.39
	6	1.50	7.0	3.55
5	3	0.60	12.0	6.00
	4	0.80	10.9	5.45
	5	1.00	10.0	5.00
	6	1.20	10.5	4.48

3.2 Yarn Elongation

After finishing process of plied compact and conventional yarns, breaking elongation of all yarns is decreased. This may be due to mercerizing process increases the crystalline region in fibers and fibers become more oriented which results in higher yarn tenacity and lower breaking elongation. After yarn finishing process, for both yarns, with the increase of ply twist factor, yarn elongation increases to a maximum and then declined at high levels of twist ratio. Decrease (%) in breaking elongation by finishing is lower for compact plied yarns than corresponding conventional plied ring yarns. For both compact and conventional yarns, at different single yarn twist levels, decreasing in plied yarn breaking elongation due to finishing gets lower as ply twist gets higher up to α_{ep} 5, then the decrease in breaking elongation increases. It is evident that ply twist factor has maximum influence on the yarn breaking elongation and the improvement (%) in breaking elongation after finishing process. After finishing compact yarns have higher elongation compared to conventional yarn by a ratio between 6.3 to 9.7% (before finishing it was 4.9-7%).

3.3 Yarn Hairiness

Compact plied yarns after finishing have the same trend of yarns before finishing process. Hairiness (H) is reduced by a ratio ranged from 43.6 to 70% and 7.5 to 50% for conventional and compact respectively. The higher conventional yarns improvement ratio is due to high hairiness values of raw yarns and the effect of singeing process. Results show that ply twist factor has maximum influence on the yarn hairiness and the hairiness improvement (%) after finishing process.

3.4 Feasible region

The feasible region i.e. the region which fulfills some required properties is constructed as follows: The individual contour maps are drawn from the regression equations and then overlapped one after the other. The required parameters are given, and the closed area represents the region fulfills different properties. The independent variables are chosen according given criteria. Contour maps for conventional and compact yarns which are shown in Figure 3 revealed that to achieve finished conventional yarn tenacity > 34 cN/tex, elongation > 4%, irregularity < 10% and hairiness < 2.8, a single twist factor ranging from 3.7 to 4.4 and ply twist factor ranging from 4.6 to 5.3 can be used and to achieve finished compact yarn tenacity > 38 cN/tex, elongation > 4.5%, irregularity < 6.7% and hairiness < 2, a single twist factor ranging from 4 to 4.5 and ply twist factor ranging from 4 to 6 can be used.
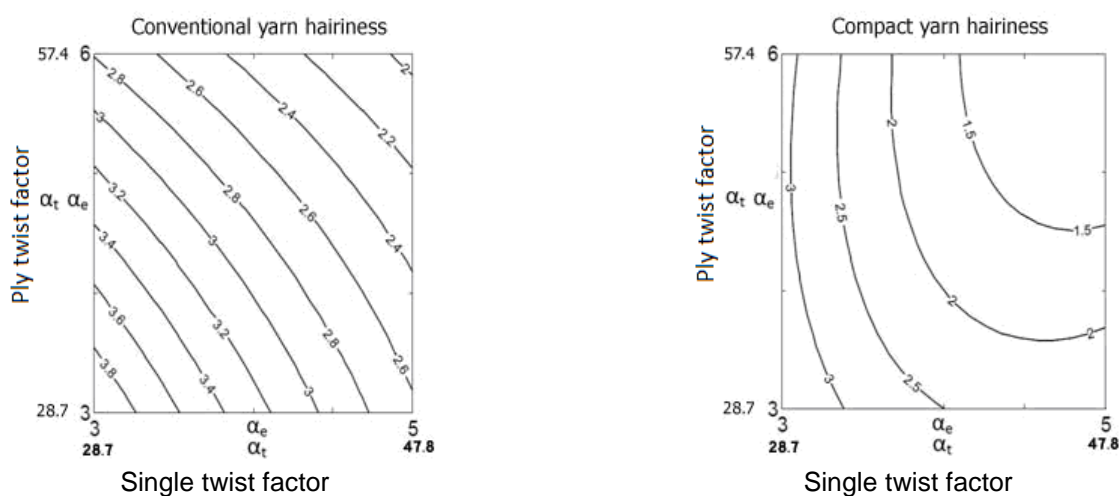
Figure 2 Contour representation of finished conventional and compact yarns hairiness
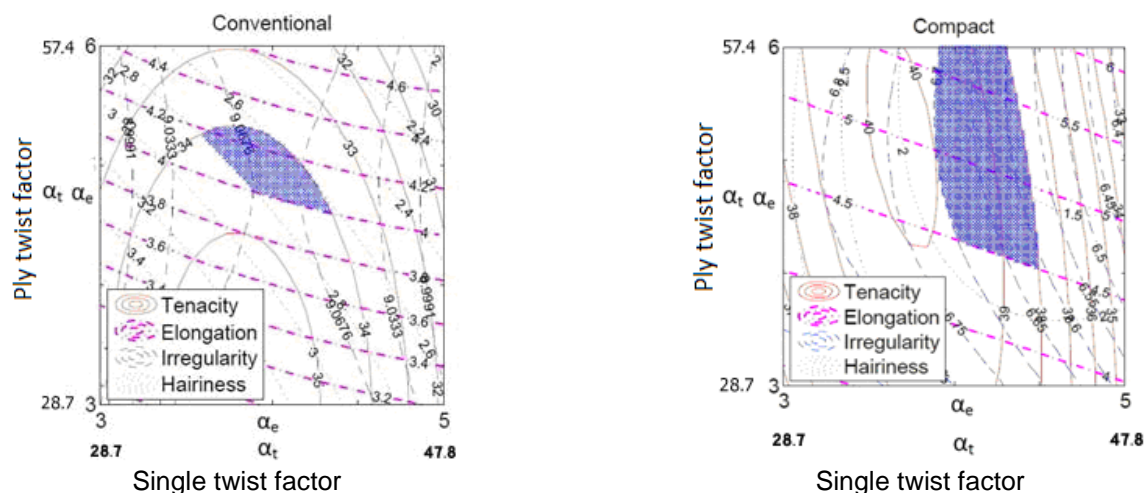
Figure 3 Contour maps used for conventional and compact yarn quality investigation

These results are also approved by the mathematical results done using the Matlab code. Comparison of compact and conventional yarns' feasible regions showed that compact yarn has different zone than conventional yarn to produce the same yarn with better quality level. Contour analysis showed that finishing process displaced the feasible region for both conventional and compact yarns.

4   CONCLUSIONS

In this study, conventional ring spun and compact yarns with different single and ply twist factor are produced and effect of finishing process is investigated. It is evident that tensile strength of both plied compact and conventional ring yarns is significantly improved by finishing process and the percentage improvement is higher for conventional ring yarns. Response analysis determined the feasible region for optimized yarn properties and this region is displaced after finishing process.

5   REFERENCES

1. Nilgun O., Esen O., Alparslan D., Tulin O.: A Comparative Study of The Characteristics of Compact Yarn-Based Knitted Fabrics Fibres&Textiles in EE 13(2), pp. 39-43, 2005
2. Jackowski T., Cyniak D., Czekalski J.: Compact Cotton Yarn, Fibres&Textiles in EE 12(4), pp. 22-26, 2004
3. Nikolic M., Stjepanovic Z., Lesjak F., Stritof A.: Compact Spinning for Improved Quality of Ring-Spun Yarns, Fibres&Textiles in EE 11(4), pp. 30-35, 2003
4. Brunk N.: Reflections on The Spinning of Two-Ply Yarns with EliTwist CompactSet, Spinnovation, No. 20, pp. 10-13, 2004
5. Brunk N.: Elite compact set-Versatile Method of Yarn Compactation, Melliand Int. 10(1), pp. 24-27, 2004
6. Barella A.: Yarn hairiness: the influence of twist Journal of textile institute 48, pp. 268-280, 1957
7. Coulson A.F.W. and Dakin G.: The influence of twist on the strength and certain other properties of two-fold yarns, Journal of Textile Institute 48, pp. 207-231, 1957
8. Can Y.: Researching the effects of some finishing process on strength and elongation characteristics of compact and ring spun yarns, Tekstil ve Konfeksiyon 19(1), pp. 56-60, 2009
9. Yeşilpınar S.: Analysis of the Performance of Sewing Threads Manufactured from Conventional and Compact Ring-spun Yarns, Fibres &Textiles in EE 14(2), pp. 20-23, 2006

COMPUTED TOMOGRAPHY APPLICATION FOR INVESTIGATING THE INTERNAL STRUCTURE OF AIR-JET YARNS

Mohamed Eldessouki[1,2] and Sayed Ibrahim[3]

[1]TU Liberec, Faculty of Textile Eng., Dep. of Materials Engineering, Liberec, Czech Republic
[2]Mansoura University, Faculty of Engineering, Dep. of Textile Engineering, Mansoura, Egypt
[3]TU of Liberec, Faculty of Textile Eng., Dep. of Textile Technology, Liberec, Czech Republic
eldesmo@auburn.edu

Abstract: The internal arrangement of fibers inside the yarn defines the yarn structure and affects its final properties and performance. Therefore, studying the detailed structure of yarns is one of the important research issues over the years where the depth of this study is affected by the available technology at the time. Computed Tomography (CT) is one of the technologies that utilize the interaction of x-rays with a rotated physical object to reconstruct a digital 3D model of the scanned object based on the transmitted x-rays intensity at different angles. In this study, a low energy x-ray source coupled with high resolution detectors installed in a micro-CT scanner that is capable of imaging objects with a resolution up to 0.3 µm. An air-jet spun yarn is introduced in this work with yarn imaging and an algorithm for calculating the packing density of fibers at different slices along the scanned yarn length. The preliminary results of this study show the feasibility of the CT scanning method to study the internal structure of yarns under relaxed conditions (i.e. without the application of strains on the yarn) which promises with a better understanding of many yarn parameters such as twist distribution, fiber migration, packing density, fibers friction…etc.
Key words: Air-jet yarns, computed tomography, packing density, yarn internal structure.

1   INTRODUCTION

Computed Tomography (CT) is an imaging method that employs the tomography (from Greek words *tomos* means "*slice*" and *graphein* means "*to write*") where "digital geometry processing" is used to generate a three-dimensional image of the internals of an object from a large series of two-dimensional X-ray images taken around a single axis of rotation. The conception of the CT idea started at the end of the 1960s and the first commercially viable CT scanner was invented in 1972 by Hounsfield who won the 1979 Nobel Prize in medicine for this work. The CT technology was basically implemented in medical imaging and the clinical CT became the radiology's powerhouse as the first method to non-invasively acquire images of the inside of the human body. The method has evolved rapidly and was implemented in industrial fields by the end of the 1980s as one of the favorite Non Destructive Testing (NDT) techniques. The diversity of CT applications,

with objects of different sizes, shifted the interest from large objects (as human bodies) to smaller ones and the need for the "higher spatial resolution" scanners started to emerge. The higher spatial resolution is obtained by either using clinical flat-panel imaging systems that achieve resolutions in the order of 150-200 µm or by using dedicated micro-CT (µ-CT) scanners, such as the one used in this study, which can usually achieve a spatial resolution less than 0.5 µm.

The principle of CT scanning stems from the fact that the information available from a single projection of an object in engineering drawing is limited and another projection is necessary to obtain the third projection and ultimately reconstructing the 3D perspective of the object. This explanation in engineering drawing applies also to CT scanning, where a single x-ray projection shows a superimposition of all objects in the path of the x-ray and therefore hard to understand the volumetric structure of the object. The information can be increased by taking

two (and more) projections, however, increasing the number of projection directions (views) is of little help because the observer is not able to mentally solve the superposition problem and to "reconstruct" the internal information of the object. Fortunately it can be shown that a complete "*computed*" reconstruction of the object's interior is mathematically possible as long as a large number of views "*tomos*" have been acquired "*graphein*" over an angular range that covers an angle of at least 180°. This acquisition scheme is implemented in CT scanners by using an X-ray tube together with a detector while the object is rotating within path of the X-ray beams as demonstrated in Figure 1.
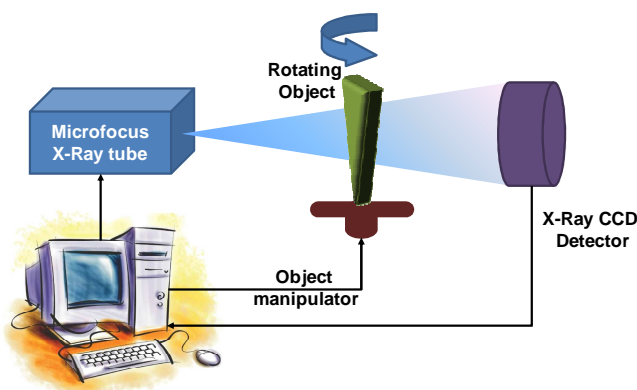
Figure 1 Schematic representation for the principle of CT scanning

Each x-ray projected image is a representation of the object's X-ray absorption along straight lines in a specific direction. For an incident x-ray with initial intensity I_0, an object of thickness d, and attenuation coefficient μ, the number I of quanta reaching the detector is given by the exponential attenuation law:

$$I = I_0 e^{-\mu d} \tag{1}$$

The negative logarithm $p = - \ln I/I_0$ of each intensity measurement I gives information about the product of the object attenuation μ and its thickness d and proportionate to the tube current I (given a constant incident intensity I_0). For nonhomogeneous objects, the attenuation coefficient is a function of $x, y,$

and z and the projection value p corresponds to the line integral along line L of the object's linear attenuation coefficient distribution $\mu(x, y, z)$:

$$p(L) = -\frac{\ln(I(L))}{l_0} = \int_L \mu(x, y, z) dL \tag{2}$$

For flat-panel CT, the line L can be parameterized by the rotation angle α and the detector coordinates (u, v). We are interested in gaining knowledge of $\mu(x, y, z)$ by reconstructing the acquired data $p(L)$ and the CT "*image reconstruction*" process is defined as the process of computing the image $f(x, y, z)$ as an accurate approximation to $\mu(x, y, z)$ from the set of measured projection values $p(L)$ [1].

2   EXPERIMENTAL WORK

2.1   Materials
A yarn made from 100% viscose of count 20 tex was produced on Reiter (J20) air-jet spinning system. The yarn was produced at a production speed of 375 m/min and an air pressure level of 6 bars. Viscose fibers used in the production were obtained from Lenzing Technik Company with 38 mm average staple length, fineness of 1.52±0.39 dtex and a tenacity of 20.65±3.72 cN/tex, as measured used the Vibroscope for 50 fiber samples. The yarn sample was straightened in a thin polyethylene tube that helps in holding the sample vertical during the CT scanning. The sample was analyzed using Bruker micro-CT SkyScan1272 scanner. The CT scanner captured 3059 images with dimensions of 3280 x 4904 pixels, the image rotation step was 0.100°, the object to source distance was 54.37500 mm, and the camera to source distance was 268.61250 mm.

The projected images were reconstructed using the CTvox software and some volumetric data was obtained using the CTVol, and the CTAn software. The analysis of the yarn packing density was performed using our developed software [2] that analyzes the cross-sectional images

obtained from the CT-reconstructed volume. The developed packing density software utilizes the Chan-Vese segmentation model to determine the yarn outer contour as well as the individual fibers contours.

2.2 Calculation algorithm

Since the yarn packing density is representation for the ratio between the area of the fibers inside the yarn and the yarn cross-sectional area, it is necessary to segment the yarn cross-sectional images for calculating these two areas. Segmentation of images based on the variational methods [3] can be obtained by minimizing the appropriate cost functionals [4]. For an image (I) with $I : \Omega \to R$, where Ω is the image domain, the segmentation can be performed by evolving the regional contours of the image in the direction of negative energy gradient using appropriate partial differential equations (PDE). This procedure is commonly known as the snakes algorithm [5] which introduces an explicit parametric curve $C : [0,1] \to \Omega$ to represent the region's contour. The parametric curve C evolves by locally minimizing the cost functional:

$$E(C) = \int |\bar{v}I(C)|^2 ds + v_1 \int |Cs|^2 ds + v_2 \int |C_{ss}|^2 ds \quad (5)$$

where C_s and C_{ss} represent the first and second derivatives of the curve C with respect to the parameter s, respectively. The first term in equation (5) represents the external energy which accounts for the image information and called the data term while the last two terms can be interpreted as the internal energy and represents the regularization terms that account for the length of the contour and its stiffness.

In this study, the Chan-Vese (CV) model [6] for active contours was used to detect the boundaries of the yarn in a given cross-sectional image. The CV model is based on techniques of curve evolution, Mumford–Shah functional for segmentation, and level sets [4, 7]. In the level set formulation, the problem becomes a "mean-curvature flow" which results in evolving the active contour until a stop condition is met on the desired boundary. Because most classical snakes and active contour models rely on the edge-function (might be calculated from the image gradient $|\nabla u_0|$) to stop the curve evolution, these models can detect only objects with edges defined by a gradient. In the CV model, however, the stopping term is based on Mumford–Shah segmentation techniques and the model can, therefore, detect contours with or without gradient (for instance objects with very smooth boundaries or even with discontinuous boundaries).

3 RESULTS AND DISCUSSION

Yarn sample was scanned and the obtained projected images were used to reconstruct the 3D digital model of the yarn as demonstrated in Figure 2. The digital model of the yarn can be manipulated in different ways where the yarn can be magnified without losing the resolution and details as shown also in Figure 2. The details of the 3D model depend mainly on the resolution of the CT scanner during the image acquisition stage not just on the resolution of the image that is magnified. The presence of the 3D digital model allows some treatments such as clipping and cutting certain parts of the structure as well as slicing the yarn structure at any required plane direction. It is, therefore, very useful to use this model and obtain cross-sectional images along the yarn length, as demonstrated in Figure 2, without the need to additional chemicals required for hardening the yarn and its physical slicing using sharp edges and the microtome.
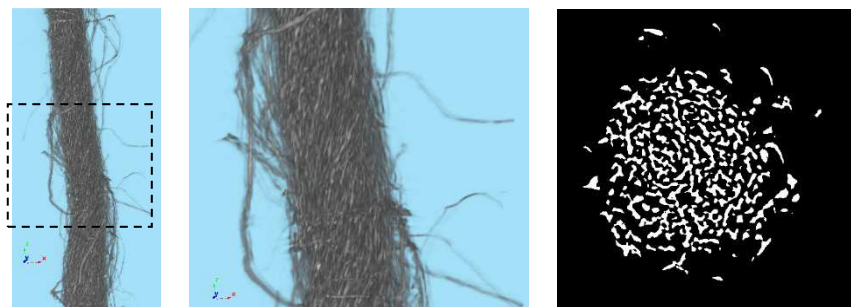
Figure 2 Reconstructed digital model of the yarn (left) that allows its visualization with a higher magnification (middle), and with cross-sectional slicing (right)

4   CONCLUSIONS

The application of CT as a non-destructive method allows the characterization of the fibrous structures (yarn) in their normal states, without the need to the chemical additives that might affect the fibers characteristics. The scanning of fibrous structures using CT technology allows the reconstruction of a digital model for the yarn that can be manipulated to trace the fiber migration inside the yarn and the calculation of different internal structure parameters. This work is a first step in studying the yarns produced on different spinning technologies and the digital yarn model will allow better understanding and possible modifications of the current mathematical models that analyze the yarn structure.

5   REFERENCES

1. Semmler W. and Schwaiger M.: Molecular Imaging I. Springer, 2008
2. Eldessouki M. and Ibrahim S.: Chan-Vese Segmentation Model For Faster And Accurate Evaluation of Yarn Packing Density, Text. Res. J., In Press
3. Mitiche A. and Ben Ayed I.: Variational and level set methods in image segmentation, Vol. 5. Springer, 2010
4. Cremers D., Rousson M., and Deriche R.: A Review of Statistical Approaches to Level Set Segmentation: Integrating Color, Texture, Motion and Shape, International Journal of Computer Vision 72. pp. 195-215, 2007
5. Kass M., Witkin A., and Terzopoulos D.: Snakes: Active contour models, Int. J. Comput. Vis. 1(4), pp. 321-331, 1988
6. Chan T. and Vese L.: An active contour model without edges, in Scale-Space Theories in Computer Vision, Springer, pp. 141–151, 1999
7. Osher S. and Fedkiw R.P.: Level Set Methods: An Overview and Some Recent Results, J. Comput. Phys. 169, pp. 463-502, 2001

DEVELOPMENT OF ADVANCED COMPATIBLE MATERIALS FOR THE RESTORATION OF CULTURAL HERITAGE ASSETS (MYTHOS): ARTIFICIAL AGEING OF BAST FIBRES

H. Fischer[1], H. Wiese[1], C. Radulescu[2] and P. Rödel[3]

[1]*Faserinstitut Bremen e.V. -FIBRE-, D-28359 Bremen, Germany*
[2]*National R&D Institute for Textiles and Leather Bucharest (INCDTP)*
16 Lucretiu Patrascanu, 030508 Bucharest, Romania
[3]*Institut für Pflanzenkultur e.K., D-29465 Schnega, Germany*
fischer@faserinstitut.de; clara.radulescu@certex.ro; roedel@pflanzenkultur.de

Abstract: *For the restoration and preservation of textile cultural heritage objects it is essential to use similar or identical materials for e.g. testing cleaning or restoration processes before treating the unique and irreplaceable originals. Main focus of the MYTHOS project is to develop such reference materials for enhanced restoration and conservation of hemp and linen based ancient arts. The project work started with development of adapted analysis scheme. Due to the nature of the samples analysis methods have to be either non-destructive or restricted to minimal sample amounts. Consequently only small subsamples of the textiles have been taken, e.g. yarn pieces from the hem. Fibre tenacity and elongation have been analysed in a single-element test (diastron). The fibre width distribution has been assessed by Fibreshape. In parallel a genetic analysis of original samples was performed to identify actual hemp and flax species close to the ancient varieties. This presentation reports the results obtained from selected original textiles and based on these the development of a scheme for defined artificial ageing for new fibre materials by use of enzymatic treatment. The results are compared to data of actual hemp and flax fibres and differences are discussed.*
Key words: *Textile restoration; fibre analysis; genetic analysis; artificial ageing; fibreshape; diastron.*

1   INTRODUCTION

Restoration and conservation techniques applied today on textiles use extra materials (glues, additives, fibres etc.) that are incorporated directly in the original textile. There are no experimental materials appropriate to the different type of textiles in historical objects, in terms of technical and biological similarity that can supplement and enhance the restoration and conservation techniques directly on the work of art. MYTHOS project proposes to develop novel ways of treating and restoring textile based European arts. The main objective of the project is to develop a set of reference materials, to be used by the cultural national and international organizations. The reference materials will have similar biological and technical characteristics as the ancient textile arts which are on based hemp (Cannabis sp.) and flax (Linum sp.).

Due to the value of historical textiles for the cultural heritage and the necessity to preserve them for the future generations all the investigations will be micro-destructive or non-destructive. The analysis of such objects requires cooperation between researchers from different areas of science. In the frame of this project it is necessary to collect data about the tenacity of the original fibres to have initial target information for the new breed variants and the ageing processes in the later phases. This is normally not essential for the description of historical textiles and thus rarely reported in the literature. After the new cultivars with old genetic profiles are obtained they will be cultivated. The bast plants will be now used for obtaining the fibres, threads and new reference materials. This paper describes first

results obtained from artificial ageing of new hemp fibres and compares the results of their mechanical analysis to those of samples taken from historical textiles.

2 EXPERIMENTAL

2.1 Materials

Historical fabrics, yarns and fibres were supplied by the National Peasant Museum, Bucharest. For the first analytical approach samples were selected which could be supplied in larger amounts than usual: fibres from preserved complete bobbins / clews and material used as decorative fibres from historical objects. Some of the samples are displayed in Figure 1. For comparison two samples of technical flax and hemp fibres are added. Both are grown in Germany and were mechanically separated. Detailed data about the reference materials can be found in [1]. A raw flax fabric (linen, #00 1818 00), 175 g/m², was purchased from Leineweberei Hoffmann, Neukirch/Lausitz, DE.

Up to now the mechanical and fineness analysis of the fibres as well as artificial ageing of actual reference fibres by use of enzymes have been performed as described below and will be reported here. Actually a genetic analysis of the sample materials is in progress to prove their origin, to identify the varieties in detail and to identify actual species as close as possible to the historic ones. This will be reported later.

2.2 Methods

The samples have to be conditioned in standard climate at 20℃ and 65% relative humidity according to DIN EN ISO 139. The mechanical characterisation is conducted on single elements based on DIN EN ISO 50798 (1996), using a Dia-Stron System (Dia-Stron Ltd., Andover, UK) with clamping length 3.2 mm [1]. In addition the tenacities of enzyme-treated fibres have been examined in a collective test by Stelometer as described previously [2]. Fineness analysis was performed using the image processing system Fibreshape as described in [1].
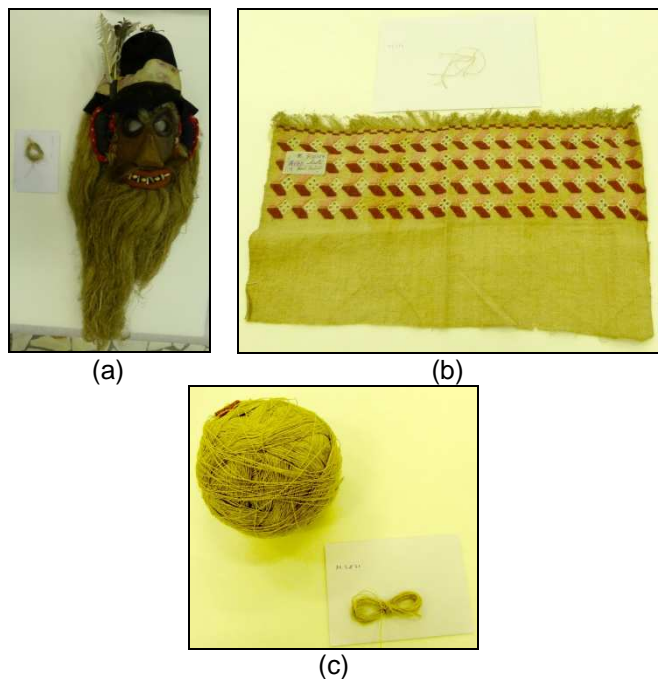
Figure 1 Images of historical fibre samples (a) B 5843, (b) M 173 and (c) M 3871

The enzymatic fibre treatments were carried out in 300 mL Erlenmeyer flasks containing 10 g hemp fibres GDE02 and 200 mL of reaction solution as described in [2]. First the fibres were washed in soda solution (concentration w/v of 0.5%) at 90℃ for 1 h. Enzyme treatments were carried out using up to 1 mL or 1 g of Texazym® AB or APN (both cellulases, purchased from INOTEX s.r.o., CZ) at 30℃ and 50℃ for 20 min. Finally the fibres were dried for 1 h at 105℃.

3 RESULTS AND DISCUSSION

Hemp sample GDE02 from actual production has been used as reference material for enzyme treatments. As displayed in Figure 2, enzyme treatments both by Texazym® AB and Texazym® APN cause a decrease of fibre tenacity from 30 cN/tex down to below 15 cN/tex. The effect of enzyme is more intensive at 50℃ than at 30℃. Due to the reaction volume of 200 mL the maximum amount of enzyme (1 g or 1 mL, resp.) represents a concentration of 0.5% (w/v). For comparison the values of the untreated raw material and a sample with only pre-treatment in soda solution are added.

These values obtained from a collective tenacity test cannot be directly compared to tenacity values from a single-element test, but the tendencies in both methods are known to be similar [3]. For this reason the results of the historic fibres (converted into cN/tex) are compared to that of the newly measured Texazym AB series as single-element tenacity test in Figure 3, displayed as box-and-whisker plots. The plots comprise the upper and lower deciles ($X_{0.90}$ and $X_{0.10}$) as outer dots, the upper and lower quartiles ($X_{0.75}$ and $X_{0.25}$) as box limits, and the median ($X_{0.50}$) denoted inside the box. It is obvious that most historical samples are in the same range of tenacity (24 to 31 cN/tex), only sample L 7024 is with median 13.7 cN/tex significantly lower. Only samples G m, B 5843 and the technical fibres from actual production (GDE 02) display a higher tenacity around 40 cN/tex combined with a much broader distribution to higher values with $X_{0.75}$ values of 60 - 70 cN/tex.

The enzyme treated variants are in the same range like most of the historic samples. The tenacity of most of the historic samples (all 'M'-samples, marked by the greenish box) can be reached easily by mild treatment of standard hemp from actual production with low amounts of Texazym® AB (0.5 - 1.0 g in 200 mL for 20 min at 50℃). The lower tenacity of e.g. sample L 7024 could easily be reached by the more intensive treatment in 0.5% of Texazym® APN for 20 min at 50℃. Higher tenacities like that of samples G m or B 5843 are directly corresponding to those of actual hemp and can thus be reached without special treatment.

All enzymatic treated samples have in addition been analysed for their fineness, and no significant differences were detected. For this reason it is necessary to select actual fibre lots with similar fineness to replace historic fibres. The tenacity can be adjusted to the level of the historic materials by enzymatic treatment.
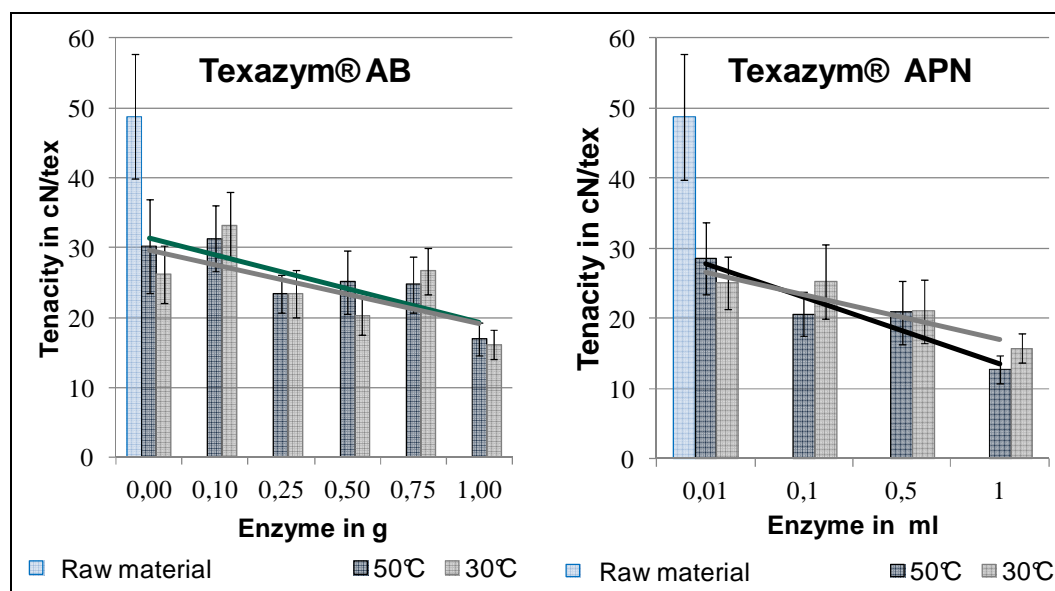
Figure 2 Influence of cellulase treatment in different concentrations on the tenacity of hemp GDE02
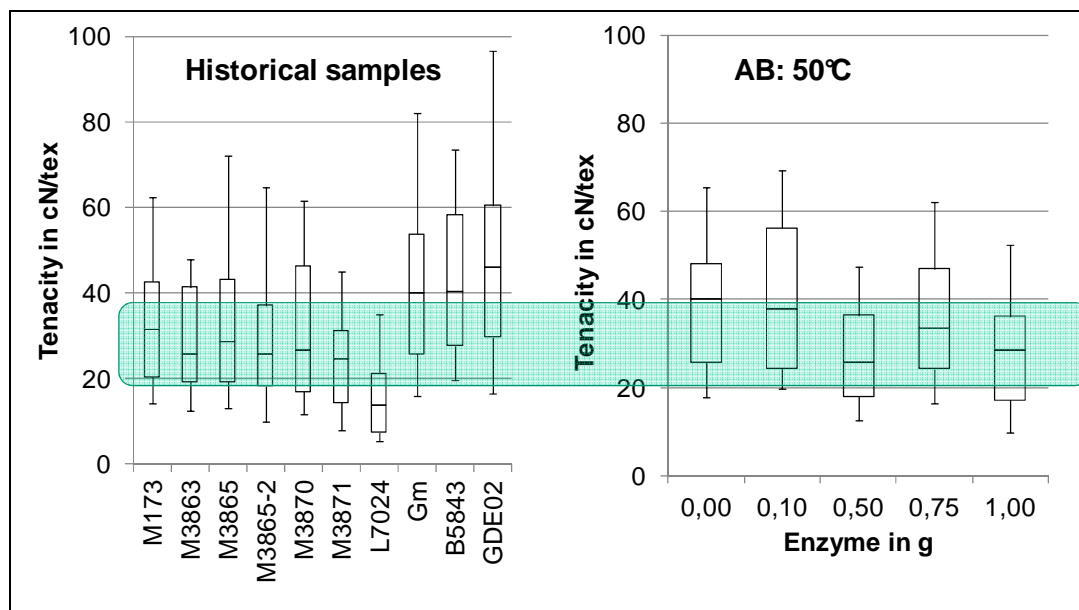
Figure 3 Tenacity (single-element test by dia-stron) of historic and standard hemp samples compared to enzymatic treated standard hemp

4   CONCLUSIONS

All historical samples assessed here are at the lower end of the literature range [3] in terms of tenacity and below the literature range in terms of fineness. Based on these results it was possible to set up a scheme for artificial ageing of new fibres to adapt them to the properties of the historic originals. Best results were obtained with artificial fibre ageing in low amounts of Texazym® AB. Lower tenacities are reachable by use of Texazym® APN. Both enzymes have been proven not to influence the fibre fineness, making the process control easy.

5   REFERENCES

1. Müssig J., Cescutti G. & Fischer H.: Integrated quality management for bast fibres in technical applications, Chapter 10 in Bouloc P., Allegret S. & Arnaud L. (eds.): Hemp - Industrial Production and Uses, CAB International, Wallingford, Oxfordshire, UK, pp. 162-186, 2013
2. Fischer H., Müssig J., Bluhm C., Marek J. & Antonov V.: Enzymatic Modification of Hemp Fibres for Sustainable Production of High Quality Materials: Comparing Different Commercial Enzymes, In Team of Authors (eds.): 11th International conference STRUTEX (Proceedings). Technical University of Liberec, CZ, pp. 301-308, 2004
3. Müssig J., Fischer H., Graupner N. & Drieling A.: Testing Methods for Measuring Physical and Mechanical Fibre Properties (Plant and Animal Fibres), Chapter 13 in Müssig J. (ed.): Industrial Applications of Natural Fibres - Structure, Properties and Technical Applications, Wiley-VCH, Weinheim, DE, pp. 269-309, 2010

MANUFACTURING OF PLANAR TEXTILE FABRIC STRUCTURES BONDED BY PERPENDICULAR LAYING OF POLYMER MELT

Brigita Kolčavová Sirková, Karol Ježík and Filip Sanetrník*

Technical University of Liberec, Faculty of Textile Engineering, Dep. of Textile Technologies
*Department of Nonwovens and Nanofibrous Materials, Liberec, Czech Republic
brigita.kolcavova@tul.cz, karol.jezik@tul.cz, filip.sanetrnik@tul.cz

Abstract: *The article is focused on the introduction and description of the technology for manufacturing of planar textile fabrics bonded by the perpendicular lying of polymer melt as well as the structure of output fabrics. Technological solution consists of two primary parts: 1) A basic bearing construction of machine with a parallel thread winding package, 2) A mobile head with a feeding device forming an exactly defined layer of polymer melt for the optimum fixation of the warp. Textile fabrics manufactured using proposed technology are distinctive by being made of longitudinal parallel wound threads (the so-called warp) fixed in place by a perpendicular layer of polymer melt. This layer form ensures the integrity and shape of the fabric. The innovation is in the actual way of manufacturing of planar textile fabrics and the principle of fabric creation, whereby a fabric and its longitudinal thread structure are bonded with minimal bending and tension. For manufacturing is possible to use the special fibers or threads with low bending rigidity, for example: optical fibers, threads with nano-coating, hollow (tubular) fibers, glass fibers as well as, carbon fibers, etc.*
Key words: *Textile, polymer, structure, warp, melt, manufacturing, fiber.*

1   INTRODUCTION

Production of fabrics is based on interlacing of individual yarns of one, two or more systems of threads. Conventional technology for production of planar textiles using mutual interlacing of the threads is technology of weaving and knitting. On the basis of these technologies is possible to produce the fabric of defined parameters and final properties.

Weaving consists of making textile from yarn. In the weaving process the threads are stretched parallel on the weaving machine. These stretched threads are known as warp threads (wound on the warp beam). Weft (filling), are inserted one by one through a gap (the shed) in the warp threads, at right angles to them. The basic principle has remained unchanged throughout the centuries. A textile is formed by weaving the filling threads one by one between the warp threads.

In a conventional loom, the filling threads are inserted by a flying shuttle. In modern weaving machines, however, they are inserted by rapier (gripper), air jet, water jet or projectile technology. The type of weaving machine, the technology used and the filling threads are determined by the type of textile to be produced [2].

Knitting processes in which fabrics are produced by set of connect loops from a series of yarns in warp or weft direction. Different knitting machines are use to perform this techniques. Warp knitted fabrics: In a warp knitted structure, each loop in the horizontal direction is made from different thread and the number of thread used to produce such a fabric is at least equal to the numbers of loops in horizontal row. Weft knitted fabric: A horizontal row of loops can be made using one thread runs in horizontal direction.

The conventional manufacturing of planar textile fabric, using the traditional knitting and weaving technology involves a lot of tension and bending strain on threads due to the interlacing of the thread. Specific brittle threads with low bending rigidity cannot be processed without preparing operation (coating, sizing, twisting, etc.).

2   RESULTS AND DISCUSSION

Technology for manufacturing of planar textile fabrics bonded by the perpendicular lying of polymer melt consists of two primary parts:
1) a basic bearing construction of machine with a parallel thread winding package,
2) a mobile head with a feeding device forming an exactly defined layer of polymer melt for the optimum fixation of the warp. Textile fabrics manufactured using proposed technology are distinctive by being made of longitudinal parallel wound threads (the so-called warp) fixed in place by a perpendicular layer of polymer melt. This layer form ensures the integrity and shape of the fabric. The innovation is in the actual way of manufacturing of planar textile fabrics and the principle of fabric creation, whereby a fabric and its longitudinal thread structure are bonded with minimal bending and tension.

Figure 1 3D prototype model of technology for manufacturing of planar textile fabrics bonded by the perpendicular lying of polymer melt

The longitudinal thread system in the tensioned state is kept from a vertical position to a horizontal position in space of the nozzle, where the vertical laying of the polymer melt is fixed in the transverse direction. Polymer melt can be placed on the longitudinal threads in the different intervals as well as the defined width. On the bases of the properties of the polymer melt is possible to apply different melting temperatures, depending on the material in the longitudinal thread system and the final application of planar fabrics. The longitudinal thread system, as in weaving technology, it is possible to process using the bobbins from the creel or the warp beam.

Figure 2 Prototype machine for manufacturing of the planar fabric

Electronically controlled the drive mobile head with a dispensing mechanism is able to deliver the polymer melt continuously or intermittently relative to the width fabrics, and in various defined spacing relative to the length of the fabric.
The thickness of the resulting bonded polymeric melt is dependent on the melt viscosity, deposition rate, and pressure as well as the nozzle profile.
The structure and geometry of threads in woven fabrics is based on mutual interlacing [2]. The fabric binding point is defined in dependence on the type of interlacing. Basic distribution of fundamentals weaves is divided into plain and non-plain (float) weaves. Plain weave is composed of crossing warp and weft threads. This is the most densely binding with the least possible density of the thread. The float part on the bases of non-interlacing sections creates a looser weave but with the possibility of achieving higher threads densities [1].

Longitudinal threads in the structure of planar textile fabric bonded by the perpendicular lying of polymer melt have parallel winding with a defined spacing. Longitudinal set of threads is not stressed by bending. In the manufacture of fabrics does not arise crossing parts of threads, and hence it is possible to achieve a maximum density of the yarns.

Figure 3 Prototype machine for manufacturing of the planar fabric – the mobile head and the application of polymer melt on longitudinal threads
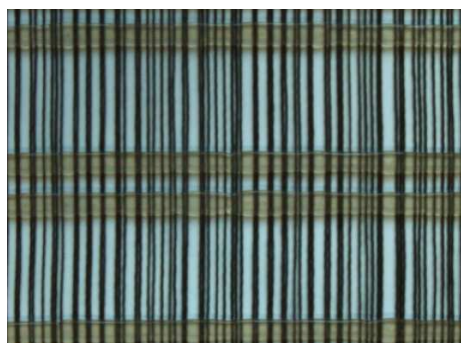
Figure 4 Basalt planar textile fabric bonded by the perpendicular lying of polymer melt
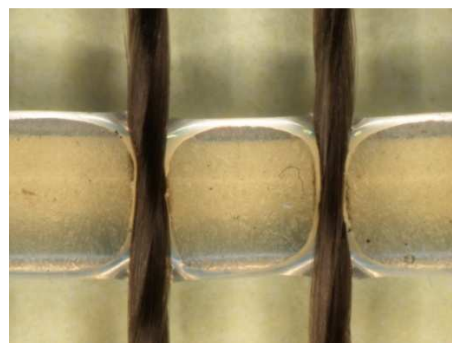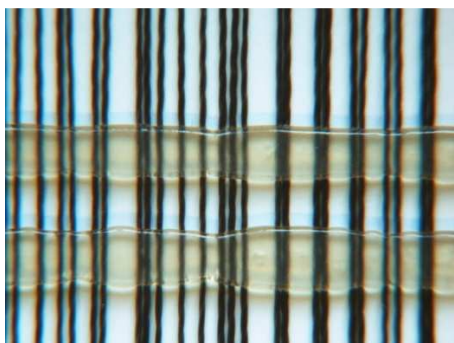
Figure 5 Basalt planar textile fabric bonded by the perpendicular lying of polymer melt (detail)

3   CONCLUSIONS

Textile fabrics manufactured using proposed technology are distinctive by being made of longitudinal parallel wound threads fixed in place by a perpendicular layer of polymer melt. The innovation is in the actual way of manufacturing of planar textile fabrics and the principle of fabric creation, whereby a fabric and its longitudinal thread structure are bonded with minimal bending and tension. For manufacturing is possible to use the special fibers or threads with low bending rigidity, for example: optical fibers, threads with nano-coating, hollow (tubular) fibers, glass fibers as well as, carbon fibers, etc. The application of fabric structures is assumed in composites and automotive and mechanical industries etc. Fabrics with nanofibre yarns will be used as biomass carriers in fluid bioreactors that will allow the faster incorporation of the purific plant. Using biomass carriers provides a tech. advantage for sustaining slow-growth microorganisms in waste water treatment bioreactors.

4   REFERENCES

1. Sirková B.: Theses, Mathematical model for description of thread's interlacing in fabric using Fourier series, Liberec 2002
2. Nosek S.: The structure and geometry of the woven fabrics, Liberec 1996
3. Picanol Group. The Basic Principle of Weaving. http://www.picanolgroup.com/PICGROUPSITE/EN/COMPANY/WEAVING/

IMPACT OF TEXTILE MATERIALS' PARAMETERS ON BEHAVIOUR/TENSION LOADS OF VIRTUAL GARMENTS USING SITTING POSTURE BODY MODELS

Tatjana Kozar, Zoran Stjepanovič, Simona Jevšnik and Andreja Rudolf

University of Maribor, Slovenia, Faculty of Mechanical Engineering
Department of Textile Material and Design
andreja.rudolf@um.si; tel.: +386 2 220 7964, fax: +386 2 220 7990

Abstract: *The contribution presents a research into the impact of textile materials' parameters on behaviour and tension loads of virtual garments. Described is the importance of fabrics' characteristics for reliable garment prototyping and visualisation using developed sitting posture 3D body models.*
Key words: *Virtual garments, 3D body models, sitting posture, knitted fabrics, mechanical properties.*

1   INTRODUCTION

Modern garment manufacturing process involves garment's virtual prototyping by 2D garment pattern construction, as well as physically-based mechanical simulation of fabrics for reproducing the shape and the motion of the garment on the virtual body models. One of the basic objectives of garment's simulation technologies is to simulate garment's realistic drape behaviour and fit appearance such as in real time [1]. Namely, fabrics exhibit visco-elastic behaviour with characteristics of liquid- and solid materials. Due to their complexity and anisotropic structure, an adequate simulation is not easy to provide. Simulation systems with computation algorithms have been developed for simulating not only simplified and static textile materials, but also complex dynamically moving garments [2].

2   THEORETICAL PART

Simulation systems are not only influencing the quality of garment's simulation. Namely, a set of input parameters are playing an important role. Therefore, adequate measuring of fabric's mechanical and physical characteristics in necessary to provide by using systems for their

characterization, such as: Kawabata evaluation system for fabrics (KES-F) and Fabric Assurance by simple Testing (FAST) [3]. A second objective of garment's simulation technologies is to design aesthetic and comfortable garments taking individual's body characteristics into consideration. Comfortable garments are special important for people with paraplegia state, which are exposed to a sitting position in daily life. Regarding garment's simulations, researcher are focusing to reproduce accurate fabric's and consequently garment's fit appearance and drape behaviour on three dimensional body models in a standing position [1, 4-6]. In recent years, we developed three dimensional body models in a sitting position by using different optical scanning systems, such as Vitus Smart scanner and an conventional optical scanner GOM Atos II 3D [7, 8]. Furthermore, a researcher identified the differences between the standing and sitting position in order to develop appropriate garments for paraplegics and to assess their fit appearance on the observed 3D body model in a sitting position [9]. Garment's virtual prototyping of pants and T-shirt for people with paraplegia state was also discussed in [10], where the 3D body model posture was adapted trough kinematic skeleton construction inside the scanned

mesh of a human body in a standing position. Its accuracy was evaluated in [11], trough calculating change values and change rates of the observed virtual- and real human measurements and through calculating surface areas in square centimetres, which were extracted from image vector silhouettes.

2.1 Scanning and reconstruction of 3D body models

Today, different 3D body scanners are used for capturing the body characteristics, extracting of measures and acquiring of 3D models for garment prototyping and virtual try-on. For this research, the test person was scanned in standing position using a conventional body scanner GOM Atos II 400. The test persons in a standing posture were scanned with feet apart hands extended. Several individual scans from different heights and angles were observed and combined into one independent mesh, Figure 1, using the software Atos V6.0.2.

Figure 1 Combined individual scans in a global coordinate system using Atos V6.0.2 software

To obtain an optimal surface description of a test's person's body, we performed the noise reduction through cleansing and removing those points which did not correspond to the body surface, such as the unnecessary digital data of the mesh at the armpits and the ground. The mesh has also contained holes, which were repaired manually by using different graphic programs like MeshLab and its tool "Poisson" and Blender for smoothing the remaining

irregularities on the meshed surface by using its tool "Sculpt Mode-Smooth", Figure 2.

Figure 2 3D body model after processing with Blender's tool "Sculpt Mode-Smooth"

For this purpose, the digital data of a scanned body were imported in a form of a .stl (STereoLitography) file into the graphic programs.

2.2 Body model's posture adaptation

For enabling 3D body model's posture adaptation, the construction of a kinematic skeleton inside the watertight mesh was performed. The "Armature Modifier" was used to construct a hierarchical skeleton of 20 bones and 15 joints, Figure 3. Firstly, in "Edit Mode" the spinal cord construction was carried out by selecting the tail of each particular constructed bone through extruding it to a new bone. The skeleton construction continued for the shoulder and upper limbs at the left and right sides and completed at the lower limb for the Left and Right sides.
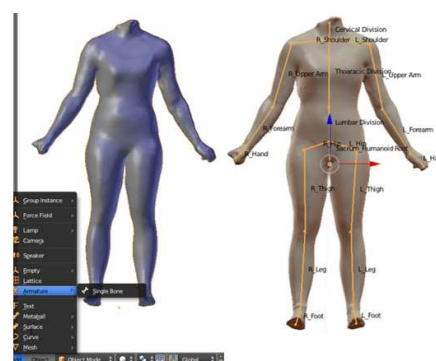
Figure 3 Blender's »Armature modifier« for skeletal construction

Achieved 3D body models, ready for posture adaptation, can be completely adapted to the desired position/posture required for virtual garment prototyping and/or virtual try-on. Figure 4 represents the body posture adaptation to a female tennis player during wheelchair tennis at the Paralympic Games of the year 2012 [12].

Figure 4 3D body model after processing with Blender's tool "Sculpt Mode-Smooth"

3   EXPERIMENTAL PART

In this study the virtual prototyping of garments for the upper body to a sitting 3D body model in different postures was performed with the aim to explore the possibilities of sports garments' development for a sitting position in terms of ergonomic requirements of garments. The garments fitting were investigated depending on the mechanical properties of the applied knitted fabrics. In addition, characterization of the knitted fabrics' deformations, and tension and stretch along any weave direction of the garment to the human body were observed, respectively.

3.1   Materials
Two knitted fabrics were used in order to carry out the research related to influence of knitted fabric's stretch on garments fitting. Knitted fabrics were produced on a raschel knitting machine RSE 4-1. The basic properties of these knitted fabrics are represented in Table 1.
The elastic components for the production of the knitted fabrics were Dorlastan and Lycra. Therefore, they can be characterised as

highly elastic knitted fabrics for women's underwear.

Table 1 Properties of the knitted fabrics

Fabric type	Raw material	Knitwear density		Fabric weight, gm^{-2}
		Wales d.	Courses d.	
S1	85% PA6 15% Dorlastan	22	80	50
S2	73% PA6 27% Lycra	22	156	95

3.2   Sport shirt pattern design and 3D virtual prototyping
The sport shirt pattern design was performed using a construction system M. Muller & Sohn and the OptiTex PDS computer program, Figure 5. The 3D virtual prototyping of the sport shirts was performed on a sitting 3D body model in different postures, Figure 6.
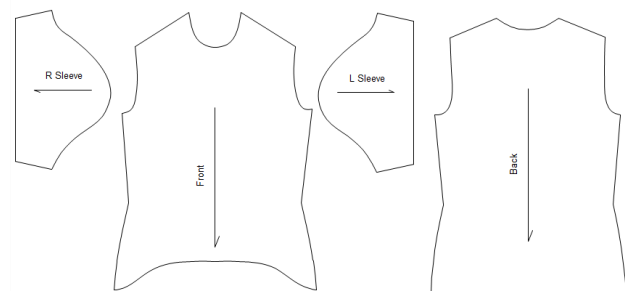
Figure 5 Sport shirt 2D pattern design
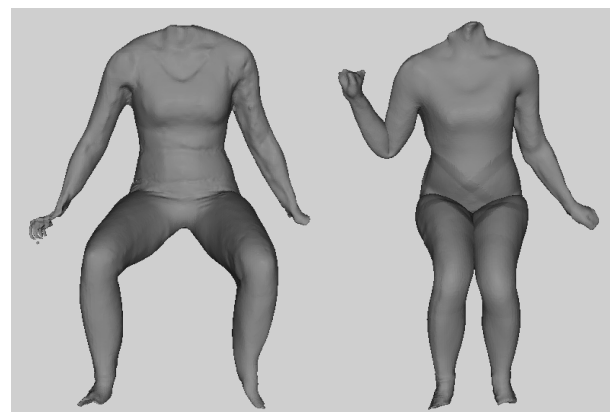
Figure 6 Sitting 3D body model in different postures

3.3 Determination of mechanical parameters of knitted fabrics

The knitted fabrics' mechanical parameters (extensibility, bending rigidity, shear rigidity, compression) were determined by using the FAST measuring system. Mechanical parameters of the knitted fabrics are collected in Table 2.

Table 2 Mechanical parameters of the knitted fabrics measured by FAST measuring system

Measurements	Direction	Units	Knitted fabric mark	
			S1	S2
Extensibility	wales	%	/	/
	courses	%	/	/
Bending rigidity	wales	μNm	0.3	1.6
	courses	μNm	0.6	1.2
Shear rigidity		Nm^{-1}	17	46
Surface thickness		mm	0.054	0.047
Surface mass		gm^{-2}	50	95

Necessary extensibility for the garment simulation was measured at tensile load of 98.07 Nm^{-1}. Since the knitted fabrics' extensibility exceeded the measuring range of 20%, the knitted fabrics' stretch of 23% was used from the fabrics list of the OptiTex program for a similar knitted fabric.

4   RESULTS AND DISCUSSION

Fitting of the sport shirts using different mechanical properties of the knitted fabrics for virtual prototyping and preview of the sport shirts tensions on the virtual human body is represented in Figure 7. The sport shirts tensions and stretches deformations along any weave orientation have been examined on a sitting 3D body model in different postures.

There can be seen some obvious differences in tension maps of both garment. They are caused by the differences in structural and physical/mechanical properties of applied knitted fabrics. Based on these results we can analyse the impact of textile materials' parameters on behaviour/tension loads of virtual garments using sitting posture body models.
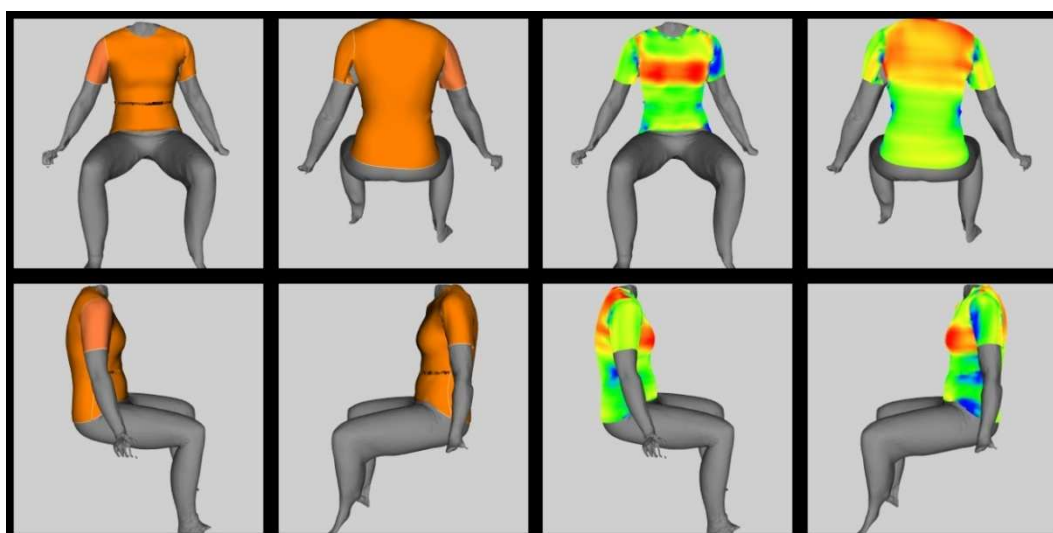
Knitted fabric S1
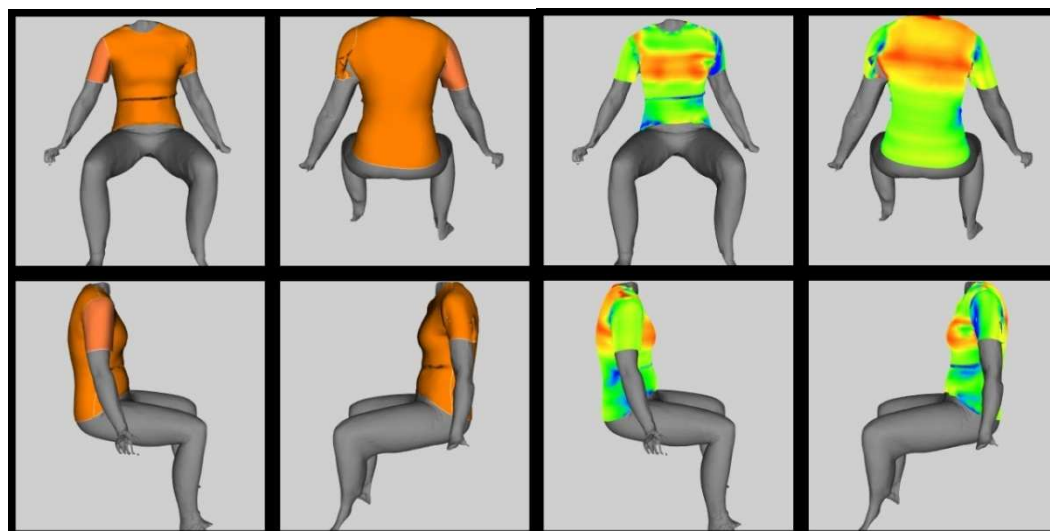
Knitted fabric S2

Figure 7 Fitting of the sport shirts using different mechanical properties of the knitted fabrics - tensions preview

5   CONCLUSIONS

In this contribution we have presented a study of the impact of textile materials' parameters on behaviour and tension loads of virtual garments. Importance of fabrics' characteristics for reliable garment prototyping and visualisation was studied using two types of warp knitted fabrics with different structural and physical/mechanical properties. For the purpose of virtual garment prototyping and visualisation we have developed standing and sitting posture 3D body models. Using the tension maps we can analyse the impact of textile materials' parameters on behaviour/tension loads of virtual garments using sitting posture body models. Furthermore, this can serve as a basis for engineered projection/planning of textile fabrics and garments to be produced.

6   REFERENCES

1. Lim H., Istook C.L.: Drape Simulation of Three-Dimensional Virtual Garment Enabling Fabric Properties, Fibers and Polymers 12(8), pp. 1077-1082, 2011
2. Magnenat-Thalmann N.: Modeling and Simulating Bodies and Garments, Springer (London), 2010
3. Behery H.M.: Effect of mechanical and physical properties on fabric hand, Woodhead Publishing (Cambridge), 2005
4. Magnenat-Thalmann N., Luible C., Volini P., Lyard E.: From Measured Fabric to the Simulation of Cloth, Computer-Aided Design and Computer Graphics, 10th IEE International Conference, 2007
5. Kim H.S., Na M.H.: Effects of Bending Properties and Drapability on the Hand and Appearance of Wool-Blended Fabrics: Comparison of Real Clothing with Online and 3D Virtual Garments, Fibers and Polimers 14(12), pp. 2148-2156, 2013
6. Ancutiené K., Sinkeviciute D.: The Influence of Textile Materials Mechanical Properties upon Virtual Garment Fit, Retrieved September 9, 2014, Web site:
7. http://www.researchgate.net/publication/215607812_The_Influence_of_Textile_Materials_Mechanical_Properties_upon_Virtual_Garment_Fit
8. Kozar T., Rudolf A., Jevšnik S., Stjepanović Z.: Developing the accurate sitting position 3D body model for garment prototyping, Proceedings of 4th International Scientific-Professional Conference Textile Science and Economy, University of Novi Sad, Zrenjanin, pp. 133-138, 2012
9. Rudolf A., Kozar T., Jevšnik S., Cupar A., Drstvenšek I., Stjepanović Z.: Research on 3D body model in a sitting position obtained with different 3D scanners. V: The International Istanbul Textile Congress 2013, May 30th to June 1th, Istanbul, Turkey, Innovative and functional textiles: book of abstracts, pp. 6, 2013
10. Rudolf A., Kozar T., Jevšnik S., Cupar A., Stjepanović Z.: Development of appropriate

garment pattern design for a sitting position 3D body model. In: The 10th Conference of Chemists, Technologists and Environmentalists of Republic Srpska, 2013

11. Kozar T., Rudolf A., Jevšnik S., Cupar A., Stjepanović Z.: Adapting human body model posture for the purpose of garment virtual prototyping, Proceedings of 4th Int. Scientific-Professional Conf. Textile Science and Economy, University of Novi Sad, Zrenjanin, pp. 133-138, 2013

12. Kozar T., Rudolf A., Jevšnik S., Cupar A., Priniotakis G., Stjepanović Z.: Accuracy evaluation of a sitting 3D body model for adaptive garment prototyping, Proceedings of AUTEX 2014 Conference, Bursa, 2014

13. http://www.paralympic.org/taxonomy/term/34/www.london2012.com?page=83, Accessed: 2014-06-22

EVALATION OF LINE LIGHT SOURCES ILLUMINATION INTENSITY

Dana Křemenáková, Jiří Militký and Juan Huang

Department of Material Engineering, Textile Faculty, Technical University
46117 Liberec, Czech Republic
dana.kremenakova@tul.cz, *tel.00420 48 5353209*

Abstract: *In the side emitting plastic optical fibres (SEPOF) the light leaks out from their surface. The main aim of this contribution is evaluation of SEPOF loss of illumination intensity in dependence on the distance from light source. The special device for measurement of light intensity on surface at various distances from light source is used. The dependence of light intensity on the distance from light source is expressed by the linear piecewise function (LLF2 model) composed from two straight line parts with attenuation factor as the rate parameter. The influence of the SEPOF diameter on the mean attenuation rate is quantified.*
Key words: *Polymer optical fibers, attenuation, piecewise model, fiber characteristics.*

1 INTRODUCTION

Standard polymer optical fibre (POF) is a dielectric waveguide transferring light or infrared radiation across its axis by the mechanism of total internal reflection on the interface of two materials with different refractive indices [1]. The main requirement for classical POF is to prevent side emission causing loss of transferred light. In the side emitting plastic optical fibres (SEPOF) the light leaks out from their surface. Side emission occurs if the light incidence angle is smaller than critical angle. This effect can be obtained by the increasing of cladding refractive index, decreasing of core refractive index or by the change of incident light angle. It is also possible to use multiple micro-bending of core or cladding; additives causing reflection or fluorescence into core/cladding or to create geometric asymmetry in the core/cladding system [2]. The SEPOF can be used for creation of optically active textile structures providing opportunities to highlight people and objects without the need for external light exposure. Due to the transmission loss, the intensity of radiation emitted in any direction decays along the straight fibre axis as a function of distance from the light source [4].
The main aim of this contribution is evaluation of SEPOF loss of illumination intensity in dependence on the distance from light source. The dependence of light intensity on the distance from light source is expressed by the linear piecewise function. The influence of the SEPOF diameter on the mean attenuation rate is quantified.

2 EXPERIMENTAL

2.1 Materials

Polymeric side emitting optical fibers "Grace" (produced by company Grace POF Co., Ltd. China) with different diameter were used for measurement of illuminating intensity in straight and bent states (see Table 1). Surface of "Grace" fiber and its cross-section are shown in Figure1.

Table 1 Optical fiber specification

core / cladding	PMMA / polycarbonate
core / cladding refractive index	1.49 / 1.41
numeric aperture / maximal input angle	0.48 / 57.4°
mass density / tensile strength	1190 kgm^{-3} / 78 MPa
wave length / temperature of use	400-900 nm / 20-70°C
POF diameter [mm]	0.25, 0.3, 0.4, 0.75, 1

The POF end connected with light energy source was prepared by heated wire cutting

and then by polishing with diamond powder. Illumination system with light emitting diode (LED) was created and used as light source for side emitting optical fibers.

a) cross-section   b) surface
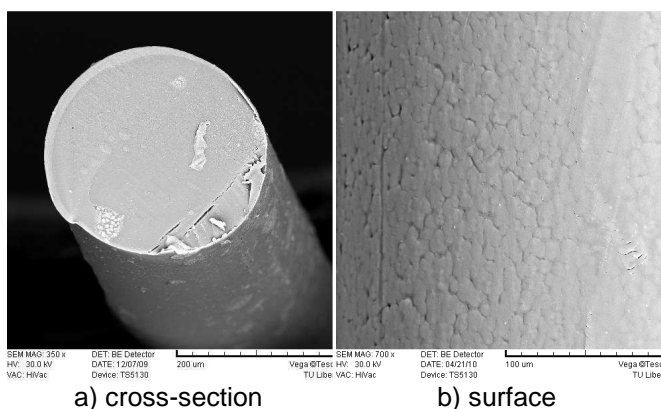
Figure 1 Polymeric side emitting optical fiber "Grace"

2.2 Methods

For measurement of illumination intensity changes of these fibers the special device was constructed [3]. The scheme of this device is shown in the Figure 2.
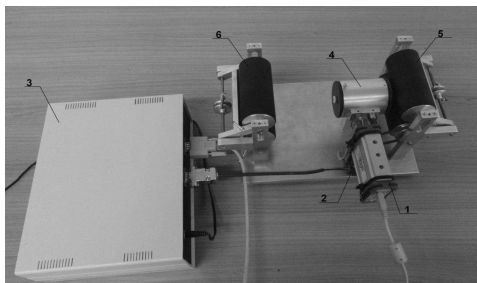
Figure 2 Device for measurement of POF illumination intensity decay

This device was used for characterization of length dependent optical attenuation. Device was composed from light sensor 1, step driver 2, control unit 3, measuring channel 4, input rolls 5 and output rolls 6. Illumination source consist from light emitting diode (LED), control circuit and power source was used as light source for side emitting optical fibers. Illumination intensity was measured along the length 1000 mm (Figure 3). Mean value of illumination intensity and 95%

confidence interval based on ten repetition of measurement on polymeric optical fiber „Grace" was calculated by using of statistics for small samples [5]. The experimental variances were used as weights in regression analysis.

3 RESULTS AND DISCUSSION

Due to the transmission loss, the power of radiation emitted in any direction decays exponentially along the fiber axis with increasing distance from the light source of the fiber while the percentage of light emitted per unit length is uniform over the entire fiber length. The attenuation coefficient α [dB] is in fact equal to logarithm of ratio between two powers on the input $P(0)$ and on the output $P(L)$

$$\alpha = 10\log(P(0)/P(L)) \tag{1}$$

The mean attenuation rate α_L is defined as the ratio of attenuation coefficient and the distance L between measuring powers. The unit of the mean attenuation rate is dB per unit length. The mean attenuation rate α_L is ideally constant, but generally may be a nonlinear function of the length L. Theoretical illumination intensity can be calculated by rearrangement of Eq. (1) into form

$$P(L) = P(0)\, 10^{-\alpha_L L/10} \tag{2}$$

This model is practically not able to properly fit the experimental data. Piecewise solid line in Figure 3 is so called LLF2 model.
LLF2 model is linear piecewise function consist from two different sections created by straight lines. This model is based on the assumption that in short distances from light source there are some no uniformity in side emission due to accommodation to aperture and critical angle. In second phase the illumination intensity is slowly decreasing with distance from source L (system is accommodated).
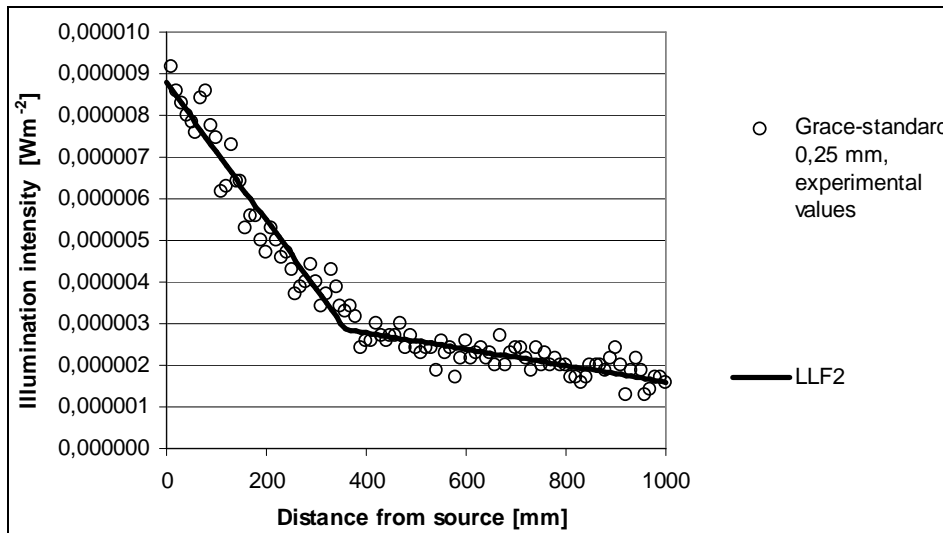
Figure 3 Typical decay of illumination intensity and LLF2 model

Local slopes of LLF2 are in fact sensitivity coefficients a_1, a_2. Corrected illumination intensity on the fiber input is $P_c(0)$. LLF2 model is described by equation

$$P(L) = P_c(0) + a_1 L + a_2 (L - L_c)_+ \qquad (3)$$

where function $(x)_+ = 0$ if x is negative and if x is positive, function $(x)_+ = x$. L_c is distance of transition between first and second phase. By using of special linear regression [4] parameters of LLF2 were found: The parameters of model (3) were evaluated from illumination decay experimental curves of

Grace flexi SEPOF with diameters 1, 2, 3, 6, 11 and 14 mm.
The influence of SEPOF fibers diameter on the parameter $P_c(0)$ and intercept of second straight line b is shown in the fig. 4. The power type models were used for parameter smoothing. It is clearly visible that both parameters are convex increasing function of diameter. The sensitivity coefficients a_1 and a_2 (see model (3)) are shown in fig. 5 as function of SEPOF fibers diameter. It is visible that in both cases the dependence is nearly linear.
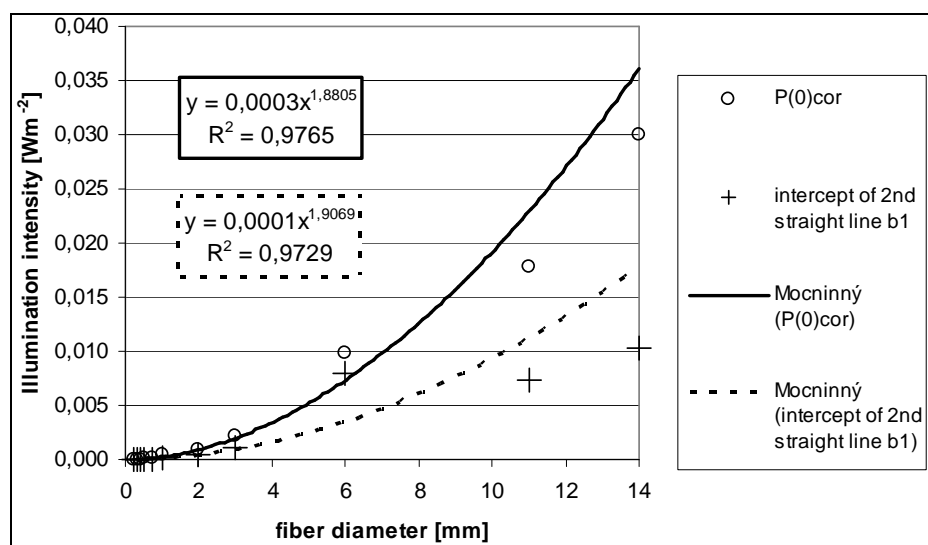
Figure 4 Dependence of intercepts of LLF2 model on SEPOF fibers diameter
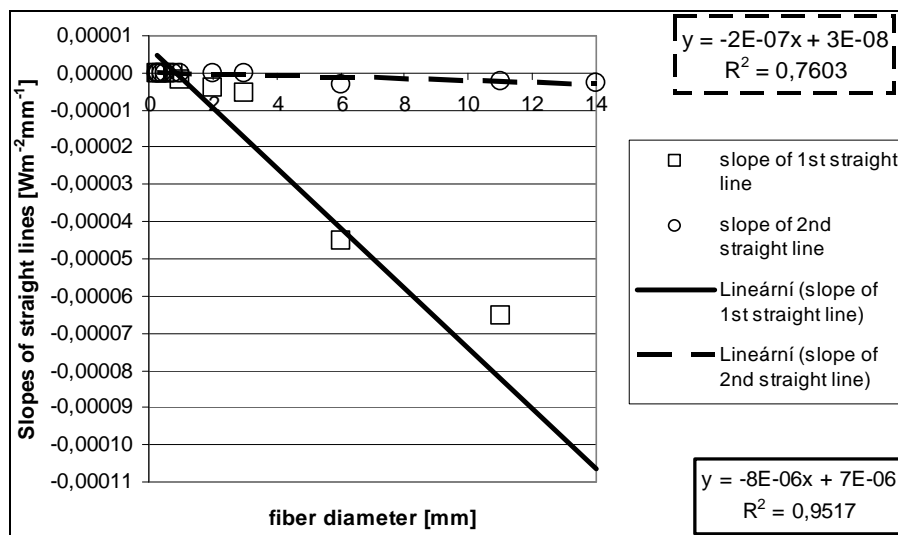
Figure 5 Dependence of sensitivity coefficients of LLF2 model on SEPOF fibers diameter

The slope of first line is decreasing function of diameter and slope of second line is nearly constant.

4   CONCLUSIONS

Optical fibres with higher diameter have higher illumination intensity. Higher fiber diameter is therefore better from point of view of total illumination at all distances from light source. It is suitable to divide this dependence to two phases, first represents no uniformity in side emission due to accommodation to aperture and critical angle and second with slow decline of mean attenuation rate i.e. LLF2 model.

5   REFERENCES

1. Zubia J, Arrue J.: Plastic optical fibers-an introduction to their technological processes and applications, Opt Fiber Technol. 7, pp. 101-140, 2001
2. Harlin A., et al.: Development of polymeric optical fiber fabrics as illumination elements and textile displays, AUTEX Res. J. 3, pp. 1-8, 2003
3. Lédl V.: Device for measurement of optical fiber illumination, Internal report, TU Liberec, 2010
4. Křemenáková D., Mishra R., Militký J., Mareš J., Šesták J.: Selected properties of functional materials, WBU Pilzen Publ House, 2013
5. Meloun M, Militký J.: Statistical Data Analysis, Woodhead Publ. India, 2011

INVESTIGATION ABOUT THE INFLUENCE OF THE YARN TENSION OVER THE MECHANICAL PROPERTIES OF TUBULAR BRAIDED FABRICS

Yordan Kyosev[1], Aurelie Nicolau[1,2], Laurence Schacher[2], Dominique Adolphe[2], Priscilla Reiners[1,2] and Frank Heimlich[1]

[1]*Hochschule Niederrhein – Univeristy of Applied Sciences, Mönchengladbach, Germany*
[2]*Ecole Nationale Supérieure d'Ingénieurs Sud Alsace, Laboratoire de Physique et Mécanique Textiles, Mulhouse Cedex, France*
yordan.kyosev@hs-niederrhein.de

Abstract: *This work reports about experimental investigation of the influence of the yarn tension during tubular braiding over the geometrical and mechanical properties of the ropes.*
Key words: *Braiding, yarn tension, elastic properties.*

1   INTRODUCTION

One of the most common application areas of braided products are ropes for different applications. For ropes the most important properties are the tensile properties like breaking force and elongation, but the elasticity and the bending rigidity too. There are several investigations about the influence of the braiding angle over the mechanical properties of the ropes [1, 3-5], based on analytical relations between the geometry of the yarns in one braid and the properties of the braid. Another researchers are trying to simulated the elastic behavior using FEM in order to predict the properties [6], where the most simulations are for overbraiding of mandrels on radial braiding machines, where there are negligible changes of the yarn length between the braiding point and carrier or are based on kinematic simulations, where the yarn tension is not important [2] so much as the yarn orientation.

For normal tubular or flat braiding machine actually the yarn tension remains seldom constant during the braiding process. There are several factors, which leads to fluctuations of it – the unwinding geometry of the bobbins, the differences of the distance between the carrier and the braiding point (Figure 1) at the different positions of the

carrier, the type of the carrier and especially the type of the compensation mechanisms.

The old carriers and some of the modern carriers for very thin and very thick ropes are still weight balanced [3]. Because the weight remains constant during the braiding, the yarn tension is kept as well constant. But the fast running braiding machines for the normal range of yarn fineness are using springs for keeping the yarn under some tension. As known from the mechanics, the spring changes its force depending on the deformation Δx:

$$F = k \cdot \Delta x \tag{1}$$

During the compensation of the yarn length differences the spring of the right hand side carrier on the Figure 1 (for Point B) will be significantly more deformed (pressed) than the spring in the carrier C (left hand side), because the left one receive the superfluous yarn length. This difference cause to different yarn tension at these points, and this difference is as higher as higher the spring stiffness k is. Each braiding machine can be set with different springs in the carriers – softer for more fine materials and stronger springs for the thicker materials. The used set of the springs determine the yarn tension and determine as well the forces at the braiding point, where the new braid is build. Some

influence over the properties of the braid can be as well expected, because the higher tension forces should lead to more compact braid. The goal of the current work is to investigate experimentally the variations in the yarn tension on a tubular braiding machine and its influence over the braid parameters.
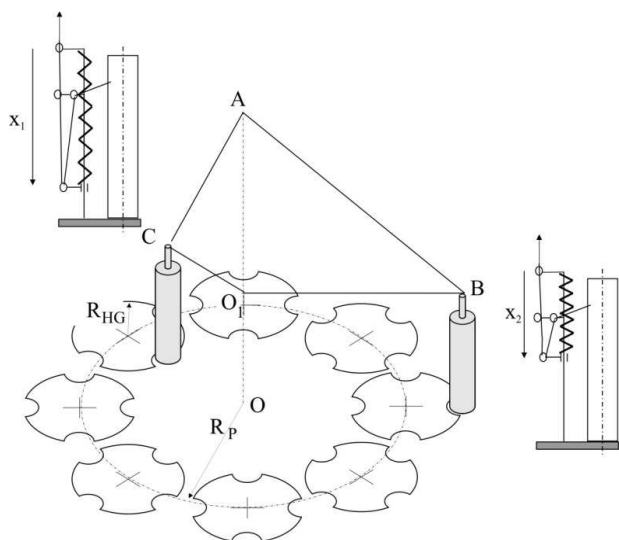
a)

b)

Figure 1 a) The distance between the carrier and the braiding point changed during the braiding process and causes difference in the yarn tension on the machines with spring balanced carriers [3]; b) Measurement of the yarn tension on the braiding machine

2 EXPERIMENTAL

During this investigation the samples was produced on a tubular braiding machine Seng 16/80-1 of the company A. Herzog, Oldenburg. PA6.6 multifilament yarn with 250 Tex was winded on bobbins on a universal winding machine FC of the company Jakob Muller, Frick, Switzerland, keeping the yarn tension during the winding constant, using tension regulation unit of the company BTSR.

The carriers are arranged "one full - one empty", so that 2:2-1 structure (two over two as a group of one yarn) according to [3] is produced. The trials are done with set of three take off speeds (8, 16 and 21 m/min) and was performed with three sets of springs – white, black and blue.

The measurement of the real yarn tension on the machine was performed as following. First the machine starts until a steady state of the braiding process at the current settings is achieved. Then the machines is stopped and the yarn tension is measured (Figure 2) using hand measuring device of the company Hans Schmidt GmbH with range up to 1000 cN, but every time it is as well marked which carrier exactly is measured so, in order the tension fluctuations on single carriers to be detectable. The yarn tension is measured at three places - once, when the carrier is on its most outer position, once as it is on the transfer point between two horn gears (middle position) and once as it is on the most inner position. The geometrical properties diameter and braiding angle are determined as mean values from a series of measurements using microscope. The bending rigidity is determined with the help of the cantilever test and the tensile properties using standard testing machine Zwick.
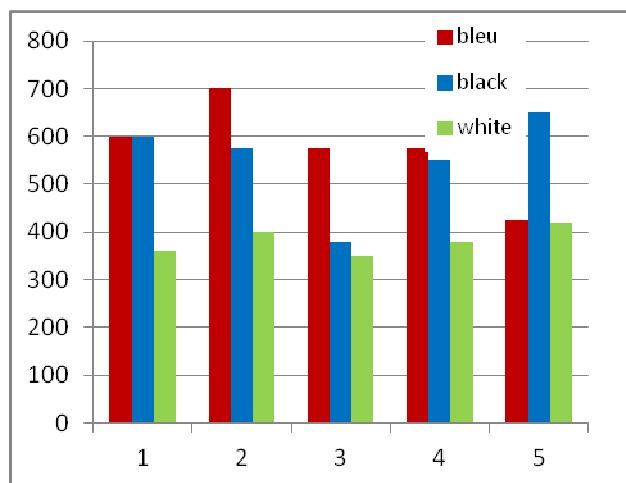
Figure 2 Yarn tension in cN at five carriers, measured for different springs (springs with different color identification have different stiffness)
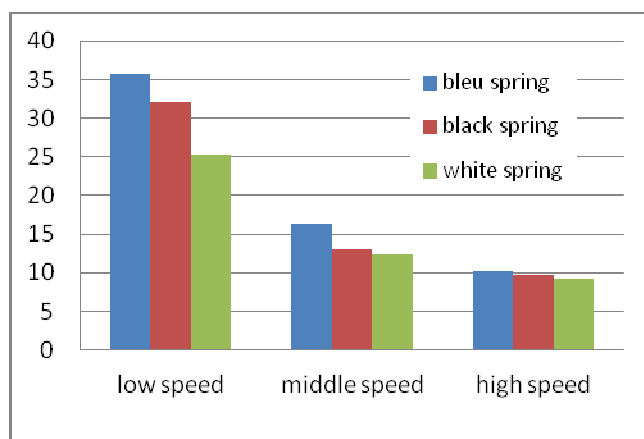
Figure 3 Bending length from cantilever test in cm for the samples at different take off velocities produced with different springs

3   RESULTS AND DISCUSSION

The measurement of the yarn tension at the different carriers shows some irregularities in the tension between the carriers (Figure 2). These can be reason of the unwinding geometry [3] but as well based on different state of the carriers as oil, friction, abrasion on some places etc. Currently running is as well experimental test about the stiffness of the springs of each group, in order to determine the tolerance between these because the differences in the stiffness will cause immediately differences in the yarn tension too.

The experimental investigation of the braids shows some influence of the yarn tension to the diameter of the braids and more significant over the bending rigidity (Figure 3) as the cantilever test shows. The higher take-off speed leads to lower bending rigidity and softer spring (white is the softer one and blue is the stiffest one) leads to lower bending rigidity too. (The complete calculations cannot be given in the abstract because of the page limitation.)

4   CONCLUSIONS

The investigation demonstrates that the yarn tension during the braiding has influence over the bending rigidity of the braids and some influence as well to the rope diameter.

5   REFERENCES

1. Du G.W., Popper P.: Analysis of a Circular Braiding Process for Complex Shapes, Journal of the Textile Institute 85(3), pp. 316-337, 1994
2. Kessels J.F.A,; Akkerman R.: Prediction of the yarn trajectories on complex braided performs, Composites, Part A: Applied Science and Manufacturing 33(8), pp. 1073-1081, 2002
3. Kyosev Yordan K.: Braiding technology for textiles: Principles, design and processes, Woodhead Publishing Limited, 2014
4. Omeroglu Sunay: The Effect of Braiding Parameters on the Mechanical Properties of Braided Ropes, Fibres&Textiles in EE 14(4), pp.53-57, 2006
5. Phoenix S.L.: Mechanical Response of a Tubular Braided Cable with an Elastic Core, Textile Research Journal 48(2), pp.81-91, 1978
6. Pickett A.K., Sirtautas J., Erber A.: Braiding Simulation and Prediction of Mechanical Properties. Applied Composite Materials 16(6), pp. 345–364, 2009

RASCHEL MESH STRUCTURES - YARN CONSUMPTION OF THE WARP INLAY

Irena Lenfeldová

Technical University of Liberec, Department of Textile Technologies
Studentská 2, 460 17, Liberec, Czech Republic
irena.lenfeldova@tul.cz, +420 48 535 3328, +420 48 535 3542

Abstract: *The several two guides bar warp-knitted structures (pillars and inlay) were designed and manufactured with the aim to predict this yarn consumption on the bases only of the geometrical structural models of these textiles, on the bases of thread diameter and the raschel machine setting together with the known warp-knitted pattern. This prediction of the yarn consumption of the inlay was verified in the dense - "compact" structure which was described only of the yarn diameter.*
Key words: *Yarn consumption, warp-knitted structure, geometry model, prediction.*

1   INTRODUCTION

An inlaid yarn is never formed into a knitted loop. Inlaid (laid-in) fabric consists of a ground structure of knitted or overlapped (warp knitted) threads that hold in position other non-knitted threads which were incorporated (laid-in) into the structure during the same knitting cycle [1-3]. The specification of the loop head and position of the threads which pass into and pass from the loop head and specification of the height are suitable for the right application of the structural properties on the planned characteristic, i. e. surface properties.

2   EXPERIMENTAL

The structures in the Figure 1 were produced with the same warp-knitted machine setting (RML-6-F, Karl Mayer, ER 24, 9.2 course/cm)

for the experiment measurement of the yarn consumption. The pillars were connected with the threads of GB 2 which don't create the loops and joined together the columns of the opened loops - pillars (Figure 2).

2.1   Specification for knitted fabrics
The material specification for fully set threading ground bar (GB 1 and GB 2) of warp-knitted fabrics was: polyester filament 167dtex x 2, f 36. These structures were designed according to the raschel machine conditions and the designed method:

- Repeat units – 8 courses (due to the machine pattern equipment),
- Two ground bars with fully set (same material),
- Maximal length of the inlay – three needle space (pitch).
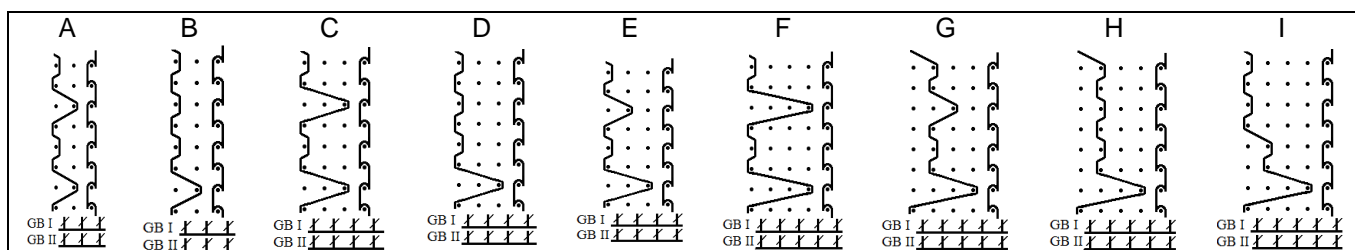
Figure 1 Lapping of the two guide bar warp-knitted fabrics (Structure A – I)
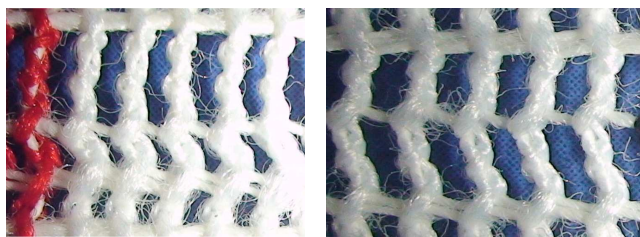
Figure 2 Photography of the designed two guides bar warp-knitted structures (Structure H and I)

2.2 Methods for calculation of yarn consumption

Some geometrical models of yarn in knitted head of the loop were designed for the calculation of yarn consumption. For that method, it was used the experimental value of the thread diameter [4] and machine setting (machine density, 920 m^{-1}). The binding area can be specified, see Figures 3, 4 and Table 1.
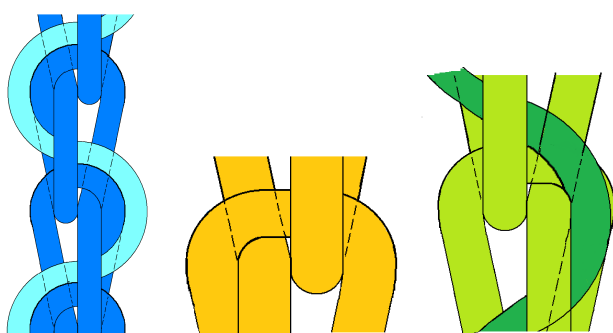
Figure 3 Contact regions of threads in knitted loops, especially in needle heads

In the case, when the produced structure has smaller ratio l/d and the loops are tight, fabrics are not full, is "compact", not excessively opened or transparent, the replacement of the thread axis can be approximated in the needle head as circle or ellipse or combination with the tangent – table 1. According of the approximation type the height of the course is designed to be the axis with the continuous curve.

The result is dependence of the yarn consumption on the yarn diameter. Theoretical area of the occurrence of these values can be shown in Figure 4. With the aspect to the expected dependence on the height of the course the yarn consumption of

the more compact model (mod. 3, 1, 2) is smaller.

Table 1 Comparison the geometrical model of designed structures

	Replacement of the inlay axis	Height of course
mod 7	1/2 circle, r=5/2d	5d
mod 6	1/2 ellipse, a=5/2d, b=2d	5d
mod 5	1/2 circle, r=2d and part of line	4d
mod 4	1/2 ellipse, a=5/2d, b=3/2d	5d
mod 3	1/2 circle, r=3/2d	3d
mod 2	1/2 ellipse, a=2d, b=3/2d	4d
mod 1	1/4 circle, r=d a part of tangent	4d
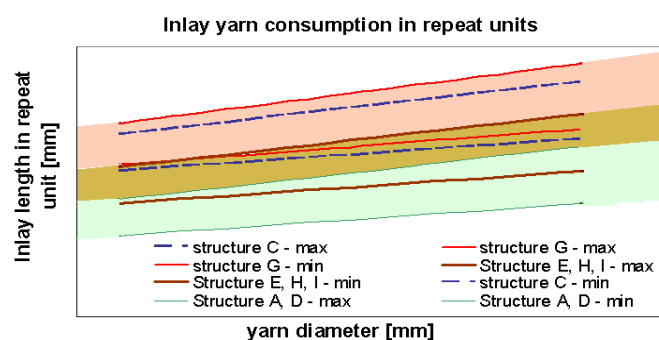
Figure 4 Diagram of the predicted values of yarn consumption

3 RESULTS AND DISCUSSION

The experimental values of yarn consumption of both ground bar (GB 1 and GB 2) were measured during manufacturing the warp-knitted samples. The results are shown in Figure 5. Although the machine setting was same, after relaxation process (not wet) some differences were appeared in the case of the pillar stitches. The mechanical impact and the effect of the take-up rollers causes these differences together with the yarn bending properties which influences these nine structures in different way. Structure H and I are similar, with another arrangement of the inlay threads in the structure, but the modeled length of the yarn in the repeat units is the same. The predicted yarn consumption and experimental value are identical, Figure 5.

The modeled values of yarn consumption (seven approximations) of the inlayed yarn

are shown in Figure 6. In the same Figure, the calculated values of yarn consumption (points in that diagram) on the base of experimental value of yarn diameter (experimental packing density) are compared with the experimental yarn consumption (horizontal line) carrying out during knitting process.
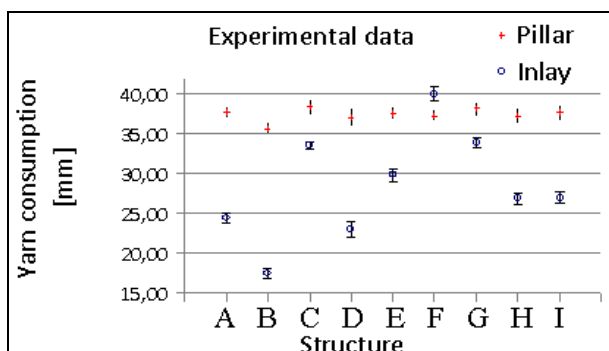
Figure 5 Measured value of yarn consumption of GB 1 (pillar) and GB 2 (inlay)
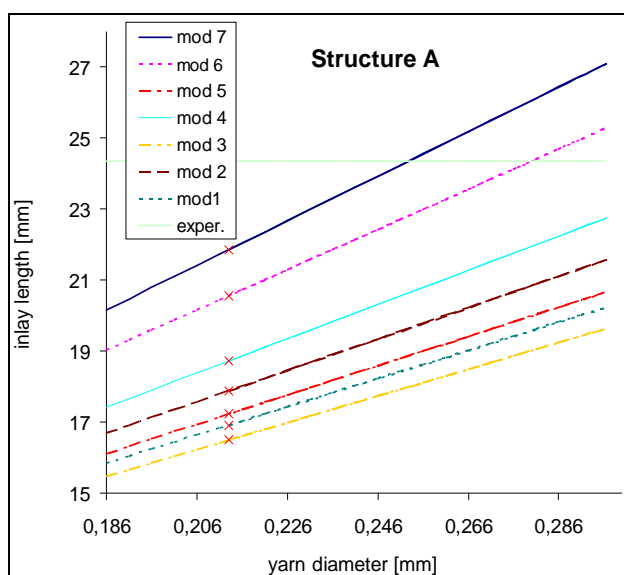
Figure 6 Yarn consumption of the inlay - structure A

The inlay length is defined in the repeated units – eight courses and the threads connect only adjacent pillars twice in this area. This chosen structure A is not lightweight from the other; it is medium with sufficient dimension stability.

4   CONCLUSIONS

From now, it is necessary to focus on the basic research of the yarn diameter in knitted structure. Even in the compact warp knitted geometry it influences the predictions and yarn consumption calculation with the bending rigidity of the yarn which creates the loops. The threads are turned through the textiles and created the new properties and influences. The loop models enable to plan the using of the knitted fabrics as textiles for special purposes, i.e. textiles to the moisture distribution, light permeability, transmission, textiles for impregnation, saturation, printing and other characters with have something to do with surface properties.

The other object is in the case of the manufacturing of the elastic thread. These structures will have the compact model in most of examples of various elasticized yarns, in comparison to equivalent structures made from conventional yarns [5].

The long-expected aim - structural model depending on the input data as are: machine setting, pattern and properties of the using thread (packing density) [6]. Focus on the area of the crossing point and bending rigidity of the yarn in the very small area given by the parameters of the gauge and take-up mechanisms of the warp-knitted machines.

5   REFERENCES

1. Grosberg P.: 3-The Geometry of warp knitted fabrics, J. Textile Institute Transactions 51(1), 1960
2. Spencer D.: Knitting technology-A comprehensive handbook and practical guide, 3rd edition, Woodhead Publishing, (Cambridge), 2001
3. Zhuo N.J., Leaf G.A.V., Harlock S.C.: The Geometry of Weft-inserted Warp-knitted Fabrics Part I: Models of the Structures, J. Textile Institute 82(3), pp. 361-371, 1991
4. Plachá I.: Charakteristika osnovní pleteniny - struktura a mechanické vlastnosti, Doctoral thesis, Technical University of Liberec, 2001
5. Pavko-Cuden A., Hladni, A. and Slug, F.: Loop Length of Plain Single Weft Knitted Structure with Elastane, J. Eng. Fibres and Fabrics 8(2), pp. 110 - 120, 2013
6. Kovar R., Kyosev Y.: Limit packing density of woven fabrics, Romanian Textile Journal V.1, pp. 35-42, 2004

TEMPERATURE DISTRIBUTION ON SEWING NEEDLE AT HIGH SPEED INDUSTRIAL SEWING LOCKSTITCH MACHINE

Adnan Mazari, Kausik Bal and Antonin Havelka

Department of Clothing, Technical University of Liberec, Czech Republic
adnanmazari86@gmail.com

Abstract: *This paper explains the experimental technique to measure the needle temperature at 3 different points of needle during high speed sewing. The results show that the needle heat is highest at the needle eye and nearly 40℃ less temp erature is observed at the needle holder. The results are further used to analyze the thermal heat loss by conduction and convection during the sewing process.*
Key words: *Sewing needle, lockstitch needle heat.*

1   INTRODUCTION

Industrial sewing is one of the most common manufacturing operations. Its application can be found in the manufacturing of garments, shoes, furniture and automobiles. Every day, millions of products ranging from shirts to automotive airbags are sewn. Hence, even small improvements may result in significant corporate benefits. Heavy industrial sewing, such as that used in the manufacture of automobile seat cushions, backs and airbags, requires not only high production but also high sewing quality (i.e. good appearance and long-lasting stitches). Typically, the material being sewn includes single and multiple plies of synthetic fabric or leather, sometimes backed with plastics, and needle heat-up is a major problem on the sewing floor. In recent years, in order to increase production, high-speed sewing has been extensively used. Currently, sewing speeds range from 60~100 stitches/sec. In heavy industrial sewing, typical sewing speeds range from 16~50 stitches/sec.

Depending on the sewing conditions, maximum needle temperatures range from 100℃ ~300℃ [1]. This high temperature weakens the thread, since thread tensile strength is a function of temperature [2], resulting in decreased production [2]. In addition, the final stitched thread has 30-40% less strength than the parent thread [3].

Various methods for measuring needle temperature, such as infrared pyrometer, thermocouple and temperature sensitive waxes, have been used [6]. Because the needle is moving extremely fast during the sewing process, it is quite difficult to measure the exact temperature [4]. There are few theoretical models available to predict sewing needle temperature [4, 5], but experimental verification has been done by thermal cameras, which is influenced by emissivity issues [7]. Sondhelm [10] used a lacquer painted in the needle groove to observe a change of colour with temperature. Laughlin [11] tried to measure needle temperature through infrared measurement from the needle using a lead-sulphide photocell. Another technique using thermocouples was later developed by Dorkin and Chamberlain [12]. As a result of improved understanding of the causes of sewing damage, many technical developments, such as improved needle design [13, 17], tension devices [14], fabric finishes [14], thread lubrication and needle coolers [15] have taken place over the years.

2   EXPERIMENTAL WORK

For this research inserted thermocouple method is used to measure the sewing needle temperature of an industrial lockstitch machine (BROTHER Industries). Conditions for all experiments were kept constant at

26°C and 65% RH. There are many different ways of experimentally measuring the needle heat for industrial sewing machine but inserted thermocouple method proved to be the most efficient way of measurement .The previous work of author [11, 13] compares different experimental method of needle temperature measurement and shows the inserted thermocouple with highly repeatable results.

Figure 1 shows the sewing needle with the inserted thermocouple. A thin thermocouple is inserted inside the needle groove and needle temperature is measured wirelessly to computer during high speed sewing.

The devices and materials used for the experiments are listed below:

- Lockstitch machine (Brother Company, DD7100-905).
- Thermocouple by Omega (K type 5SC-TT-(K)-36-(36)) for the inserted method.
- Thermocouple by Omega -wireless device and receiver (MWTC-D-K-868).
- Needles (Groz-Becker 100/16) R- type.
- Fabric: 2/1twill 100% cotton with 257 g/m^2
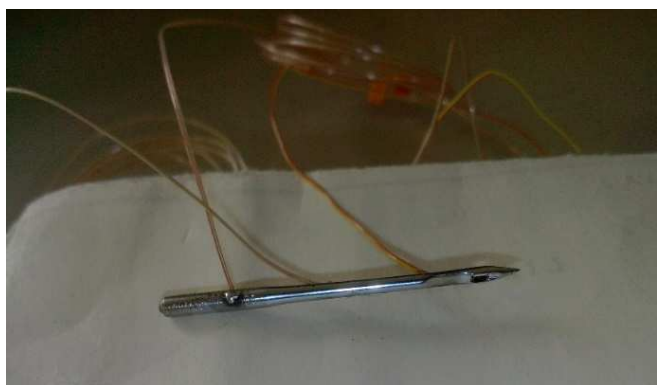
Figure 1 Needle attached with 3 thermocouples

3 RESULTS AND DISCUSSION

The sewing process is performed with 80 tex polyester core spun thread. The positions of temperature measuring thermocouples is shown in Figure 2 and Table 1 shows the average temperature at each position measured after 40 seconds of continuous sewing.

Table 1 Needle temperature [°C] at different positions of needle

Thermocouple position		1	2	3
with 80 tex thread	at 1000 r/min	99	76	64
	at 2000 r/min	143	108	89
	at 3000 r/min	213	145	115
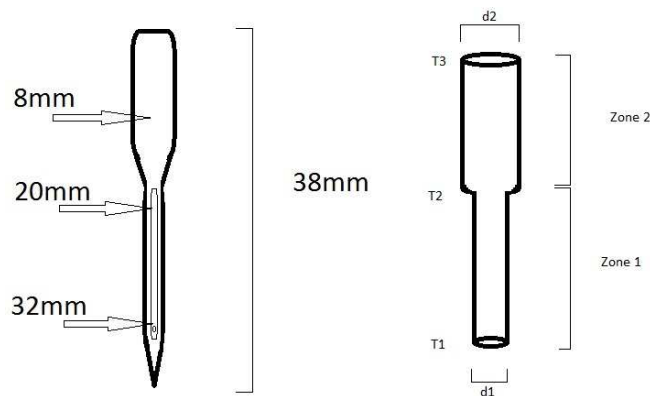
Figure 2 Technical design of needle

$$Q_{conduction1} = Q_{conduction2} + Q_{convection2} \qquad (1)$$

$$Q_{cond1} = \lambda.A_{c1}^{2}.\left(\frac{T_1 - T_2}{L_1}\right) = \lambda.\left(\frac{\pi d_1^{2}}{4}\right).\left(\frac{T_1 - T_2}{L_1}\right) \quad (2)$$

$$Q_{cond2} = \lambda.\left(\frac{\pi d_2^{2}}{4}\right).\left(\frac{T_2 - T_3}{L_2}\right) \qquad (3)$$

$$Q_{convection2} = h_2.A_{p2}.(T_{2m} - T_a) \qquad (4)$$

$$h_2 = \frac{Nu_{m2}.\lambda}{L_2} \qquad (5)$$

$$Re_{m2} = \frac{v.L_2.\upsilon}{\mu} \qquad (6)$$

$$T_{m2} = \frac{T_2 + T_3}{2} \qquad (7)$$

$$Pr_{m2} = \mu_a.C_p/\lambda_a \qquad (8)$$

$$Nu_{m2} = 0.0296.Re_{m2}^{0.8}.Pr_{m2}^{1/3} \qquad (9)$$

$$Q_{conduction1} = Q_{conduction2} + Q_{convection2}$$

$$\lambda . \left(\frac{\pi d_1^{\,2}}{4} \right) . \left(\frac{T_1 - T_2}{L_1} \right) = \lambda . \left(\frac{\pi d_2^{\,2}}{4} \right) \left(\frac{T_2 - T_3}{L_2} \right) + \quad (10)$$

$$+ \, h_2 . A_{p2} . \left(T_{m2} - T_a \right)$$

Checking the equation 10 with our experimental results shows less than 5% error, which is possible as needle is considered cylindrical but in actual has needle groove and taper design with the zone 2 of the needle.

4   CONCLUSIONS

The research work concludes that:
- Needle temperature is highest near the needle eye, whereas the point near the holder shows nearly 40$^{\mathrm{o}}$C loss due to heat loss by conduction and convection.
- Needle temperature is higher for all 3 positions of thermocouple for sewing with thread as compared to dry sewing.
- Further analysis of thermal equations shows that heat loss by conduction by region one is equal to heat loss by conduction and convection in region two with an error of less than 5 %.

5   REFERENCES

1. Qinwen Li, Liasi E.: A study on the needle heating in heavy industrial sewing part-1, International Journal of Clothing Science and Technology 13(5), pp. 351-367, 2001
2. Hersh S., Grady P.: Needle heating during high speed sewing, Textile Research Journal 39, pp. 101-120, 1969
3. Midha V.K., Mukhopadhyay A, Chatopadhyay R, Kothari V.K.: Studies on the changes in tensile properties of sewing thread at different sewing stages, Textile Res. Journal 79, pp. 1155-1167, 2009
4. Qinwen Li, Liasi E.: A study on the needle heating in heavy industrial sewing, part II, International Journal of Clothing Science and Technology 13(2), pp. 87-105, 2001
5. Trung N., Kùs Z.: Computer Simulation of Sewing Needle Heating, CSCC'99 Proceedings, pp. 1991-1994, 1999
6. Mazari A., Havelka A.: Tensile properties of sewing thread and sewing needle temperature at different speed of sewing machine,Advanced Materials Research 627, 2013
7. Li Q., Liasi E., Simon D., Du R.: Heating of industrial sewing machine needles: FEA model and verification using IR radiometry, in Thermosense XXI, Proc. SPIE, R.N. Wurzbach, D.D. Burleigh eds., 3700, pp. 347-357, 1999
8. TEXTILCHEMIE DR. PETRY GMBH: Infrared needle temperature measurement, accessed 1 October 2013
9. http://www.drpetry.de/fileadmin/user_upload/petry/pdfs/Infrared_needletemperature.pdf
10. Trung N.C., Kùs Z.: Theoretical Analysis of Sewing Needle Temperature, In: Young Textile Science '95, Liberec, Czech Republic, 1995
11. Sondhelm W.S.: Causes of seam damage: Needle heating, J. Textile Institute 44, pp. 580-585, 1953
12. Laughlin R.D.: Needle temperature measurement by infrared pyrometry, Textile Research Journal 33(1), pp. 35-39, 1963
13. Dorkin C.M., Chamberlain N.H.: The facts about needle heating, Clothing Institute Technical Report No.13, 1963
14. Anon.: Finding solutions to needle problems, Bobbin, February 1981, pp. 180-187
15. Anon.: Sewing Solutions, Apparel International, pp. 9, January 1996
16. Lewis J.: Clothing finishing procedure for preventing sewing damage in wool and wool/synthetic fiber double jersey fabrics, Clothing Research Journal 1(3), pp. 3-19, 1973
17. Yukseloglu M., Citoglu F., Catinkaya B.: A study on the needle heating in polyester blend upholstery fabrics, Industria Textila 63(5), pp. 246-25, 2013

MEASURING OF YARN CRIMP IN WOVEN FABRIC

Iva Mertová and Bohuslav Neckář

Department of Textile Technologies, Faculty of textile engineering
Technical University of Liberec, Studentska 2, 46117 Liberec, Czech Republic
iva.mertova@tul.cz

Abstract: A new method to measure the warp or weft yarn crimp in fabric was developed. The method is based on the analysis of yarn tensile characteristics. In this method, the yarns with predetermined distance are removed from fabric and clamped between the jaws of tensile-strength machine (Instron) without any pretension in the yarn and accordingly yarn crimp is measured. The results were also compared with other two existing methods. The results of yarn crimp in warp and weft direction of the fabric are found to be sensitive to selection of applied force range. Observed results from all methods have statistically significant correlations. It is monitoring influence of fabric and yarn parameters on yarn crimp value.
Key words: Fabric parameters, tensile curve, yarn crimp, woven fabric.

1   INTRODUCTION

The crimp of warp and weft yarn in woven fabrics are influenced by various factors, such as loom setting, type of fabric, sets of fabric, fabric weave, yarn diameters, weft and warp yarn bending rigidity, compression of yarns (at binding points) etc. The yarn crimp also changes during the fabric production on the loom, fabric relaxation in cloth roll and chemical processing of the fabrics. The yarn crimp also influences the economics of the fabrics due to change in fabric contraction, extensibility of fabric during finishing, fabric tensile properties, fabric weight and thickness and shape stability. It means, yarn crimp is highly governed the consumption of material to a specific application of a fabric. Crimp, crimp amplitude and length of the yarn axis are generally used as input data to predict the fabric properties but these parameters are complicated to define and measure.

Several researchers have studied the phenomenon of yarn crimp in the fabric and proposed different models of cloth geometry [1-5, 15 and 16]. The existing methods have their own merits and demerits while studying the cloth geometry. The study of real geometry of crimp in a woven fabric is very tedious due to variation in fabric structure because each wave is independent and differs from other wave, yarn is not uniform and it is often problematic to find out the position of yarn axis.

The main difference between existing methods and our proposed method is processing and comparison of stress-strain curves of two yarns: pull-out yarn and parent yarn.

We use the term pull - out yarn for yarn removed from fabric (yarn which is crimped). The parent yarn is yarn from cone, which was used for fabric production.

Existing methods are inaccurate, complicated or expensive for praxis. Our effort was to find new, more precise method but method which isn't demand on laboratory equipment and time-consuming.

The following objectives are framed for this paper:

- To verify the method to measure the crimp in a woven fabric on different types of fabric.
- To compare the results of proposed method with other existing methods for different types of woven fabric.
- To compare the measured results with predicted values using linear model.

2   THEORY OF METHOD

The theory is based on the analysis of tensile curves of parent yarn and yarn taken-out from

the fabric with crimp. The whole derivation is presented in [17].

According this theory the "best" value of parameter λ is obtained:

$$\lambda = \frac{\sum_{i=1}^{n}\{[\varphi(\sigma_i)+1][\psi(\sigma_i)+1]\}}{\sum_{i=1}^{n}[\varphi(\sigma_i)+1]^2} = \frac{\sum_{i=1}^{n}\{[\varepsilon_{h,i}+1][\varepsilon'_{h,i}+1]\}}{\sum_{i=1}^{n}[\varepsilon_{h,i}+1]^2}. \quad (1)$$

Then, we calculate the crimps of pulled-out yarn in the fabric and it is defined by the following equation:

$$s = l_0/h_0 - 1 = \lambda - 1 \quad \text{(dimensionless)} \quad (2)$$

Once we calculate the value of λ from equation (1) then the calculation of yarn crimp becomes very simple by using of equation (2).

3 EXPERIMENTAL

The method was used form crimp measuring of two sets of experimental fabric. The first was set of polyester staple yarns; the second fabric set was from cotton yarns.

Polyester staple yarns of three different linear densities i.e. 16.5, 25 and 40 tex are used to produce thirty plain weave fabrics with different combinations of warp and weft density to study the influence of yarn fineness, warp and weft density on yarn crimp. Cotton yarns of linear densities 8.4 (warp yarn) and 10 tex (weft yarn) are used to produce ten simple jacquard fabrics with different weaves. The details of yarn and fabric parameters of both experimental fabric sets are given in Tables 1 and 2.

Two points at a distance of 500 mm along the length of yarns of the considered woven fabric are marked for both warp and weft directions. For the present study 50 yarn specimens, each from warp and weft direction, are pulled-out from the fabric. Pulled-out yarns consist of undulations or waves introduced during weaving process. While pulling-out the yarn from the fabric, utmost precautions were taken that yarn should not get strained and untwisted.

Table 1 Yarn and fabric parameters - Set of experimental fabric I

Fabric Code	Yarn linear density (tex)		Yarn sets (1/cm)	
	warp	weft	warp	weft
1/25/19	16.5	25	24	19
2/25/19	16.5	25	27.8	19
2/25/22.4	16.5	25	27.8	22.4
3/25/19	16.5	25	31.8	19
3/25/22.4	16.5	25	31.8	22.4
3/25/26	16.5	25	31.8	26
1/40/15	16.5	40	24	15
2/40/15	16.5	40	27.8	15
2/40/18	16.5	40	27.8	18
3/40/15	16.5	40	31.8	15
3/40/18	16.5	40	31.8	18
3/40/21.2	16.5	40	31.8	21.2
4/25/19	25	25	19	19
5/25/19	25	25	22.4	19
5/25/22.4	25	25	22.4	22.4
6/25/19	25	25	26	19
6/25/22.4	25	25	26	22.4
6/25/26	25	25	26	26
4/40/15	25	40	19	15
5/40/15	25	40	22.4	15
5/40/18	25	40	22.4	18
6/40/15	25	40	26	15
6/40/18	25	40	26	18
6/40/21.2	25	40	26	21.2
7/40/15	40	40	15	15
8/40/15	40	40	18	15
8/40/18	40	40	18	18
9/40/15	40	40	21.2	15
9/40/18	40	40	21.2	18
9/40/21.2	40	40	21.2	21.2

Table 2 Yarn and fabric parameters – Set of experimental fabric II

Fabric Number	Yarn linear density (tex)		Yarn sets (1/cm)	
	warp	weft	warp	weft
1 till 10	8.4	10	66	55

Subsequently, the yarn was clamped on Instron tensile-strength tester with a gauge length of 500 mm assuring that the marked points on the yarn exactly match with nip point of the jaws. Now, yarn is allowed to break and average specific stress-strain curve of 50 yarns are plotted with the help of the software. For comparison, the average specific stress-strain characteristics of

original parent yarn are also evaluated from an experimental set of 50 individual curves.

We compared the curves of parent yarn and pulled-out yarn at an interval of specific stress values $(\sigma_{min}, \sigma_{max})$. The right λ-value describes the comparison of parent and pulled-out curves in a suitable range of specific stresses. We tried to use different values from following interval $(\sigma_{min}, \sigma_{max})$ on the place of lower limit σ_B. For each selected value of σ_B the corresponding λ-value was determined using equation (1) and then the yarn crimp from equation (2).

4   OTHER METHODS OF YARN CRIMP MEASUREMENT

Experiments are also carried out to measure the yarn crimp using two other different methods.

For first method, soft cutting and image analysis method [11] was used to prepare and process the cross sections of considered fabrics.

Second method is the old "raveling" or "thumb-method". In this method, the yarn specimen from fabric part length h_0 is pulled-out, then the yarn is straightened with thumbs (by a subjectively sensed down-pressure) and the length l_0 of un-crimped yarn is measured. Accordingly, the yarn crimp is determined using the equation (2).

5   COMPARISON OF RESULTS

Table 1 illustrates the observed correlation coefficients between experimental methods. The correlation coefficients between experimental methods are statistically significant for both fabric sets.

Table 3 Correlation coefficients of yarn crimp

Correlated methods	warp	weft
Instron – Image Analysis	0.88	0.79
Instron - Raveling	0.91	0.86
Image Analysis - Raveling	0.86	0.83

Experimental results confirm the influence of warp and weft sett and yarn count on yarn crimp values. Fabrics from polyester staple yarn have nonstandard behavior.
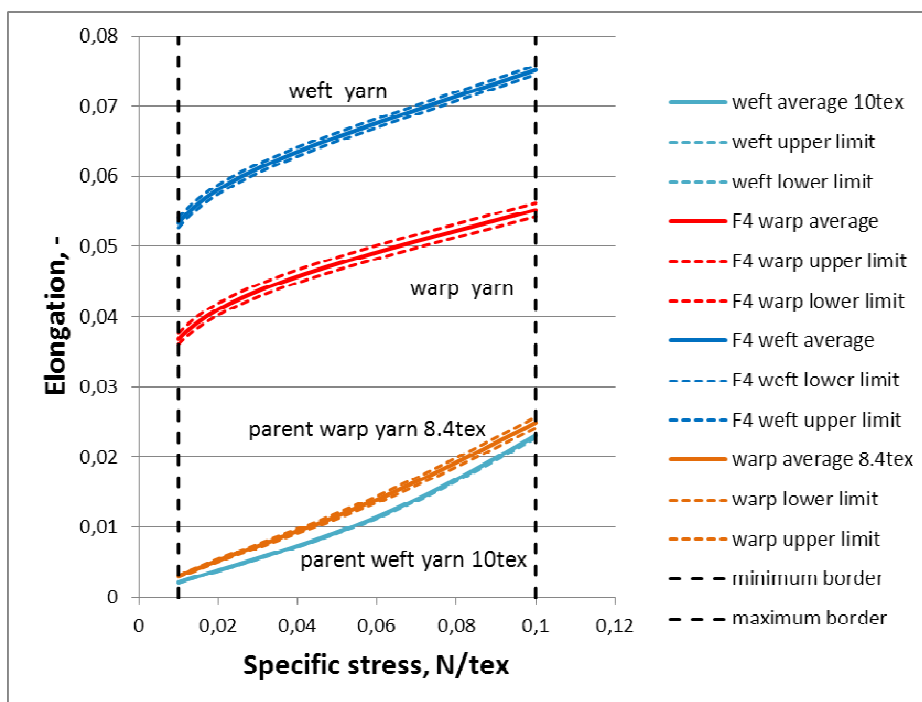
Figure 1 One example of inverse functions of specific stress-strain average curves in interval of specific stress values, cotton fabric no.4

The high warp set in combination with yarn count leads to reverse behavior of both treads systems. All fabrics have higher crimp in warp directions than weft directions, see Figure 3.

The same phenomenon refers to fabric elongation in both directions. Nonstandard behavior leads to nonstandard dependences. Warp crimp increase with higher warp set value and decrease with higher weft set. Crimp in weft direction decrease with higher warp set and increase with higher weft set, see Figure 4.
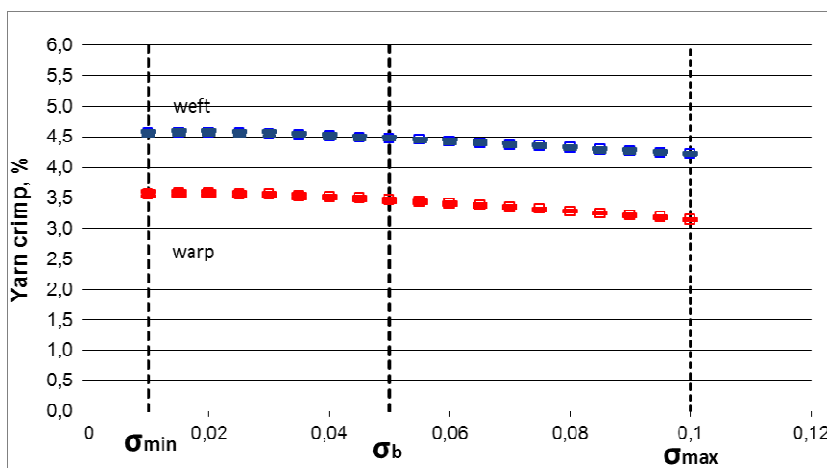
Figure 2 Evaluated yarn crimp in relation to the introduced value σ_B
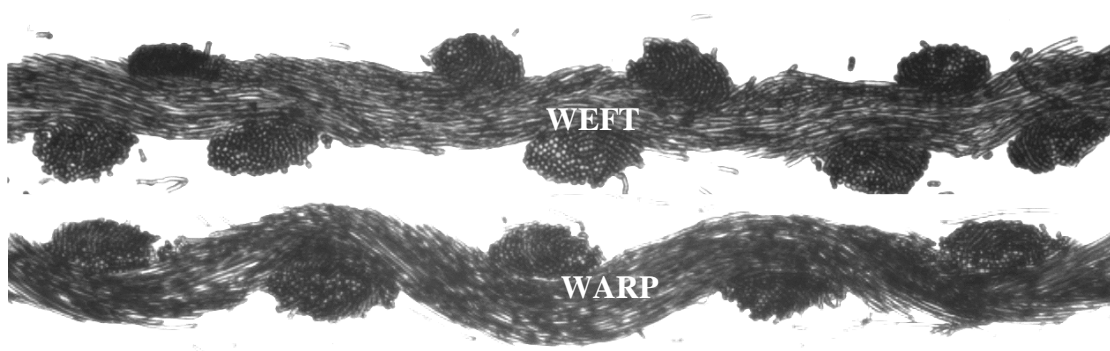
Figure 3 Transversal and longitudinal cross section images – example, fabric 3/25/19
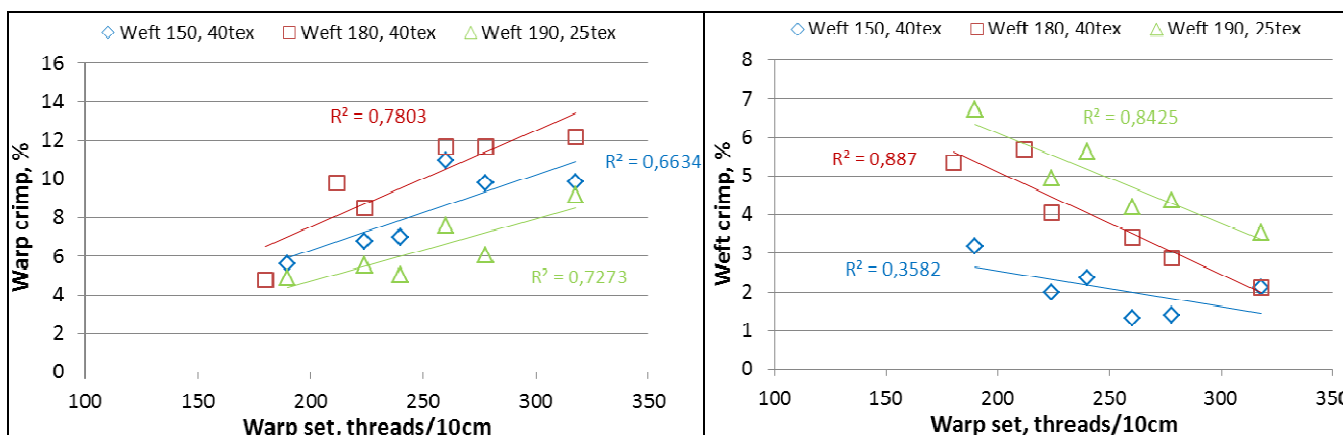
Figure 4 Influence of warp set on yarn crimp in warp and weft direction

6 CONCLUSION

The measurement of yarn crimp in fabric and fabric thickness on two considered methods and proposed methods is somewhat influenced by inherent problems of measurement techniques and yarn characteristics. Therefore, it was difficult to arrive at "fully right" values of yarn crimp in fabric and fabric thickness for comparison and testing of different method used.

Nevertheless, the method is relatively easy and more accurate to measure and reproduce the warp and weft crimp. The proposed method has great potentials for adaptation in industrial laboratories. And the method is possible to use for measuring yarn crimp in simple jacquard fabric with full area design.

7 REFERENCES

1. Hu J.: Structure and mechanics of woven fabrics, Woodhead publishing Ltd., Cambridge, p. 61, 2004
2. Sirková B.: Mathematical model for description of thread's interlacing in fabric using Fourier series, PhD Thesis, Technical University of Liberec, 2002
3. Kovar R., Krula M.: Crimp of Woven Fabric. In: 3rd ITCDC, Dubrovnik, Croatia, 8-11 October 2006, pp. 622-626
4. Kovar R.: Length of the yarn in plain weave crimp wave, Journal of The Textile Institute 102(7), pp. 582–597, 2011
5. Lin Jeng-Jong: Prediction of Yarn Shrinkage using Neural Nets, Textile research Journal 77(5), pp. 336-342, 2007
6. Chen X.: Modelling and predicting textile behaviour, Woodhead Publishing Ltd., Cambridge, pp.144, 2010
7. Leaf G.A.V.: The mechanics of plain woven fabrics, International Journal of Clothing Science and Technology 16(1/2), pp. 97-107, 2004
8. ISO 7211-3. (2196). Textiles - Woven fabrics - Construction. Methods of analysis, Part 3: Determination of crimp of yarn in fabric
9. ASTM D 3883 - 99 Standard Test Methods for Yarn Crimp and Yarn Take-up in Woven Fabrics
10. Kovar R.: Crimp of woven fabric measuring, 15th International Conference Strutex, Liberec, Czech Republic, 1-3 December 2008, pp. 117-123
11. IS 46-108-01/01 Recommended procedure for preparation of samples. Soft and hard sections (slices)
12. IS 23-108-01/01 Definition of the geometry of thread interlacing in a woven fabric from cross-sections
13. Kolčavová Sirková B., Vyšanská M.: Methodology of Evaluation of Fabric Geometry on the Basis of Fabric Cross-section, Fibers&Textiles in Eastern Europe 20, pp. 41-47, 2012
14. Neckar B.: Morphology and structural mechanics of fibrous assemblies (in Czech), Technical University of Liberec, Liberec, pp. 16, 1998
15. Peirce F.T.: The Geometry of Cloth Structure, Journal of Textile Institute 28, 1937
16. Oloffson B.: A general model of a fabric as a geometric mechanical structure; J. Textiles Inst. Transactions 55(11), pp. 541-557; 1964
17. Mertová I., Neckář B., Ishtiaque S.M.: New method to measure yarn crimp in woven fabric, Textile Research Journal, submitted for publication, 2015
18. Kolcavova Sirkova B., Mertová I.: Modeling of Warp and Weft Crimp in Jacquard Woven Fabric Structure, The Fiber Society Technical Conference, Liberec, 2014

CHARACTERIZATION OF FIBROUS STRUCTURES THERMAL INSULATION

Jiří Militký, Dana Křemenáková and Guocheng Zhu

Department of Material Engineering, Textile Faculty, Technical University of Liberec
46117 Liberec, Czech Republic
jiri.militky@tul.cz, tel.00420 48 5353228

Abstract: *To keep the human bodies warm in very cold conditions, the clothing must have good thermal insulating properties. Textiles thermal insulation is closely related to a material's thermal insulating properties, the structure of fibers and porosity of textiles. The thermal resistivity characterizing of thermal insulation can be simply predicted from thermal conductivity as intensive characteristics. For textile structures is overall porosity relatively high and this factor is playing major role in their insulation. Second important factor is thickness of textile layer. The type of fiber is usually not so very important. Nowadays, a lot of synthetic fibers with different shape and hollow are produced. Shape is in fact influencing of porosity. The heat insulation of hollow fiber alone is better in comparison with conventional fibers.*
Main aim of this contribution is to investigate simple two phase model for prediction of thermal conductivity of textile structures with various porosity composed from regular and hollow fibers. The influences of porosity and fiber thermal conductivity on thermal conductivity of textile structures are quantified. The influence of hole portion of hollow fibers on the textile structures thermal conductivity are predicted as well.
Key words: *Prediction of thermal conductivity, hollow fibers, noncircular shape fibers, overall porosity, textile structures.*

1 INTRODUCTION

Comfort occurs when body temperatures are held within narrow ranges, skin moisture is low, and the physiological effort of regulation is minimized [1].The relevant clothing material characteristics are thermal insulation, water vapor resistance and moisture absorption. The major insulating effect of clothing is based on the still air layers between the skin and the different clothing layers, which reduce conduction losses to the environment. Clothing resists convective losses by preventing convection currents from forming next to the body and by providing a barrier against air currents in the environment. Clothing also reduces radiant heat loss by serving as a thermal radiation barrier and evaporative heat loss by restricting the evaporation of sweat produced by the body. The thermal insulation effect of an individual textile layers is dependent on their material properties i.e. usually thermal conductivity and porosity, the looseness or tightness of fit,

the body surface area covered by the clothing and the accessible surface area for heat loss. Nowadays, a lot of synthetic fibers with different shape and hollow can be produced due to the advanced manufacturing technologies. Hollow fibers have many unique properties and have found numerous applications as well. For example, hollow fibers can provide great bulkiness with less weight and are often used to make insulated clothing materials. The heat insulation properties of hollow fiber are better than those of conventional fibers [2, 5]. Therefore, it is very important to know the thermal property of fibers, to design and optimize the structure of fibers for various applications. By the detailed inspection of thermal conductivities of textile structures containing special cross sections and hollows it can be found that the main role are playing the planar mass and fabrics thickness which are responsible for fabric total porosity. [3]. Due to limitation of measuring for fiber's thermal conductivity, the numerical simulation method

becomes a very useful and effective way to evaluate the fiber's thermal conductivity. In this work, some kinds of fibers with different circular hollow size are studied. The influence of planar mass and fabric thickness on the fabric thermal conductivity is quantified.

2   EXPERIMENTAL

2.1   Materials

The typical fibers with holes or special cross section (Coolmax, Coolplus, Thermocool, Thermolite) and round polyester fibers were used (see Figure 1). Air volume portion P [%] of hollow fibers was evaluated from microscopic images. The fiber fineness are given in the Table 1. From these fibers the ring spun yarns were prepared.

Basic characteristic of fibers and yarns are given in the Table 1.

Samples of gray plain knitted fabric with using of staple yarns mention above on the Tricolab device were produced. Parameters of knitting fabrics were: row density 13 rows per cm, column density from 8.5 to 9 column per cm according yarn fineness, tension force cca 50-60 mN and speed cca 200-250 m/min [4].
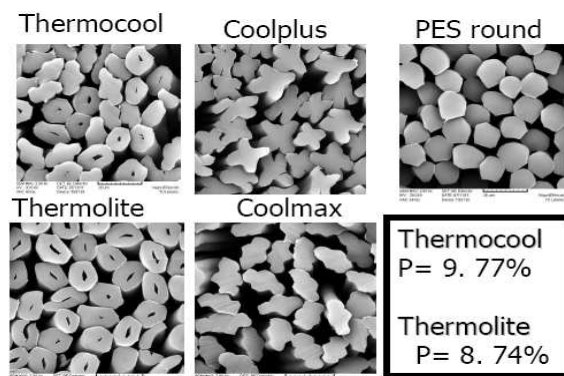
Figure 1 Cross section of selected fibers

Table 1 Basic parameters of fibers and yarns

Fiber type	Yarn fineness (tex)			Yarn twist (m⁻¹)			Fibers number	Fiber fineness (tex)
	Mean value	Limits of 95% confidence interval		Mean value	Limits of 95% confidence interval			
Coolmax	16.4	16.2	16.5	706	686	727	85	0.192
Coolplus	16.3	15.8	16.7	619	606	632	92	0.177
Thermocool	17.1	16.8	17.4	738	724	753	92	0.186
Thermolite	16.7	16.4	17.0	776	749	803	90	0.186
PES round	16.4	16.1	16.7	546	530	562	104	0.158

Table 2 Basic characteristics of knitted fabrics

Sample type	Thermal conductivity (Wm⁻¹K⁻¹)			Thickness (mm)			Thermal resistance (Km²W⁻¹)		
	Mean value	Limits of 95% confidence interval		Mean value	Limits of 95% confidence interval		Mean value	Limits of 95% confidence interval	
Coolmax	0.0390	0.0387	0.0394	0.750	0.734	0.766	0.0192	0.0195	0.0188
Coolplus	0.0400	0.0397	0.0402	0.909	0.899	0.919	0.0227	0.0229	0.0226
Thermocool	0.0384	0.0382	0.0386	0.763	0.756	0.771	0.0199	0.0201	0.0197
Thermolite	0.0393	0.0391	0.0396	0.879	0.860	0.899	0.0223	0.0228	0.0219
PET round	0.0402	0.0398	0.0406	0.890	0.873	0.907	0.0222	0.0225	0.0218

Table 3 Air permeability and Gsm of knitted fabrics

Sample type	Air permeability (l.m⁻².s⁻¹)			Gsm (g.m⁻²) grey fabric
	Mean value	Limits of 95% confidence interval		
Coolmax	9572	9587	9557	104
Coolplus	9624	9652	9596	101
Thermocool	9624	9643	9605	106
Thermolite	9626	9643	9609	110
PET round	9811	9841	9781	107
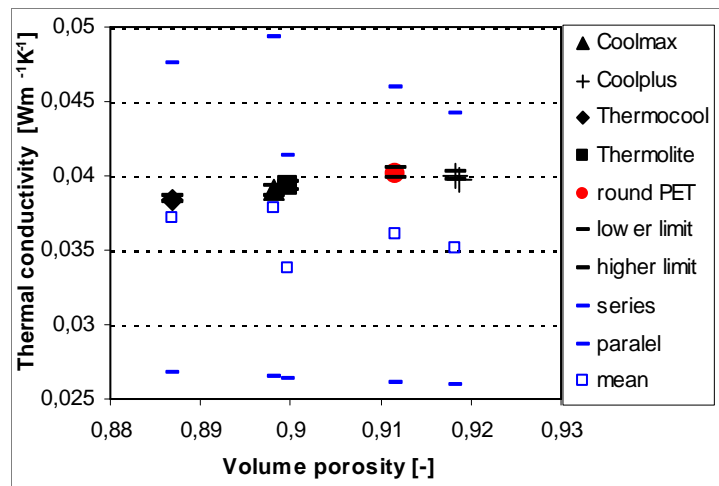
Figure 2 Dependence of knitted fabrics measured thermal conductivity on their porosities

2.2 Methods

Thermal conductivity, thickness and thermal resistance with using device Alambeta (pressure 200 Pa) were measured and they are given in Table 2. Air permeability with using device FX3300 (pretension 1000 Pa) and areal density (Gsm) were measured and they are given in Table 3.

The fabrics volume porosity was calculated from relation

$$P_F = \frac{W}{\rho_F \, H} \qquad (1)$$

where ρ_F is polyester fibers density (1360 kg/m^3), W is planar mass (usually [g m^{-2}]) and H is thickness (usually [cm]).

Dependence of knitted fabrics thermal conductivity on their porosities P_F is shown in the Figure 2. Bars are here indicating 95%-th confidence intervals and empty squares are predictions calculated from model (2).

3 RESULTS AND DISCUSSION

For expression of thermal conductivity of hollow fibers it is simple to replace cylindrical geometry (for round fiber) by two phase model consist from fibrous (polymeric) phase having thermal conductivity λ_f and air phase with thermal conductivity λ_a in serial) or parallel arrangements. Relative portion of air phase is equal to air volume portion P and

relative portion of fibrous phase is $1 - P$. The thermal conductivity of hollow fiber is then

$$\lambda_h = 0.5 \left(P \, \lambda_a + (1-P) \, \lambda_f + \frac{\lambda_a \, \lambda_f}{P \, \lambda_f + (1-P) \, \lambda_a} \right) \qquad (2)$$

The thermal conductivity of knitted fabrics are computed form similar equation where porosity P_F is used instead of hole portion in fibers P.

Because the real fabric porosities are much over 70% the influence of hole portion is not very important (Figure 3) and better thermal insulation can be obtained by combination of planar mass a thickness.
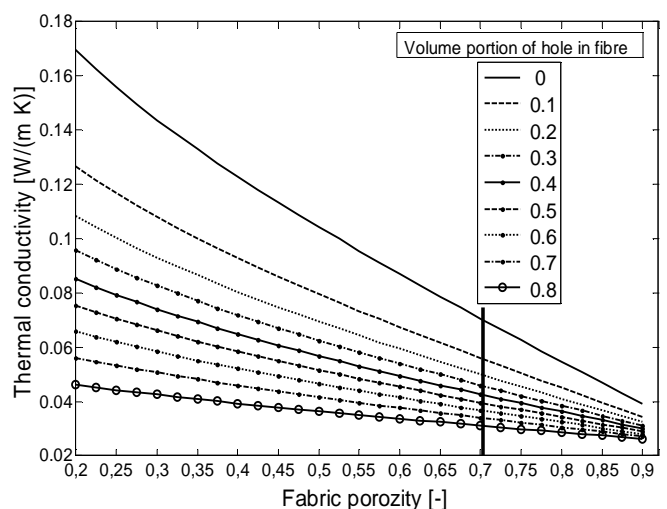
Figure 3 Dependence of fabric thermal conductivity on their porosity for hollow fibers with various relative volumes of holes

In study [5] the knitted structures created from above mentioned special fibers are described and their thermal properties are discussed in details. Here it can be only mentioned that the differences between thermal conductivities for similar structures are very small. Much higher is influence of fabric construction (Figure 3).

4 CONCLUSIONS

The simple prediction is useful for rough calculation of hollow fiber thermal conductivity as well. In fabrics the influence of holes in fibers are not so important as influence of planar mass and fabric thickness (porosity). The changes in these construction parameters are simple in the case of nonwovens but limited in the case of woven or knitted fabrics

5 REFERENCES

1. Anonym: 2009 ASHRAE Handbook Fundamentals SI Edition, chap. 9, American Society of Heating, Refrigerating and Air-conditioning Engineers, Inc., Atlanta 2009
2. Karaca E., Kahraman N., Omeroglu S., Becerir B.: Effects of Fiber Cross Sectional Shape and Weave Pattern on Thermal Comfort Properties of Polyester Woven Fabrics, Fibers&Text in EE 20(3), pp. 67-72, 2012
3. Lizák P., Murárová A., Majundar S.C.: Heat transfer through a textile layer composed of hollow fibers, J. Therm. Anal. Calorim. 108, pp. 851-857, 2012
4. Militký J., Křemenáková D.: Current state in the field of thermal barrier properties of textiles, Res. Rept. for project ADAPTEP, March 2013
5. Petrulis D.: Fundamental study of the effect of the fiber wall thickness and inner diameter on the structure of polyamide and polypropylene hollow fibers, J. Appl. Polym. Sci 92(3), pp. 2017-2022, 2004

INFLUENCE OF DRAFTING ON MASS IRREGULARITY OF COTTON RING YARNS

Eva Moučková, Petr Ursíny, Petra Jirásková and Yuliya Kim

Technical University of Liberec, Faculty of Textile Engineering, Department of Textile Technologies, Studentská 2, 461 17 Liberec 1, Czech Republic
eva.mouckova@tul.cz; tel. +420 48 535 3274; fax +420 48 535 3542

Abstract: *In the present paper the issue of transformation of mass irregularity of fibers product by drafting arrangement of the ring spinning machine is analyzed. The experimental procedure for samples collection of carded as well as combed cotton rovings and ring yarns are used. Theoretical model of transformation of mass irregularity is presented. Tendency of behavior of experimentally determined modulus and theoretical modulus of relative transfer function of drafting system are compared.*
Key words: *Mass irregularity, ring yarn, roving, modulus of relative transfer function, draft.*

1 INTRODUCTION

Drafting processes in the spinning technology significantly affect (deepen) level of mass irregularity of fibrous product. Causes of negative impact of draft on the yarn irregularity and generally, analysis of whole drafting process are described in a large number of research papers, for example [1-5]. The irregularities added to yarn by the apron drafting arrangement of the ring spinning machine were studied in the work [6]. The variance-length curve of mass irregularity of worsted rovings and yarns were analyzed also in the work [7]. To determine conditions that ensure optimal course of drafting process it is important to know the influence of draft on the structure of mass irregularity. From that, among others, requirements on a supply product in the corresponding technological stage in the spinning technology result together with the possibility of eventual shortening of given spinning technology.

In this work, the influence of draft on mass irregularity in the drafting mechanism of ring spinning machine is analyzed. The impact of draft on the extent of change of corresponding harmonic components of mass irregularity is studied using the experimentally determined modulus of relative transfer function. The results are compared with a theoretical modulus of relative transfer function of defined ideal drafting process.

2 METHODS AND MATERIALS

Generally, the modulus of relative transfer function is a ratio of amplitudes of corresponding harmonic components of output and input signal related to the respective mean value of fineness of output and input fibrous product [8]. In this work we analyze the experimentally determined modulus of relative transfer function of drafting system of ring spinning machine, which we define by formula (1):

$$\left| F_{\exp}^{*}(\lambda) \right| = \frac{CV_1(\lambda)}{CV_0\left(\dfrac{\lambda}{P}\right)} \tag{1}$$

where: $\left| F_{\exp}^{*}(\lambda) \right|$ is the experimentally determined modulus of relative transfer function of drafting mechanism, $CV_1(\lambda)$ is the variation coefficient of harmonic component with wavelength λ [m] of yarn mass irregularity [%], $CV_0(\lambda/P)$ is the variation coefficient of harmonic component with wavelength λ/P [m] of roving mass irregularity [%], P is the total draft of drafting mechanism of ring spinning frame.

The variation coefficients of harmonic components at wavelength λ, respectively λ/P we read from the spectrogram of yarns, respectively rovings, which were obtained from the measurement of mass irregularity using the device Uster Tester IV-SX. We compared the modules with each other. Tendencies of behavior of these experimentally modules of relative transfer function we also compared with behavior of theoretical modulus of relative transfer function of drafting mechanism calculated according to formula (2).

$$\left| F_p^*(\lambda) \right| = \left| P \frac{\sin \dfrac{\pi\, l}{\lambda}}{\sin \dfrac{\pi\, l\, P}{\lambda}} \right| \qquad (2)$$

where: $\left| F_p^*(\lambda) \right|$ is theoretical modulus of relative transfer function of drafting mechanisms as a function of wavelength λ; λ is the wavelength of harmonic component of mass irregularity of result fibrous product [m], l is the uniform fiber length [m]; P is the draft. The theoretical modulus of relative transfer function of drafting mechanism was derived in the work [9] from the transfer function of drafting system with a general speed field [10] assuming the ideal draft, which is defined in [1]. The concept of three-roller double-apron drafting mechanism tries to approach to these conditions [9].

For the experiment we used: 100% CO combed and carded rovings and yarns. Their specification is mentioned in Table 1. Carded rovings and yarns were produced from medium-stapled cotton A1, combed rovings and yarns were manufactured from medium-stapled cotton A1 as well as from long-stapled cotton MII. The rovings used for experiment were produced from the same spinning lot as yarns.

Yarns and roving were subjected to the measurement of mass irregularity on the instrument Uster Tester IV-SX, measuring conditions will be mentioned in the full-text.

3   RESULTS AND DISCUSSION

The results of measurement of rovings and yarns mass irregularity will be mentioned and discussed in the full-text. The demonstration of experimentally determined average modules of relative transfer functions $\left| F_{\exp}^*(\lambda) \right|$ is shown in Figure 1. The black line indicates the value of the modulus $\left| F_{\exp}^*(\lambda) \right| = 1$. From the results it is evident that experimentally determined average modules of relative transfer functions increase sharply from wavelength $\lambda \cong 1$ m towards shorter wavelengths. Since the values of modulus greater than 1 indicate deepening mass irregularity [9], it can be stated that the experimentally determined modulus of relative transfer function confirmed that the draft gets worse irregularity at short wavelengths.

Table 1 Yarns and rovings used for experiment

Cotton	Technology	Nominal roving fineness [tex]	Nominal roving twist [m⁻¹]	Nominal yarn count [tex]	Nominal yarn twist [m⁻¹]	Total draft on ring sp. machine
MII	Combed	460	52	11.5	950	40
				20	680	23
A1	Combed	670	52	15.6	1000	43
				20	780	33.5
				25	650	27
				35.5	600	19
A1	Carded	840	46	25	800	33.5
				29.5	730	28.5
				42	650	20
				60	520	14

With increasing values of the draft, the rise in values of modulus is steeper and, at the same time, the wavelength, from which values of modules rise, extents.
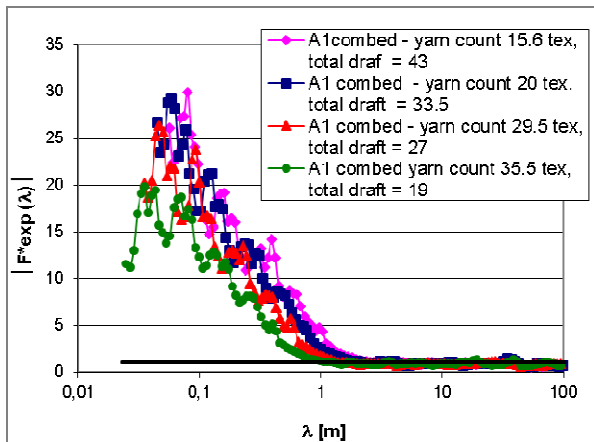
Figure 1 Experimental modulus of relative transfer function of drafting mechanism - machine G30, cotton A1, combed technology

It is the most evident in the case of carded yarns. In the range of wavelengths $\lambda \rangle 1$ m, the values of modules fluctuate around a value equal to 1 (for the detailed example see Figure 2). The fluctuation is probably given by higher irregularity of rovings at longer wavelengths and also by the fact that those length sections of roving, from which the yarns were spun, were not tested in this experiment.
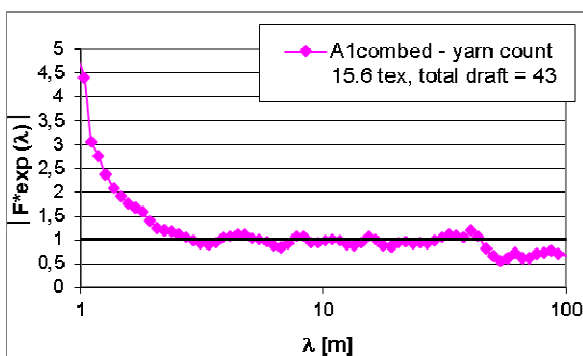
Figure 2 Detail of experimental modulus of relative transfer function

At present, in the case of yarn produced in the spinning mill (as is the case here) it is impossible. However, in the term of statistic, any significant differences were not recorded

between average values of variation coefficient of harmonic component of roving and yarn mass irregularity on corresponding wavelengths.

Behavior of envelope curves of theoretical modulus in comparison with experimentally determined modulus of relative transfer function of drafting mechanism is, for illustration, mentioned in Figures 3. For the calculation of theoretical modulus we applied mean cotton fiber lengths of used rovings and the magnitude of total draft set on the ring spinning machine.
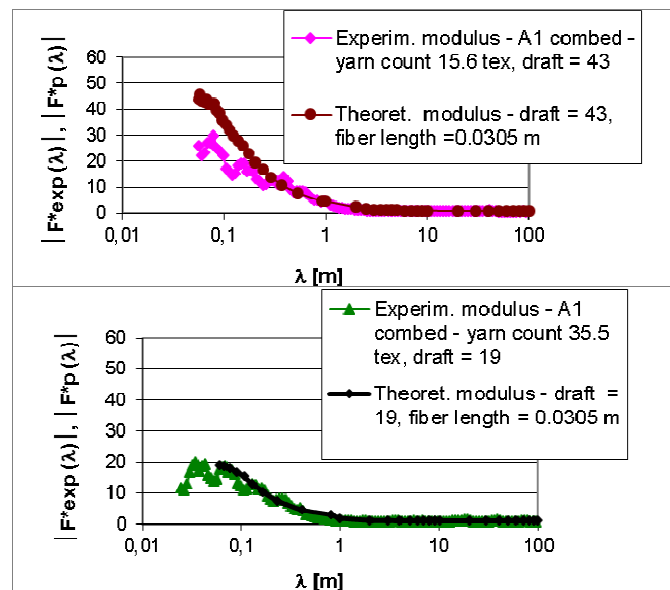
Figure 3 Comparison of experimentally determined modulus with envelope curve of theoretical modulus of relative transfer function of drafting mechanism - cotton A1, combed technology

The graphs of theoretical modulus are displayed in the real range of wavelengths of the envelope curve. From the results it is seen that tendency of behavior of dependence of experimentally determined modules on the wavelength practically coincides with the course of the envelope curve of theoretical modules. The theoretical modules reach higher values at very short wavelengths compared to the experimentally determined modules. This increase is given by defined conditions of ideal draft, especially conditions of immediate acceleration of fibers at the given point of drafting zone. In reality,

this process runs as, to a certain extent, a gradual process, which seems to be actually more favorable for harmonic components with very short wavelengths. The break-draft in the real drafting mechanism also plays a favorable role. For these reasons, the course of theoretical modulus is used for referred range of wavelengths, where congruence of tendency of course of theoretical and experimental modulus basically was confirmed.

Theoretical modulus shows steeper increase with growing draft (lower linear density of yarn [tex]), which confirms more marked deepening of mass irregularity. It is a process with immediate acceleration of fibers in given point of drafting zone and a process without any positive effect of break-draft. Influence of the break-draft asserts itself positively in the case of real drafting mechanism.

4 CONCLUSIONS

This theoretical-experimental study showed a tendency of influence of drafting mechanism of ring spinning machine on the transformation of mass irregularity. Tendencies of behavior of theoretical and experimentally determined modules of relative transfer function confirm deepening of amplitudes of the harmonic components of mass irregularity with shorter wavelengths and, on the contrary, practically negligible effect on components with longer wavelength. Influence of magnitude of draft and the fiber length was mutually confirmed as well. The reason of deepening of mass irregularity at short wavelength can be attributed to a dispersion of the accelerated points of floating fibers. Ascertained differences between courses of theoretical and experimental modules correspond to the fact,

that the process of refinement of fibrous product by the draft is very complicated from the point of view of transformation of mass irregularity. But, simultaneously, main tendencies of observed functions as well as influence of important material and technological parameters are confirmed. It creates conditions for further analyses of optimization of drafting processes.

5 REFERENCES

1. Foster G.A.R.: Fiber motion in roller drafting, Journal of the Textile Institute Transaction 42(9), T335-T374, 1951
2. Grishin P.A.: Theory of drafting and its practical applications, Journal of the Textile Institute Transaction 45(3), T167-T266, 1954
3. Lin Q., Oxenham W., Yu C.: Effect of accelerated point distribution on sliver irregularity. Part I: Characterization of accelerated point distribution, Journal of the Textile Institute 103(5). pp. 549-557, 2012
4. Lin Q., Oxenham W., Yu C.: A study of the drafting force in roller drafting and its influence on sliver irregularity, Journal of the Textile Institute 102(11), pp. 994-1001, 2011
5. Graham J.S., Bragg C.K.: Drafting force measurement as an aid to cotton spinning, Textile research Journal 42(3), pp. 175-181, 1972
6. Balasubramanian N.: A study of the irregularities added in apron drafting, The Textile Research Journal 39(2), pp. 155-165, 1969
7. Cihlářová E.: Transformation of roving mass irregularity into yarn mass irregularity, Proceedings of 5th World Textile Conference Autex, University of Maribor, Department of Textile (Maribor), pp. 494-499, 2005
8. Balda M., Bošek M., Dráp Z.: Základy automatizace, SNTL Praha (Prague), 1968
9. Ursíny P.: Předení II, Technická univerzita v Liberci (Liberec), 2009
10. Sevosťanov A.G., Chavkin V.P., Divinskij L.A.: Kinematičeskaja teorija vytjagivanija voloknistogo produkta, Izvestija vyšších učebnych zavedenij, Technologia Textilnoj promyšlennosti (5), pp. 68-75, 1967

MOISTURE MANAGEMENT OF THE FIRST LAYER SPORTS MATERIAL KNITTED STRUCTURES

Pavla Těšinová[1], Svetoslava Mladenova Doncheva[2], Denitsa Pavlinova Petrova[2], Yordanka Angelova[2] and Pavla Ryplová[3]

[1]*TU Liberec, Faculty of Textile Eng., Studentska 2, Liberec, Czech Republic*
[2]*TU Gabrovo, Department of Textiles, 4 Hadji Dimiter Str., 5300 Gabrovo, Bulgaria*
[3]*Interimex CZ a.s., Smetanova 858/19, Jablonec nad Nisou, Czech Republic*
pavla.tesinova@tul.cz; *tel. +420 48 535 3734, fax +420 48 535 3472*

Abstract: *Moisture management is a very important parameter for classification of sports materials for the first layer covered skin during sport practicing. Those materials are made from knitted structures preferably to provide the best recovery properties, tight and moving comfort. Knitted materials need to provide transport properties of humidity from the body to evaporative surface. In this paper is presented results from measurement on Moisture Management Tester, SDL Atlas, which was constructed as a simulation of sweat wettability in the fabric structure not only from one fabric surface to the other but also detect management of moisture in the direction of fabric structure along on both sides. We tested different structures of knitted material used for construction of commercial clothes in nowadays very good quality.*
Key words: *Moisture management, knitted fabrics, the first layer, sport goods.*

1 INTRODUCTION

Moisture management is a key property for the first layer of sports clothes for all outdoor and indoor activities. We focus for comfort properties for outdoor activities since good comfort affects also protection for our health. Transport of the humidity (sweat) from the body to the surface where sweat is evaporated to the air is important for cold/warm feeling.

Article [1] describes closely diffusion, sorption-desorption, convection and process, liquid water transmission, combined vapour and liquid transmission. Moisture transmission through a textile material is not only associated with the mass transfer processes, but also heat transfer is presence. Diffusion is the main mechanism for transferring moisture in low moisture content conditions. Water vapour diffusion is mainly dependent on the porosity of the fabrics which knitted materials show in the loop structure. Wicking plays an important role in moisture transmission, when the moisture content of clothing is very high, and the body is producing large quantities of liquid perspiration. Sportswear should possess very high wicking properties [1]. Consequential article summaries testing and modelling used for moisture transport through fabrics [2].

Liquid used for measurement was pre-defined as exact amount of test solution (synthetic sweat). Synthetic sweat should be defined according to the real humidity produced by men or idealised for the main ingredients only. For our purposes was used simple recipe of 9 grams of sodium chloride in 1 litre of distilled water. Anyway precise recipe for various kinds of sweat is defined in [5].

2 EXPERIMENTAL PART

It was measured 6 types of knitted structures from PES, PAD and elastane in various blending ratios. Some of materials were produced with brushed back surface for good handle and some of them were knitted with design loops from the front side for better thermal properties. It was measured at least three samples from each and statistically processed.

The following subchapters describe material identifications and testing equipment definition.

2.1 Materials

Experimental material was chosen as a set of different structures of knitted fabrics which is used nowadays for construction of sportswear for the first layer in various activities level from recreation activities, hiking etc. to exercising oh high level, climbing, long-distance skiing in quality for everyday use with easy maintenance. Samples named *basic A-F, multifil A-B, PAD basic A-B* are weft knitted with double-face rows and transferred stitches. This structure offers lighten the materials with keeping of moisture transfer properties and is widely used nowadays. Samples named *plain A-B, brushed back A-B, loops front A-C* are with classical double-face rows and affording to the name with additional loops from front side or brushed from the back side. Comparison mainly according to the structure is observed.
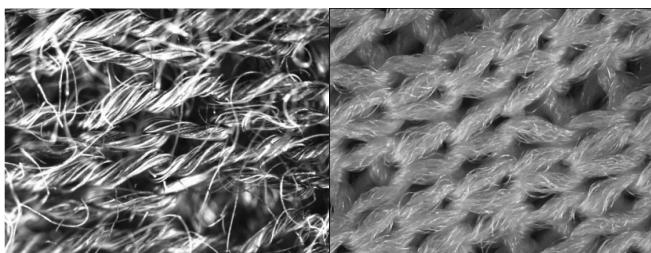
Figure 1 Structure of materials: basic, multifil, PAD basic
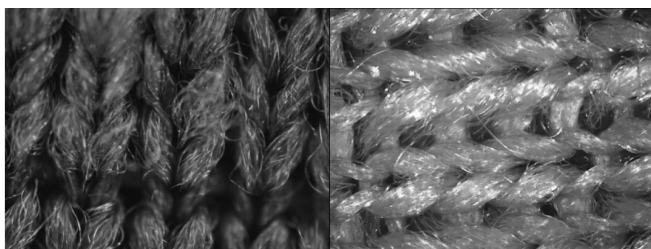
Figure 2 Structure of materials: plain, back side of loops front

2.2 Method

Moisture management Tester M290 (MMT), SDL Atlas, was chosen as testing equipment for its dynamic wicking process visualisation. According to the Instruction manual MMT is an instrument to measure the dynamic liquid transport properties of textiles such as knitted and woven fabrics in three dimensions: Absorption Rate - Moisture absorbing time of the fabric's inner and outer surfaces, One-way Transport Capability – Liquid moisture one-way transfer from the fabric's inner surface to outer surface, Spreading/Drying Rate – Speed of liquid moisture spreading on the fabric's inner and outer surfaces. This instrument consists of upper and lowers concentric moisture sensors, where the fabric being tested is placed in between the two sensors. Solution is inserted for 20 seconds after the start of the test and next 100 seconds is detected its spreading by the sensors [3]. Method is closely described by authors of the instrument [3, 4].
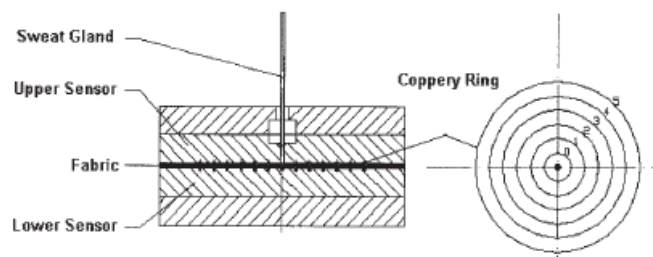
Figure 3 Visualisation of tester sensors [4]

3   RESULTS AND DISCUSSION

MMT Manual helps us with interpretation of results with definitions. Our materials visualised on Figure 4 should be defined as moisture management fabrics where medium wetting and absorption is in presence. Spreading between surfaces is just faster than expected. Materials in this kind are sufficiently effective in one way transport of humidity from the skin. Staple fibres in the yarn caused natural hair anyway so it can be effect of some spreading on the back side.

Water penetration fabric is shown on Figure 5 with small spreading area and excellent one-

way transport in exemplary state. Basic structure provides optimal transport of humidity and very good comfort. Optimal in winter weather is than to wear right up the first layer absorbing layer to remove moisture more quickly and prevent cold feeling.

On the other type on structure we can observe on Figure 6 typical example when standard weft knitted structure has got loops on the front side so spreading of moisture was found as expected but material is also good in transport to the front side (green line high slope from the very beginning of the test and feeding of the solution). Evaporation can start right after moisture in the front of material. Residual moisture in the loops can still affect some decrease of temperature but not right on the skin.
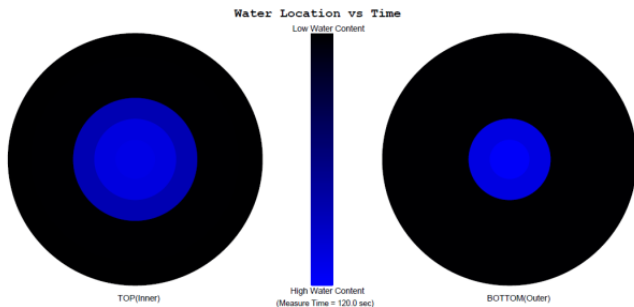
Figure 4 Typical results of material with quick transport from back side for material with basic weft knitted structure from PAD (PAD basic A)
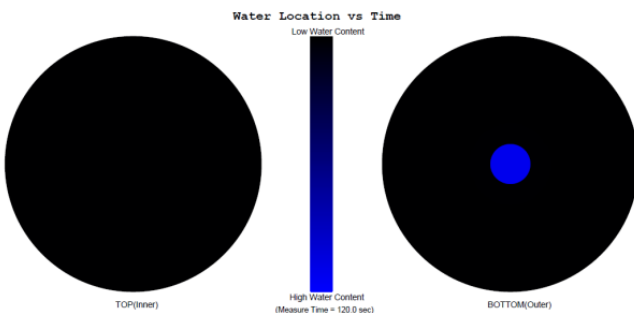
Figure 5 Typical results of material with excellent transport in spreading from back side with basic weft knitted structure with transferred stitches (basic F)
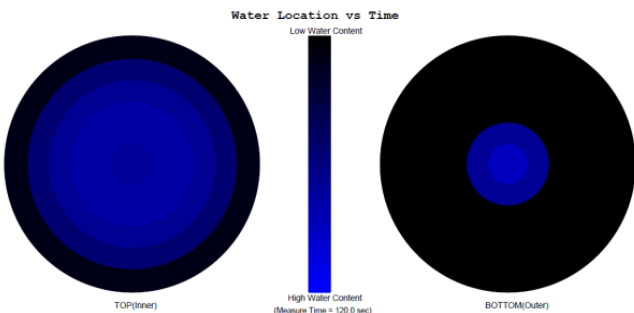
Figure 6 Typical results of material with moisture transport and spreading in back side in brushed hair weft knitted structure (loops front B)

4   CONCLUSIONS

Structure of knitted fabrics affects comfort properties including moisture transport of the material of the first layer of sport clothing. Results obtained from the measurement follow presumption of good comfort properties in the standard limits. All used structures provide satisfactory moisture transport to the front side where humidity will evaporate.

Hairy materials have also significant spreading area on the back side same as materials with loops in our case. Transportation of the moisture to the front is than slower but on the other hand it enables evaporation from the bigger area which important for complete drying.

MMT testing instrument offers response in the time of 2 minutes thus testing of the material is studied in the time when man starts perspiration. We can predict from the behaviour that spreading on the back side will start transporting in the water vapour state directly. Humidity decrease of amount or weight shall be studied also in the next projects.

5   REFERENCES

1. Das B., Das A., Kothari V.K., Fanguiero R., Araújo M.: Moisture Transmission Through Textiles-Part I: Processes involved in moisture transmission and the factors at play, AUTEX Research Journal 7(2), pp. 100-110, 2007
2. Das B., Das A., Kothari, V.K., Fanguiero, R., Araújo, M.: Moisture Transmission Through Textiles Part II: Evaluation Methods and Mathematical Modelling, AUTEX Research Journal.7(3), pp. 194-216, 2007
3. Instruction manual M290 MMT Moisture Management Tester. Rev. 4.2 (10/11), SN: 808G0007. SDL Atlas Ltd, p.62
4. Junyan Hu, Yi Li, Kwok-Wing Yeung, Anthony S.W. Wong and Weilin Xu.: Moisture Management Tester: A Method to Characterize Fabric Liquid Moisture Management Properties, Textile Res. J. 75(1), pp. 57-62, 2005
5. Marques M.R.C., Loebenberg R., Almikainzi M.: Simulated Biological Fluids with Possible Application in Dissolution Testing, Dissolution Technologies 18(3), pp. 15-28, 2011

MECHANICAL CHARACTERISTICS OF POLYESTER YARN

Petr Tumajer[1] and Martin Bílek[2]

[1] *Faculty of Textile Engineering, TU Liberec, Studentska 2, Liberec, Czech Republic*
[2] *Faculty of Mechanical Engineering, TU Liberec, Studentska 2, Liberec, Czech Republic*
petr.tumajer@tul.cz; tel.:+420 48 5353120; martin.bilek@tul.cz; tel.:+420 48 5353174

Abstract: *The paper looks at the ways of determining the modules of rigidity of warp threads from the point of view of the weaving process. Various methods are discussed here, and their shortcomings are analysed in an experimental way (on a definite textile material). The theoretical section of the paper describes a three-member rheological model, and in its final part, this model is confronted with the results of the experimental measurements. The concerned issues have been solved in connection with the determination of input parameters for modelling of the weaving process.*
Key words: *Warp, mechanical properties, rheological model, dynamic module, static module.*

1   INTRODUCTION

The mechanical properties of linear textiles exert considerable influence on their processing in the course of the weaving process [1]. During weaving, the warp threads are extended periodically at a frequency given by the r. p.m. of the weaving loom. Because of the visco-elastic properties [2] of threads, it is necessary to assume that a change in the weaving frequency brings about a change in the mechanical characteristics (of the dynamic module) of the warp. Theoretically, this phenomenon can be described by means of so-called rheological models. However, is a change in the weaving frequency the only reason for the changes in the mechanical characteristics of warp threads? Furthermore, the paper looks at the effect of the number of cycles on the change in mechanical characteristics of the threads. These issues are solved primarily in experimental form, on a definite type of linear textile. For this material there have been established values of the dynamic modules of rigidity at varied frequencies of extension by means of a special device, VibTex. [3, 4]. Furthermore, there have been established so-called static modules of rigidity by a standard test of the strength using the Instron 4411 device. The same device is employed afterwards for

analysis of the effect of the number of cycles on the change in static modules of rigidity, too.

2   THEORETICAL SECTION

Textiles are visco-elastic materials. Consequently, a mutual combination of elastic and viscous elements can be employed for their description. Then it is possible to describe these models generally by a set of linear differential equations with constant coefficients, and to employ the properties of the Laplace and Fourier transformations for the solution [2]. The manner of characterisation of dynamic modules of rigidity and of their dependencies on frequency, employing the Laplace and Fourier transformations, is described in detail in [3], and we will indicate the resulting relations for the so-called three-member model here (Figure 1).
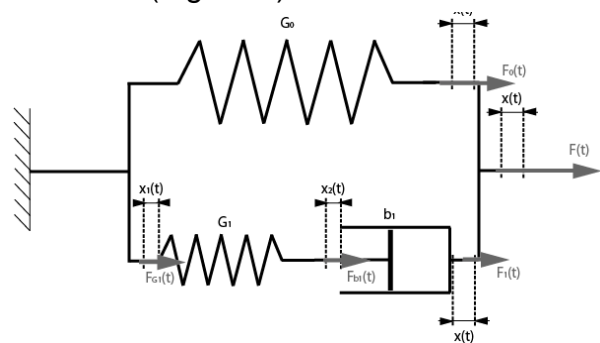
Figure 1 Three-member model

The equations in the time	The equations in operator form	
$F_0(t) = G_0.x(t)$	$F_0(p) = G_0.x(p)$	(1)
$F_{G1}(t) = G_1.x_1(t)$	$F_{G1}(p) = G_1.x_1(p)$	(2)
$F_{b1}(t) = b_1.\dfrac{dx_2(t)}{dt}$	$F_{b1}(p) = b_1.p.x_2(p)$	(3)
$x(t) = x_1(t) + x_2(t)$	$x(p) = x_1(p) + x_2(p)$	(4)
$F_1(t) = F_{b1}(t) = F_{G1}(t)$	$F_1(p) = F_{b1}(p) = F_{G1}(p)$	(5)
$F(t) = F_1(t) + F_2(t)$	$F(p) = F_1(p) + F_2(p)$	(6)

Response equation obtained by eliminating $x_1(p)$, $x_2(p)$, $F_{G1}(p)$, $F_{b1}(p)$, $F_1(p)$ and $F_0(p)$ from the system of equations (1) to (6):

$$F(p) = \left[G_0 + \frac{b_1.p}{1 + \frac{b_1}{G_1}.p} \right].x(p) =$$

$$= \left[\frac{G_0.\left(1 + \frac{b_1}{G_1}.p\right) + b_1.p}{1 + \frac{b_1}{G_{.1}}.p} \right].x(p) = T(p).x(p)$$

(7)

Frequency response, which are set-up by the substitution $p \to i.\omega$ in the transfer $T(p)$:
Dynamic module:

$$C(\omega) = \sqrt{\left[G_0 + \frac{\frac{b_1^2}{G_1}.\omega^2}{1 + \left(\frac{b_1}{G_1}\right)^2.\omega^2} \right]^2 + \left[\frac{b_1.\omega}{1 + \left(\frac{b_1}{G_1}\right)^2.\omega^2} \right]^2} =$$

$$= \sqrt{G_0^2 + \frac{2.G_0.\frac{b_1^2}{G_1}.\omega^2\left[1 + \left(\frac{b_1}{G_1}\right)^2.\omega^2\right] + \frac{b_1^4}{G_1^2}.\omega^4 + b_1^2.\omega^2}{\left[1 + \left(\frac{b_1}{G_1}\right)^2.\omega^2\right]^2}}$$

(8)

Module for low frequencies, i.e. $\omega \to 0$ (static module of rigidity):

$$\lim_{\omega \to 0}[C(\omega)] = G_0$$

(9)

Module for high frequencies, i.e. $\omega \to \infty$ (dynamic module of rigidity):

$$\lim_{\omega \to \infty}[C(\omega)] = G_0 + G_1$$

(10)

3 EXPERIMENTAL SECTION

3.1 Characteristics of the tested material and the conditions of measuring

For measuring purposes, two-fold twisted polyester yarn with nominal fineness 25x2 tex and parameters according to Table 1 were used. All tests were carried out with clamping length 500 mm and under identical climatic conditions: the temperature 20°C, the humidity 65%.

Table 1 Parameters of employed material

	Mean	95% confidence interval
Doubling twist Z_D [m^{-1}]	439	(432; 446)
Spinning twist Z_S [m^{-1}]	612	(595; 629)
Linear irregularity U [%]	6.89	(6.79; 6.99)
Quadratic irregularity CV [%]	8.69	(8.57; 8.81)
CV(1 m) [%]	2.91	(2.79; 3.04)
CV(3 m) [%]	2.22	(2.06; 2.38)
CV(10 m) [%]	1.44	(1.2; 1.69)
Num. of thin places -50% [km^{-1}]	0.5	(0.11; 1.6)
Num. of thick places +50% [km^{-1}]	4.5	(3.06; 6.78)
Burls +200% [km^{-1}]	9.5	(7.35; 12.61)
Fuzziness [-]	7.35	(7.09; 7.61)
Yarn diameter 2D [mm]	0.458	(0.452; 0.464)
CV$_{2D}$ 8 mm [%]	6.384	(6.228; 6.54)
CV$_{2D}$ 0.3 mm [%]	7.972	(7.769; 8.175)
CV$_{1D}$ 0.3 mm [%]	12.204	(11.73; 12.677)
Relative strength [cN/tex]	28.32	(27.97; 28.67)
Strength [N]	14.16	(13.98; 14.34)
Elongation at break [%]	28.55	(28.01; 29.08)

3.2 Determination of dynamic modules of rigidity by means of the special VibTex device

The characteristics of the Vibtex device are described in detail in [3] and [4]. In the present case, the device was used for harmonic extension of the thread at frequencies 20, 40, 60, 80 and 100 Hz with maximum elongation 4 mm and pretension 400 mN. A diagrammatic drawing of the Vibtex device including an example of a measured value for the frequency of thread extension 60 Hz is shown in Figure 2.
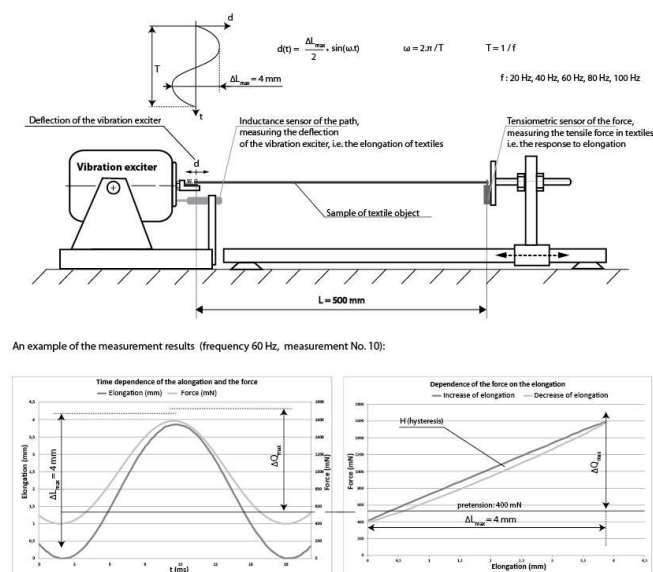
Figure 2 Scheme Vibtex device and an example of the measurement results

The records of tensile force and elongation were realised always after approximately one to two minutes from actuation of the vibration system, i. e. the recorded values correspond to the behaviour of the sample after 1,200-12,000 cycles. The length of the record is one second, and the sampling frequency 19,200 Hz.

The measured values were processed by means of the special VibTexSoft program, which is able to characterise the dynamic (complex) module C as the ratio of the maximum value of tensile force ΔQ_{max} to maximum elongation ΔL_{max} in a randomly chosen cycle of a time interval of one second.

$$C = \frac{\Delta Q_{\max}}{\Delta L_{\max}} \qquad (11)$$

Afterwards, the software in this cycle calculates, using the rectangle method, hysteresis H as the difference between the energy necessary for extension of the sample and the energy released when letting it loose. Next, it will employ this value for calculation of the mutual phase shift (loss angle) between the extension and the force according to the following relation:

$$\delta = \arcsin \frac{4.H}{\pi . \Delta Q_{\max} . \Delta L_{\max}} \qquad (12)$$

Afterwards, it is possible to characterise the real C_{Re} (elastic module) and the imaginary component C_{Im} (loss module) of the dynamic module by means of the following relations:

$$C_{Re} = C.\cos(\delta) \qquad (13)$$
$$C_{Im} = C.\sin(\delta) \qquad (14)$$

Note: The method of deduction of the above-mentioned relations and their implementation in the VibTexSoft program are described in detail in [4].

The results of processing of the measured data are shown in the following table and are presented in the form of a bar chart (see [6]).

Table 2 Mechanical characteristics of polyester yarn established by means of the Vibtex device

f (Hz)	20	40	60	80	100
Number of meas.	10	10	10	10	10
C (N/m)	292	305	303	312	296
Confidence 95%	(287; 297)	(299; 311)	(300; 306)	(305; 319)	(289; 303)
δ (°)	4.6	4.6	5.0	6.1	6.9
Confidence 95%	(4.5; 4.7)	(4.5; 4.7)	(4.9; 5.1)	(5.9; 6.3)	(6.7; 7.1)
C_{Re} (N/m)	291	304	302	310	293
Confidence 95%	(286; 296)	(298; 310)	(299; 305)	(303; 317)	(286; 300)
C_{Im} (N/m)	23.5	24.7	26.3	33.1	35.3
Confidence 95%	(22.9; 24.1)	(24.1; 25.3)	(25.9; 26.7)	(31.9; 34.3)	(34.1; 36.5)

3.3 Determination of the static module of rigidity on the Instron 4411 device

As already indicated above, the value of the so-called static module is determined during the standard strength test, i.e. during very slow extension of the thread at a constant velocity of 2 mm/s till it breaks breaks (Figure 4). The pretension in the thread was adjusted to the value 400 mN (the same as in the VibTex device).
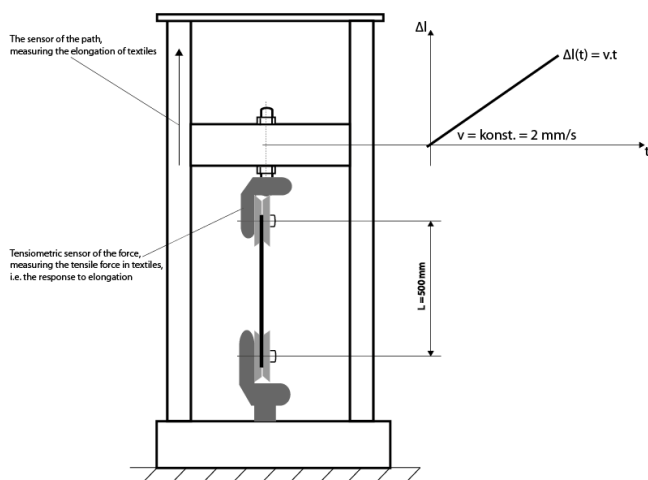
Figure 4 Diagrammatic drawing of the test realised by means of the Instron 4411

From ten strength tests chosen at random tensile curves were generated, i.e. charts of the dependence of the force on elongation, and these were used for determination of the static module of rigidity (Figure 5).
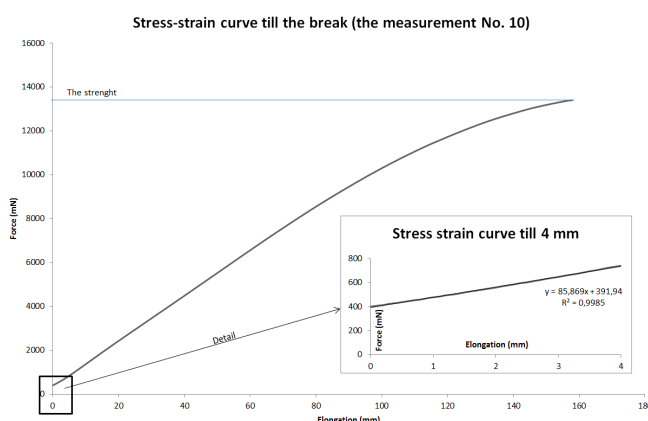
Figure 5 Stress-strain curve till the break

This module was determined so as to characterise the properties of the thread at

deformations up to 4 mm (the same as the dynamic modules established on the VibTex device).

Henceforth, data that characterise the dependence of the tensile force on elongation up to 4 mm were used. By the method of least squares, a straight line was interpolated through these values, and the respective correlation coefficient R^2 was determined. The ascertained values are shown in the following table.

Table 3 Determination of the correlation coefficient

Number of measurements	R^2	Confidence 95%
10	0.9994	(0.9991; 0.9997)

The value of the correlation coefficient R^2 draws near to one. Therefore, in this case it is possible to substitute the tensile curve in the area up to 4 mm by a linear function, and to establish the static module of rigidity as the slope of the regression straight line.

$$F(\Delta l) = K\Delta l + F_0 \qquad (15)$$

where the symbol *Δl* represents the absolute elongation and the symbol *F₀* the pretension. The ascertained value of the static module is shown in the following table.

Table 4 Value of the static module of rigidity of polyester yarn determined by means of the Instron device

Number of measurements	K (N/m)	Confidence 95%
10	108	(106; 110)

3.4 Change in static modules of rigidity during cyclical extension on the Instron device

The Instron 4411 device was also used for experimental analysis of the change in mechanical properties of the thread (static modules of rigidity) during cyclical loading (Figure 6). In this case, the thread was extended periodically in 8 cycles at a constant velocity of 2 mm/s with maximum elongation 4 mm and period 6 s, which

corresponds to the frequency 0.17 Hz. Consequently, the time dependence of the elongation is determined sequentially by a linear function which forms an "isosceles triangle". This function can be expressed by the Fourier series (see [6]).
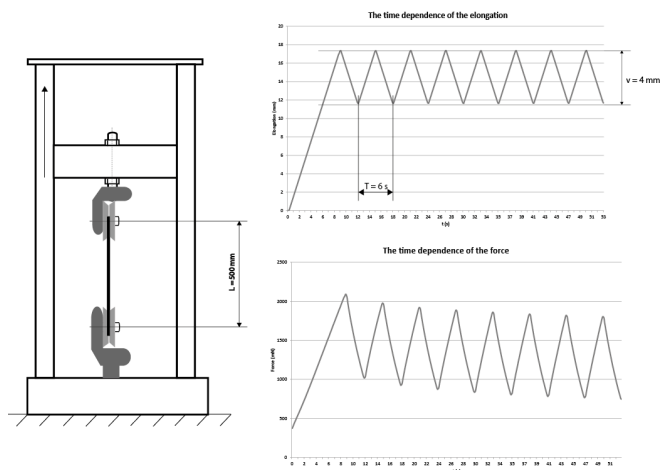
Figure 6 Diagrammatic representation of a test on the Instron device

Using the measured data, charts of the dependence of tensile force on the elongation for individual cycles, both increase and decrease, were generated. Figure 7 shows an example of the results for measurement No.10.
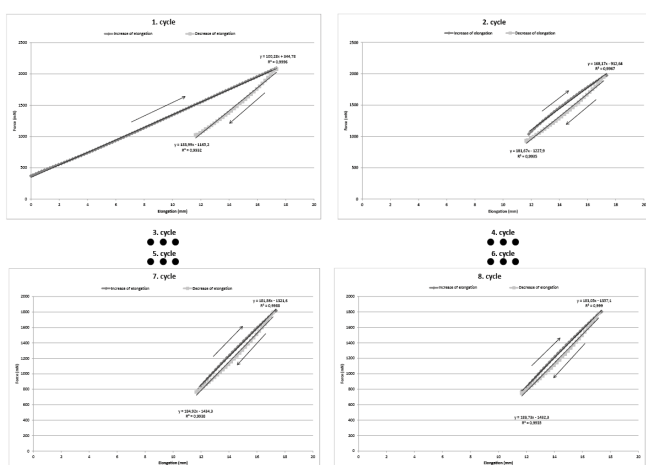
Figure 7 Dependence of tensile force on elongation

In the individual cycles, the equation of the regression straight line as well as the respective correlation coefficient, for both increase and decrease of the elongation, was established. The equation of the regression straight line for increase of the elongation is established by means of relation 16, while the equation of the regression straight line for decrease of the elongation is established by means of relation 17.

$$F_1(\Delta l) = K_1.\Delta l + F_{01} \tag{16}$$

$$F_D(\Delta l) = K_D.\Delta l + F_{0D} \tag{17}$$

The slope of regression straight lines then characterises the static module of rigidity both for increase and decrease of elongation in individual cycles. The ascertained values are presented in the form of a bar chart in Figure 8.
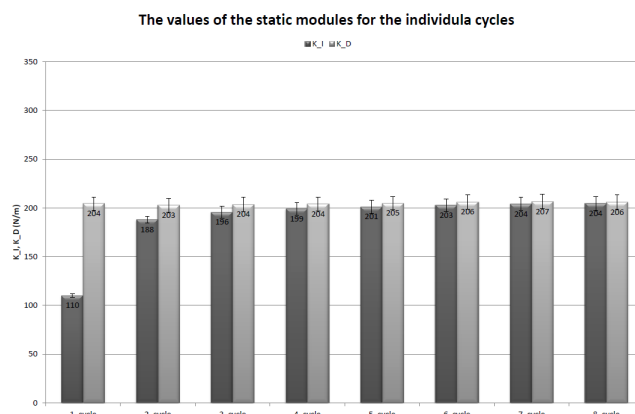
Figure 8 Mechanical characteristics of polyester yarn determined by means of the Instron device

4   CONCLUSION

4.1   Evaluation of changes in static modules of rigidity during cyclical loading

The following chart (see Figure 9) compares the static module of rigidity determined during the strength test (K_i = 108$\pm$2 N/m) with the values of static modules ascertained in individual cycles during periodical extension.

Table 5 Mechanical characteristics of polyester yarn determined by means of the Instron device

Cycle	1.	2.	3.	4.	5.	6.	7.	8.
Number of meas.	10	10	10	10	10	10	10	10
K_I (N/m)	110	188	196	199	201	203	204	204
Confidence 95%	3	6	7	7	7	7	7	7
R_I^2	0.9997	0.9969	0.9979	0.9984	0.9986	0.9988	0.9989	0.9990
K_D (N/m)	204	203	204	204	205	206	207	206
Confidence 95%	7	7	7	7	7	7	7	7
R_D^2	0.9934	0.9936	0.9937	0.9938	0.9939	0.9939	0.9939	0.9938
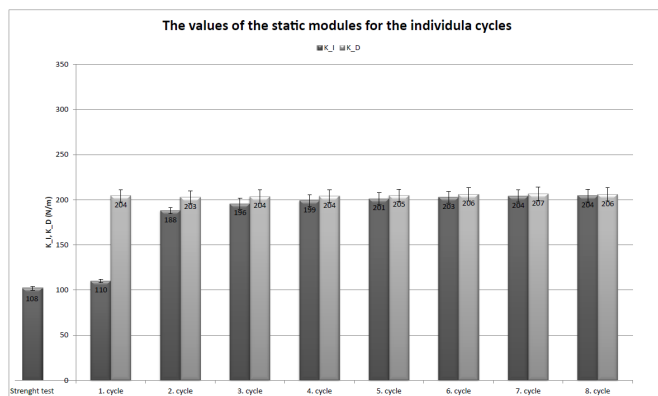
Figure 9 Comparison of static modules of rigidity of polyester yarn determined using different methods

It is evident that in the increase of elongation in the first cycle, the value of the module K_I=110±3 N/m does not differ significantly from the value K ascertained in the strength test. However, a significant increase in rigidity occurs during the decrease in elongation in the first cycle, namely to the value K_D=204±7 N/m. In the following cycles, the values of static modules of rigidity no longer differ significantly either in the increase and decrease of the elongation. The significant change in the static module of rigidity in the first cycle probably arises in consequence of the alteration of the internal structure of the thread (increased orientation of fibres), caused by its first extension.

4.2 Mutual comparison of static and dynamic modules of rigidity

The above-mentioned finding proves that the difference between the static module of rigidity K ascertained during the strength test and the dynamic module of rigidity C, or its real component C_{Re} respectively, is not caused just by the visco-elastic properties of the thread, and consequently, these differences cannot be explained by mere employment of rheological models, as has been suggested in papers published in the past [2].

Figure 10 shows a comparison of the static module of rigidity ascertained during cyclical loading on the Instron 4411 device in the 8th cycle for increase of elongation K_I=204±7 N/m and for decrease of elongation K_D=206±7 N/m with the values of the real component of the dynamic module of rigidity C ascertained at various frequencies of extension on the VibTex device.
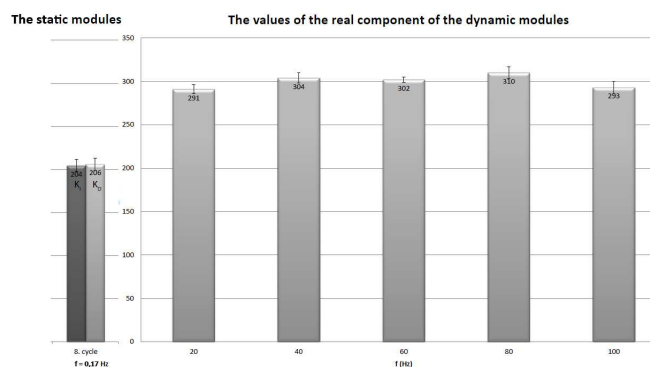
Figure 10 Comparison of the static module of rigidity of polyester yarn determined by different methods

It is obvious that the values of the real component of the dynamic module C do not differ substantially for individual frequencies. We can therefore state that in the range from 20 to 100 Hz, the value of the dynamic module of rigidity of the concerned thread is independent of the frequency and its value is approximately 300 N/m. However, the static

value of the module of rigidity ascertained during cyclical loading on the Instron 4411 device is approximately 200 N/m. This difference is probably indeed caused by the visco-elastic properties, and for its explanation we can use the three-member model described in the theoretical section. The equation (16) determines the value of the static module of rigidity by the parameter G0, which in our case is approximately 200 N/m. According to the equation (17), with increasing frequency of extension the rigidity increases to the value G_0+G_1, which in our case is approximately 300 N/m.

4.3 Influence of the module of rigidity of warp threads on the weaving process

The above-mentioned findings are rather important when determining the modules of rigidity of warp threads for the purpose of modelling of the mutual force interaction between the mechanical components of the weaving loom and the warp. It turns out that the standard strength test is practically unusable in this case, because it is not able to encompass the increase in rigidity which arises as a consequence of the first extension. Also, the difference between the static module and the dynamic one caused by the visco-elastic properties is rather considerable. Therefore, the cyclical test on the Instron 4411 device for determining the modules of rigidity is also contentious from the point of view of the weaving process. From the standpoint of the weaving process,

it is necessary to determine the respective modules of rigidity of warp threads employing a device which is able to simulate the weaving process as accurately as possible, taking into account the high number of cycles, the maximum values and frequencies of the extension (see the VibTex device).

5 REFERENCES

1. Morton W.E., Hearle J.W.S.: Physical properties of textile fibres, Manchester & London, The Textile Institute, Butterworths, 1962
2. Bílek M., Tumajer P.: Behaviour of Textiles under High Frequency stress, Acta Universitatis Cibiniensis Technical Series, vol. LVIII, pp. 8-14, 2009
3. Tumajer P., Ursíny P., Bílek M., Moučková E.: Research Methods for the Dynamic Properties of Textiles, Fibres&Textiles in Eastern Europe 19(5), pp. 33-39, 2011
4. Tumajer P., Ursíny P., Bílek M., Moučková E.: Use of the Vibtex vibration system for testing textiles, Autex Research Journal 11(2), pp. 47-53, 2011
5. Bílek M.; Moučková E., Tumajer P.; Ursíny P.; Žák J.: Deformation characteristics of linear textiles in the transition process, STRUTEX 2010 Book of abstracts, pp. 95-96, CD-Book of full texts, Technical University of Liberec, December 2010, Liberec, Technical University of Liberec, Faculty of Textile Engineering, Liberec, 2010
6. Tumajer P., Bílek M.: Mechanical characteristic of polyester yarn, STRUTEX 1014, Book of abstracts, pp. 19-23, CD-Book of full texts, Technical University of Liberec, 2014, ISBN 978-80-7494-139-9

FACTORS INFLUENCING RELIABILITY OF ON-LINE COLOR MEASUREMENTS

Michal Vik[1], Václav Čejka[2], František Founě[2] and Petr Škop[2]

[1]TU Liberec, Textile Faculty, LCAM DME, Studentská 2, 461 17 Liberec, CZ
[2]VÚTS a.s., Measurements-SW, Svárovská 619, Liberec XI-Růžodol I, 460 01 Liberec, CZ
michal.vik@tul.cz; tel. +420 485 353 226, fax +420 485 353 552
Vaclav.Cejka@vuts.cz; tel. +420 485 302 360, fax +420 485 302 402

Abstract: On-line color monitoring, properly configured and used, can produce substantial savings in dyeing and finishing operations. Fortunately, in the textile industry today there is almost universal use of the CIE (1976) colorimetric parameters, although there is still some disagreement as to whether the L*a*b* or L*C*H* dimensions should be used to describe color differences. When making measurements on goods exiting the continuous dye or finishing range, it is important for the dyer to know what color changes are occurring from one reading to the next. The dyer must readily understand the numerical color information, gathered at the end of the range, so that any appropriate corrective action can be taken for goods still to be dyed and so the color of finished goods can be accurately projected. VÚTS has developed a new color sensor for the on-line textile quality control system. This paper describes the features of this color sensor and factors influencing measured colorimetric data.
Key words: Colorimetry, textiles, on-line color measurement, dyeing, finishing.

1 INTRODUCTION

Variation in any of the processes in textile industry, which precede continuous dyeing, can results in fabrics and show variation after dyeing. By the same token, any variation in the finishing processes, which succeed continuous dyeing, can result in finished fabric as color change or color variation. The finished fabric themselves are susceptible to shade changes which can be partially reversible, but frequently irreversible and ate brought about changes in temperature, moisture content, dyestuff and chemicals concentration, fiber blending ratio, etc. and these kinds of shade changes area of particular importance to those who wish to retain physical samples, as standards, for prolonged periods.

On-line color monitoring, properly configured and used, can produce substantial savings in dyeing and finishing operations. When continuous dyer has to make an adjustment to correct a shade variation it would be of great benefit for him to know weather the change had originated on or before the dye range. Such work would be part of larger study to help the continuous dyer to rapidly distinguish between the color variations, which he can control, and those, which he cannot.

Some of companies are utilizing on-line systems for measuring and in some cases controlling color. Because of this movement, there are ever-increasing opportunities to compare on-line and laboratory measurements. Since number of companies produces both laboratory and on-line systems for different industrial applications such as pulp and paper, food industry, we get a lot of questions related to why lab and on-line measurements don't agree. There are several reasons that the instruments can disagree; yet each reading is in itself, "correct". What are those reasons?

- geometry differences between sensors
- product backing difference
- calibration basis difference
- product condition difference at time of measurement
- effect of different light source spectral content on fluorescent dyestuff or FWA
- sensor differences

In addition to these legitimate differences, there are several reasons why either the on-line or lab sensor is reading wrong:
- outside the temperature range
- contaminated sensor
- contaminated standardization tile
- power line problem fouled up data
- malfunction of part of system
- outside distance range
- wrong illumination or observer

At this point, lets examine major legitimate reasons for disagreement.

1.1   Geometry

How many different measuring geometries are used on-line? Answer typically two: 45°:0° or 0°:45° either directional (45°x:0° or 0°:45°x) or circumferential (45°a:0° or 0°:45°a). One of known exception is X-Rite VeriColor Spectro with 30°x:0° measuring geometry [1]. How many measuring geometries are used in the production lab? Answer is also typically two, but exactly more. Because diffuse measuring geometries are used in two modes: specular component included (di:8°) and specular excluded (de:8°), as addition in pulp and paper industry special diffuse measuring geometry d:0°, which is specular excluded. Of course are directional geometries used also.

It is necessary to understand that treatment of non-diffuse reflection is different for the each measuring geometry. Consider a high gloss is not captured by the receptor of directional geometries (45°:0° or 0°:45°), only diffusely reflected light. When compared with measurements made by a di:8° measuring geometry of lab instrument, the readings will be different. In the same fashion, color difference measurements between the standard and the product could be different depending on the gloss difference between the product and standard. For example color appearance of glossy samples will appear duller on di:8° device in comparison to device equipped by 45°a:0° viewing geometry.

1.2   Backing

Given the same measuring geometry, the product backing for both the lab and on-line measurement should be the same. That is, if on-line there is obviously no backing (tile, fabric, etc.), then do the same in the lab and opposite. The requirement for considering backing is simple, measure to determine the effect of a white or black backing. If the opacity is very high, then this is not a consideration.

1.3   Product Condition Differences

Often the on-line measurements are made on wet or humid hot fabric. Is it reasonable to expect that a measurement made there will be the same as a conditioned tear out sample measurement? Answer is NO! It is reasonable to expect a color difference between the product and product standard (humid and hot) to be the same as between conditioned samples? Probably not, but the difference will probably be closer than the absolute measurement, for example for wool samples dyed by acid and reactive dyestuffs.

1.4   Effect of spectral power distribution of used light source

This problem is obviously mentioned with materials containing FWA (Fluorescent Whitening Agent), which absorb UV radiation and emit in the blue region of visual part of electromagnetic spectra. But it is necessary to understand that numbers of dyestuffs are partially fluorescent and this property will caused measured color difference between measuring devices equipped by different light sources. Present day lab equipment lamp is obviously Xenon flash, which contains sufficient amount of UV radiation and spectral power distribution is near to illumination D65 in contrary to LEDs which not. That means measured result in case of warning clothing fabric will be strongly differ.

2   EXPERIMENTAL

VÚTS has developed a new color sensor for the on-line textile quality control system (Figure 1), which tries to solve all above-mentioned problems. Present day is impossible to explain full technical details of construction due to patent direction.
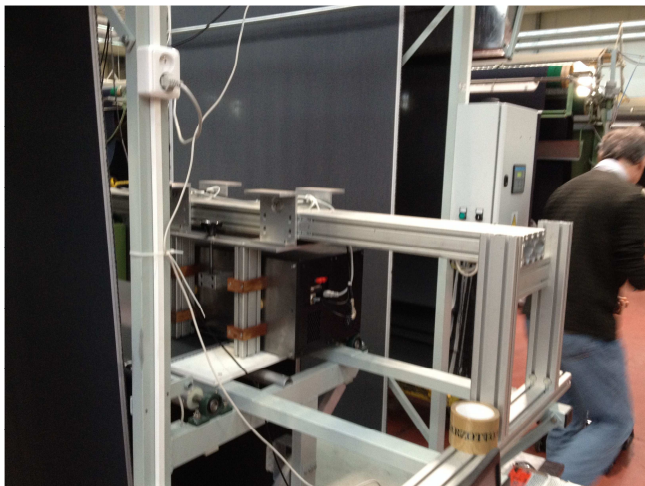
Figure 1 VUTS on-line spectrophotometer
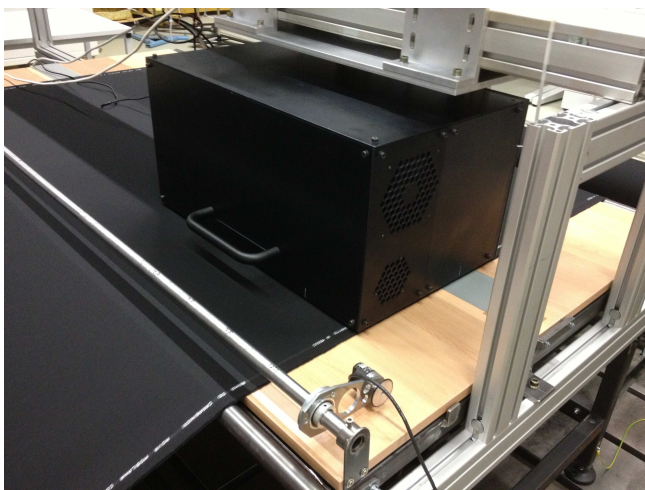
Figure 2 Measurement of testing fabric during of line tests

In our experiment was tested 30 m long loop of wool fabric dyed by selected acid dyestuffs on deep blue shade as visible on picture in Figure 2. Measurement of deep color is generally sensitive on long-term stability of device due to problem with insufficient amount of reflected light. Based on that was made set of individual readings at different section of textile fabric as a test of long term stability and variability of measured data.

3   RESULTS AND DISCUSSION

On-line measurement in contrary to off-line measurements is designed for measurement of moving fabric. It is simple to understand that speed of movement can vary due time and position of fabric on to measuring head. Based on that was tested sensitivity of colorimetric data on speed variability of measured fabric. On graph in Figure 3 it is visible that, the measured data are more sensitive on short frequencies in speed variability in comparison to high difference of speed on the start of measurement. This effect confirm to backing problem, which was mentioned before. That means speed variability will cause difference in fabric tension and consequently difference in opacity. Such problem is possible to solve by FFT filtering of measured data based on known frequency, speed variability from speed sensor of measuring device.
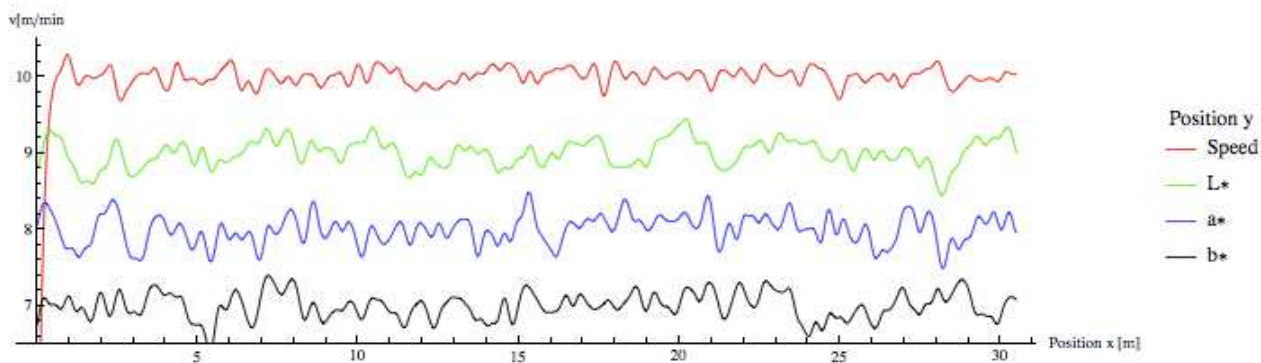
Figure 3 Comparison of colorimetric parameters of deep blue shade wool fabric and its speed variability
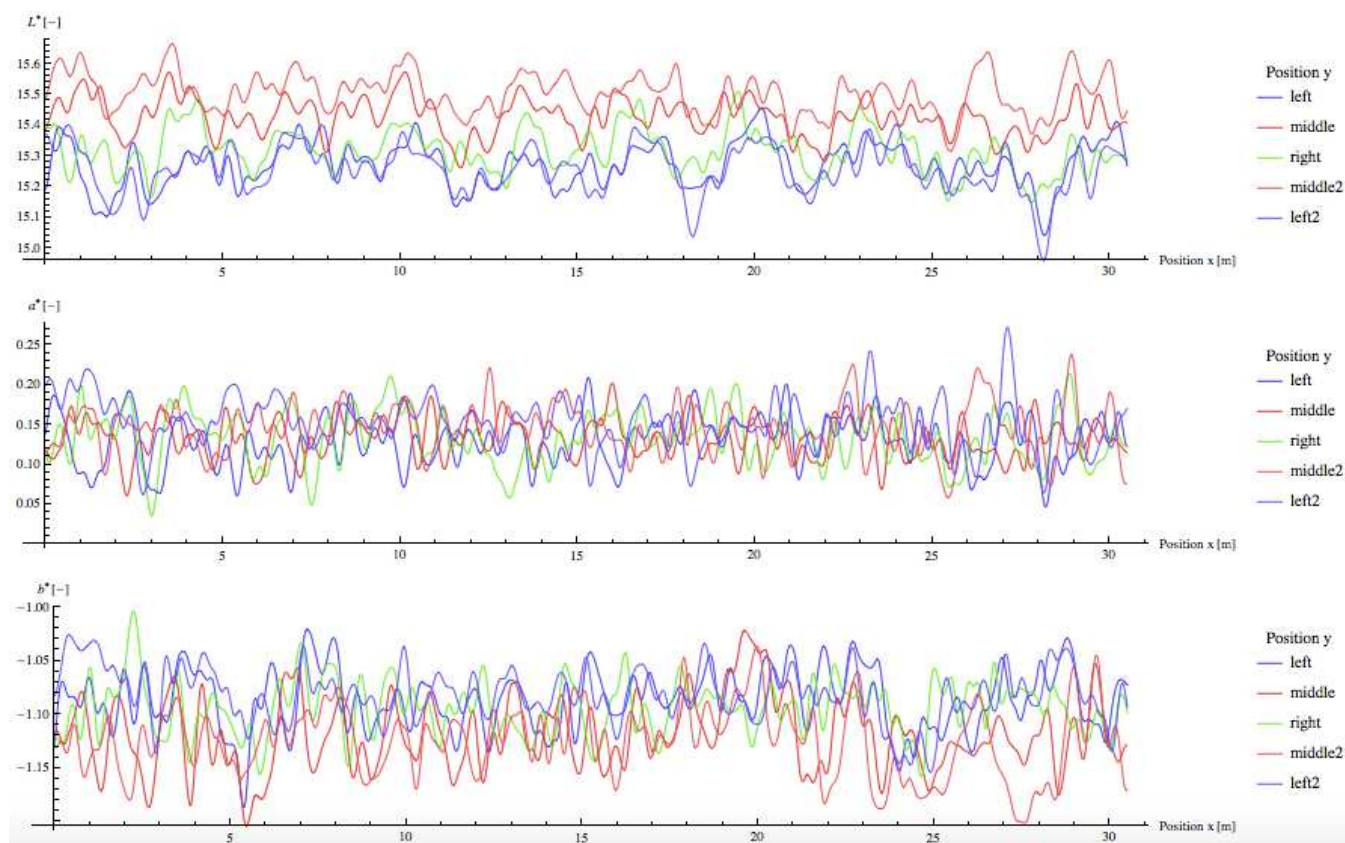
Figure 4 Colorimetric parameters of deep blue shade wool fabric

Second test was focused on long-term stability and resolution of measured position, in our case 5 line together (starting position right, two center and lefts). Presented data on graph in Figure 4 are non-filtered data; nevertheless are simple visible differences between measured positions. Long-term variability of measurements was 0.85 ΔE* unit.

4   CONCLUSIONS

This paper describes the features of this color sensor and factors influencing measured colorimetric data. VÚTS has developed a new color sensor for the on-line textile quality control system and presented results confirm usability of this unique device.

5   REFERENCES

1. *http://www.xrite.com/vericolor-spectro*

COMPLEX COLOR NON-UNIFORMITY AND SURFACE TEXTURE

Michal Vik[1], Martina Viková[1], Anna Maltseva[1] and Václav Čejka[2]

[1]*TU Liberec, Textile Faculty, LCAM DME, Studentská 2, 461 17 Liberec, CZ*
[2]*VÚTS a.s., Svárovská 619, Liberec XI-Růžodol I, 460 01 Liberec, CZ*
michal.vik@tul.cz; tel. +420 485 353 226, fax +420 485 353 552

Abstract: *The article explains the basic concepts of colorimetry and deals with issues of assessment reflectance quality of special plaster coatings in accordance with current methods of measuring spectral reflectance of the International Commission on Illumination (CIE). The results demonstrate that in the case of coatings with high gloss values (more than 70 GLS in the geometry 60) leads to a linear increase of specific purity depending on the specific increase luminance in the case of measuring devices fitted diffusion geometry. Conversely, if the angle-measuring instrument fitted geometry values of specific purity correlated with values of specific brightness. Analysis BRDF, respectively BSRDF function showed that the previously used dichromatic spectral reflectance model must be extended by an additional parameter explaining the correlation between chroma and lightness at the diffusion measurement geometry.*
Key words: *Colorimetry, color space, BRDF, CIE geometric arrangement.*

1 INTRODUCTION

The optical parameters of materials are very important in the design of lighting systems. If you turn out the light flux at the interface of two media, we can consider the case, the air-glass, there are three phenomena: reflection, absorption and passage. These values correspond to phenomena: reflectance, absorbance and transmittance. Part of the luminous flux φ_ρ is reflected, part absorbed φ_α and the last part of the material passes φ_τ. Applies the law of conservation of energy 1:

$$\varphi = \varphi_\rho + \varphi_\alpha + \varphi_\tau \tag{1}$$

Reflectance ρ can be defined as the ratio of the reflected flux to the incident luminous flux as defined in equation (2):

$$\rho = \frac{\varphi_\rho}{\varphi} \tag{2}$$

Reflectance values of the interface of two non-absorbing medium of known refractive indices n_0 and n' (n_0 the refractive index of the interface before an index of refraction of the material) for normal incidence can be determined from the Fresnel relations 2:

$$\rho = \left| \frac{n' - n_0}{n' + n_0} \right| \tag{3}$$

For example, the interface kaolin ($n' = 1.553 - 1.565$) 3 and air ($n_0 = 1.000293$) will have a reflectivity ρ value 0.0469 - 0.0484.

Equation (2), respectively (3) we can resolve and the problems passage of light and subsequently and the absorbance. A common problem is the requirement for normal incidence. To solve the issue comprehensively reflection, we have to use the theory of light transmission [4] and the ensuing two-way reflectance distribution function known as BRDF 5. The BRDF function can be most generally said, that it is an angular dependent reflectivity, or a function of angle of incidence and scattering. Indicates the sub-critical probability density (the integral may be less than 1), the light that impact fall down the surface, it is reflected in given direction. BRDF function can in radiometric (photometric) quantities defined as radiance (brightness) of the surface $L(\theta_i, \Phi_i, \theta_s, \Phi_s)$ divided by the incident irradiance (lighting) E:

$$BRDF(\theta_i, \phi_i, \theta_r, \phi_r) = \frac{L(\theta_i, \phi_i, \theta_r, \phi_r)}{E} \tag{4}$$

It is a four-dimensional function of two variables (θ_i, Φ_i) determines the direction of the incident radiation and two outgoing (θ_r, Φ_r) defining the direction of the reflected light. If examined isotropic surface, the BRDF function depends only on three variables θ_i, Φ_i, θ_r, since the reflectivity of the surface is symmetrical with respect to the plane of incidence and perpendicular to the surface does not change in the case when the surface rotates around its normal.
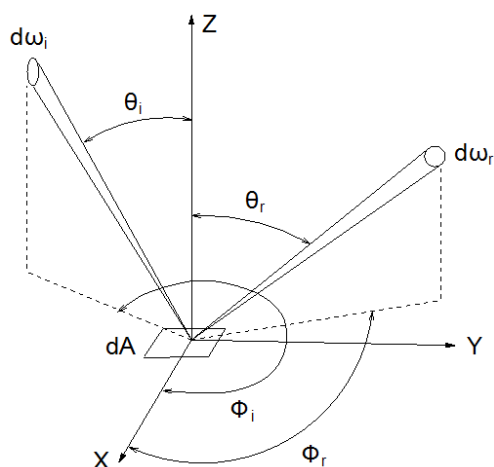
Figure 1 The geometry defining the BRDF function

Figure 2 Photometric angles and reflection components of non-homogeneous dielectric

BRDF function is usually measured using gonio-TDRs and also exist the methods, which use the image sensors (digital cameras, etc.) for the measuring and simple tools for defined lighting [6]. In terms of colorimetry, respectively description of the colorimetric properties of this approach is

inadequate because it is necessary to include both the relative spectral composition of the light source and the spectral reflectance of the measured object. In other words, it is necessary to supplement the BRDF of these spectral characteristics, so that equation (4) passes into its extended analytical expression:

$$BSRDF\left(\theta_i, \phi_i, \theta_r, \phi_r, \lambda\right) = \frac{dL_r\left(\theta_i, \phi_i, \theta_r, \phi_r, \lambda, E_i\right)}{dE_i\left(\theta_i, \phi_i, \lambda\right)} \quad (5)$$

In the beginning it was said that this theoretical solution is based on the assumption of a homogeneous dielectric when considering reflection at the interface of two media. Near of real objects is necessary to assume dielectric inhomogeneous in terms of the simplified diagram in Figure 2, where there is a reflection at the interface of two media (this reflection is often referred to as primary) and the reflection of body dielectric material (this reflection is referred to as secondary or diffusion). The resulting reflection is formed as an additive component of primary (surface) reflection L_S and secondary component (diffuse) reflection L_D:

$$L\left(i, e, g, \lambda\right) = L_S\left(i, e, g, \lambda\right) + L_B\left(i, e, g, \lambda\right) \quad (6)$$

where e is the angle of observation, g is the phase angle and i is the angle of direction of the incident beam. Shafer 7 showed that spectral characteristics of reflection at the interface and within the dielectric body itself are invariant to illumination angle. Equation (6) is reduced to form:

$$L\left(\theta, \lambda\right) = m_S\left(\theta\right)c_S\left(\lambda\right) + m_B\left(\theta\right)c_B\left(\lambda\right) \quad (7)$$

where m_S a m_B are factors geometric scaling, c_S a c_B are spectral characteristics of the reflection at the interface and inside the body, where is:

$$c_S\left(\lambda\right) = E\left(\lambda\right)R_S\left(\lambda\right) \qquad \text{and}$$
$$c_B\left(\lambda\right) = E\left(\lambda\right)R_B\left(\lambda\right) \qquad (8)$$

where $E(\lambda)$ is the relative spectral composition of the light, $R_S(\lambda)$ the spectral reflectance factor at the interface and $R_B(\lambda)$ is the spectral reflectance factor inside the body.

2   MATERIALS AND METHODS

In the company AVIS COLOR was ready to set 7 hardboard panels with a thickness of 5 mm and a square size 80x80 cm, which were applied decorative coatings Italian company OIKOS.

Figure 3 Sample painted FBA LUCIDO

Figure 4 Sample painted TRAVERTINO black

For measuring of the spectral characteristics of these fancy paints were used two portable devices with different geometric configuration: MiniScan XE (HunterLab, USA) with a geometry of 45°a:0° (circular illumination on 45°), the spectral range 400-700 nm, spectral bandwidth measurement step 10 nm, aperture diameter 30 mm, used light source: D65 simulator based on discontinuous Xenon lamps. The second device was Microflash MF200d (Datacolor International, USA) with geometry di:8° spectral range 400-700 nm extrapolated spectral measurement step 10 nm bandwidth, aperture diameter 20 mm, used light source: D65 simulator based discontinuous Xenon lamp. Each sample was measured 3 times at 16-measuring points, which formed a square coordinate grid 4x4 points. In total, 96 individual measurements in vertical and horizontal orientation of the device to the network, coordinate, which was subsequently evaluated using data treatment software Gigawiz Aabel, v. 3.0. Due to the results mentioned when it was necessary to limit the impact of different technologies on which they are based spectrophotometers above, was subsequently used spectrophotometer SHIMADZU UV3101PC, which allows alternative casting two measuring geometries: di:8° and de:8, compensated aperture holes 10 mm. Using spectral range 380-760 nm and 0.5 nm spectral step. This measuring system were measured calibration standards ceramic CCSI (Ceram Research, UK).

3   RESULTS AND DISCUSSION

Used fiberboard plates have proved advantageous, since it was possible to fix the frame in the buffer so as to ensure flatness of the plate in a tolerance of ± 1 mm to 80 cm in length. The correct position and orientation of measuring device was provided through the reticle. As documented resultant values colorimetric coordinates L*a*b*, in the case of the sample referred to as FBA LUCIDO, which amounted to 72 gloss units at 20° GLS (94.5 at 60°), there is a significant difference between the two geometries tested. The total color difference $\Delta E^* = 12.65$ is formed mainly by the difference in specific diameters $|\Delta L^*| = 11.32$. Measurement using geometry di: 8 show a significant linear trend, as illustrated in Figure 5, respectively Figure 6. This result would support the assumption of specific binding between the luminance and purity in a colorimetric system CIE1976L*a*b* discussed in the context models for the evaluation of color appearance CAM [8]. In contrast, these results of the measurement

sample using FBA LUCIDO this has not been confirmed by measuring geometry 45°:a:0°, see Figure 7. If in case the measuring geometry di:8 coefficient of determination reaches almost 90% (R^2 = 0.89), then in the case of measuring the geometry of 45°:a:0° was virtually zero coefficient of determination (R^2 = 0.07), as illustrated by Figure 8 in other words, the above assumption that the increase in specific lightness of the hue is accompanied by an increase in specific purity by measuring the geometry of 45°:a:0° does not apply and can not be considered as a native feature colorimetric system CIE1976 L*a*b*.
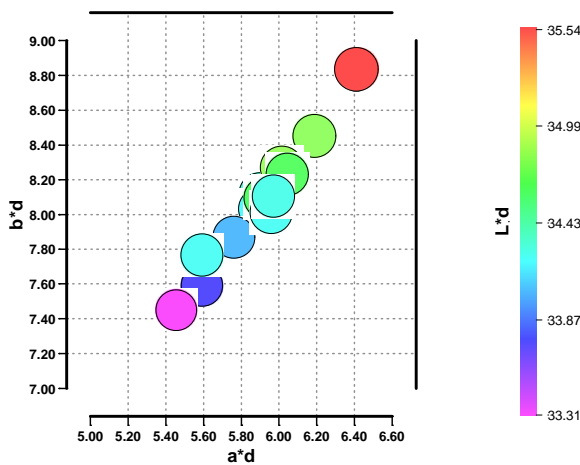
Figure 5 The colorimetric coordinates for the sample with paint FBA LUCIDO – measuring geometry di:8°
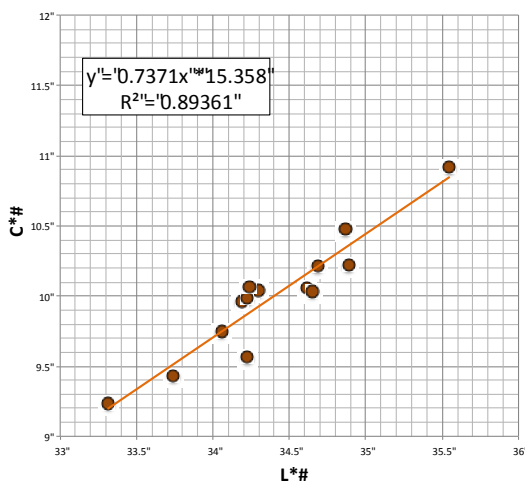
Figure 6 The colorimetric coordinates for the sample with paint FBA LUCIDO – measuring geometry 45°:a:0 °

Decorative paint TRAVERTINO black was as a comparative sample. Values colorimetric coordinates of this sample are both measurement geometries near and within industrial tolerances of these can be also exchanged. Comparing the two test samples in terms of gloss find that the smooth part of the pattern TRAVERTINO black gloss values were measured up to 5.5 GLS units at 85° (6.3° 60). In other words, the sample is compared with the sample FBA LUCIDO significantly dull. In terms of colorimetric parameters of mutual comparison of the two samples shows that the measured value of the total color difference between test measurement geometries in the case of the sample TRAVERTINO black was ΔE* = 0.99. This color difference is primarily made up of a cleanly in shade tolerance, because the difference in specific diameters |ΔL*| = 0.08 is at the limit of measurement errors, which ranged in the above cases at SD = 0.05. It can therefore be concluded that a significant difference between the measured colorimetric parameters for both test geometries occurs mainly in samples with higher gloss.
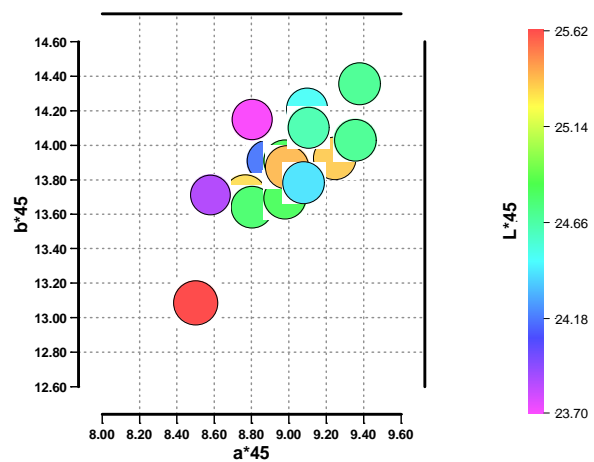
Figure 7 The colorimetric coordinates for the sample with paint FBA LUCIDO – measuring geometry di:8°
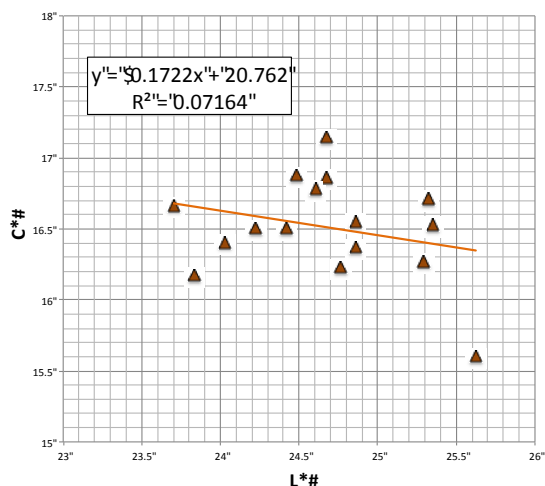
Figure 8 The colorimetric coordinates for the sample with paint FBA LUCIDO – measuring geometry 45°:a:0°

Figure 9 The colorimetric coordinates for the sample with paint TRAVERTINO black – measuring geometry di:8°

Returning to equation (7), we see that the overall character of the reflected light is additive formed at the interface reflection component and a component of the measured reflection from inside the body. If we accept the hypothesis that in the case of smooth surfaces close to them and measuring geometry 45°:a:0° due to its design neglects component reflects the $R_S(λ)$ and measure only the component $R_B(λ)$, then the spectral reflectance characteristics of the $R_S(λ)$ determined from equation (7), since the equation (8) shows that the spectral reflectance characteristic is dependent on the relative spectral representation used light $E(λ)$, which in our case the above D65 and the reflection coefficient $R_S(λ)$ and $R_B(λ)$. In other words, by subtracting the coefficient of reflection $R_{45:0}(λ)$ from $R_{di:8}$ obtained value $R_S(λ)$, since the geometric scaling factors m_B and m_S are in this case constant.

The graphs of Figures 11 and 12 show that the $R_S(λ)$ has a substantially flat nature of the local maximum in the spectral region of the stroke. This led to the suspicion that the compared data are flawed spectral resolution of both devices, which if MiniScan XE devices are natively measured data with a spectral step of 10 nm, whereas in the case of apparatus Microflash MF200 is a native of 2.67 nm spectral step.

Figure 10 The colorimetric coordinates for the sample with paint TRAVERTINO black - measuring geometry 45°:a:0°

The measured data are still at the hardware level smoothed using a cubic spline function and then exported to 10 nm spectral step.

For this reason, comparisons were made both measuring geometries, respectively measured values of the reflection coefficient $R_{de:8}(λ)$ and $R_{di:8}$ on a Shimadzu UV3101PC, when the cuvette compartment of the spectrophotometer were alternately installed reflective inserts for both measurement and geometry to eliminate the effect of smoothing the spectral data was elected spectral step of 0.5 nm. In order to eliminate unevenness in color perception

visible in decorative paints, ceramics were measured calibration standards Series II Ceram Research, which are used worldwide to calibrate reflectance spectrophotometer.
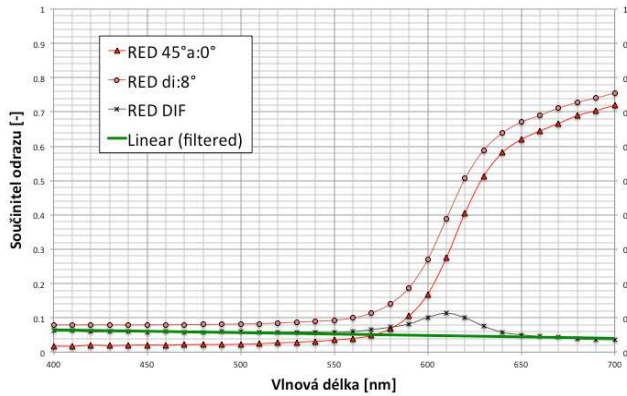
Figure 11 Spectral reflectance data of RED ceramic tile
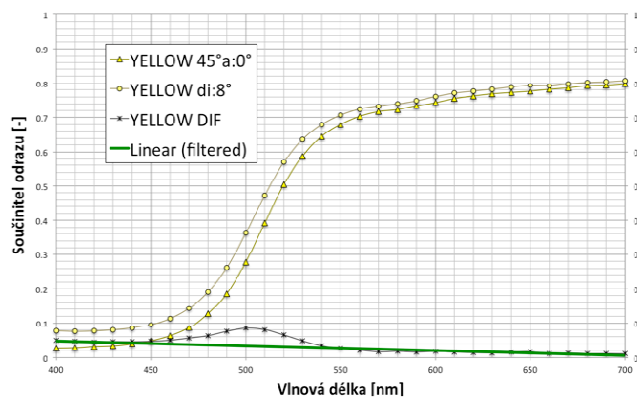
Figure 12 Spectral reflectance data of YELLOW ceramic tile
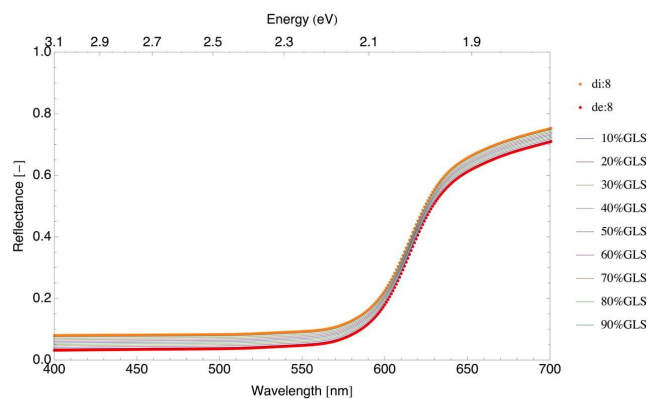
Figure 13 Spectral reflectance data of RED ceramic tile - $R_{de:8}(λ)$, $R_{di:8}$ + data wit simuated gloss enfluence on Shimadzu UV3101PC
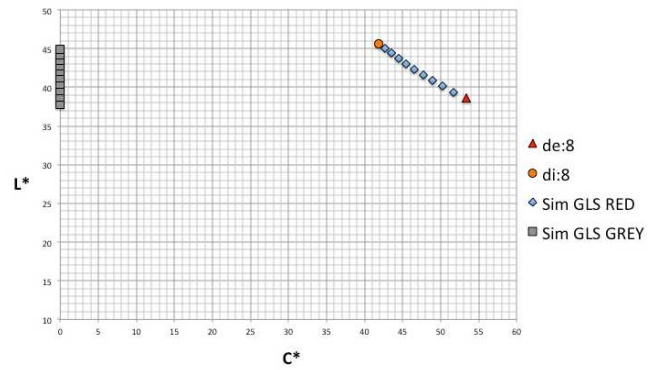
Figure 14 The colorimetric coordinates L*C* for the RED ceramic tile measured by $R_{de:8}(λ)$ and $R_{di:8}$ together with data simulation

Spectral reflectance data of RED ceramic tile from mentioned set measured by both diffuse geometries on spectrophotometer Shimadzu confirms that local maxima presented in graphs on Figures 11 and 12 are artifacts caused by limited traceability of data between tested portable devices. As documented by green lines labeled in Figures 11 and 12 as Linear (Filtered), spectral characteristic $R_S(λ)$ is linear with a decrease of 0.02 coefficients of reflection on the screen 300 nm, which is practically parallel to the abscissa. Consequently, the gloss itself can negatively influence the measured chroma **C*** as shown in graph on Figure 14. This result is in contrary to measured data of decorative paint FBA LUCIDO as documented by graph in Figures 6. If we will compare influence of simulated gloss on lightness **L*** and chroma **C*** value of achromatic color in Figure 14 Sim GLS GREY data for approx. deep grey color, it is visible that addition gloss will caused only increasing of lightness, but effect on resulting chroma is practically zero. That implies in the case of decorative coatings with high gloss is necessary dichromatic function (7) describing the spectral reflectance characteristics supplemented by other parameters explaining specific purity increase with the increase of the specific lightness. One of explanation of this effect can be based on possible effect of changes in local thickness of covering varnish layer.

4   CONCLUSIONS

The bi-directional distribution reflectivity BRDF is currently widely used in computer graphics, when synthetic textures of virtual objects can achieve a high zoom real appearance. Inverse solutions of this function, respectively its spectral expansion are less obvious and require adequate instrumentation. The measurement results showed, that in the case of decorative coatings with high gloss is necessary dichromatic function (7) describing the spectral reflectance characteristics supplemented by other parameters explaining specific purity increase with the increase of the specific diameters. For a precise definition of such a function will be to supplement the existing results on spectral reflectance measurements using multiple angle spectrophotometers, respectively gonio-spectrophotometers. Furthermore, it was shown that in the case of the comparison of the spectral data from different devices, it is necessary to perform a compensation of the spectral resolution.

5   REFERENCES

1. Bass M.: Handbook of Optics: Fundamentals, techniques, and design, Optical Society of America, McGraw-Hill 1994
2. Bukshtab M.: Applied Photometry, Radiometry, and Measurements of Optical Losses, Springer Series in Optical Sciences, 2012
3. Palik E.D.: Handbook of Optical Constants, Elsevier, 1997
4. Klein G.A.: Industrial Color Physics, Springer Science+Business Media 2010
5. Torrance K, Sparrow E.: Theory for Off-Specular Reflection from Roughened Surfaces, J. Optical Soc. America 57, pp. 1105-1114, 1976
6. Cady F.M., Bjork D.R., Rifkin J., Stover J.C.: BRDF Error Analysis, Proc. SPIE 1165, Scatter from Optical Components; doi: 10.1117/12.962845
7. Shafer S.A.: Using color to separate reflection components, Color Research and Application, 10(4), pp. 210–218, 1985
8. Fairchild M.: Color Appearance Models, John Wiley & Sons Ltd, sec. ed., 2005

DEPENDENT AND INDEPENDENT PARAMETERS OF NEEDLELESS ELECTROSPINNING

Fatma Yalcinkaya, Baturalp Yalcinkaya and Oldrich Jirsak

Department of Nonwovens and Nanofibrous Materials, Faculty of Textile Engineering, Technical University of Liberec, Studentska 2, 46117 Liberec, Czech Republic
yenertex@hotmail.com

Abstract: Electrospinning is a relatively simple method to produce nanofibers from solutions and melt of different polymers and polymer blends. There is an extensive application in future of electrospinning nanofibers. Several methods have been developed for wide scale production.
In this article, we introduced parameters of needleless electrospinning and new parameters were added to literature. It was found that each parameter play a major role on productivity and quality of nanofibers.
Key Words: Roller electrospinning, parameters, nanofiber.

1   INTRODUCTION

Electrospinning is a versatile method to produce ultra-thin fibers less than 1 µm. Nanofibers produced from electrospinning has enormous properties such as, high surface area, highly pore structure, small pore size, and electrical properties and so on. Based on specific properties of nanofibers, scientists focus on promising application area of nanofibers. Nanofibers can be used for, filtration, wound dressing, drug delivery, tissue engineering, artificial vessels, barrier textiles, sensors, carriers and so on [1-3]. Electrospinning is one of the most demanded production method. Electrospinning methods can grouped into two; needle and needleless electrospinning. There are system and process parameters which has effective role on nanofibers. Process parameters can be defined as needle diameter, distance between electrodes, feed rate, applied voltage, ambient conditions while system parameters can defined as polymer solution properties such as surface tension, viscosity, molecular weight, solvent, etc. Beside this, needleless electrospinning is useful equipment for large production in industrial scale. Niu et al. grouped needleless electrospinning system as upward and downward [4]. One of the most popular upward needleless electrospinning systems is

roller electrospinning system which was developed by Jirsak et al. [5]. Despite many research about parameters of needle electrospinning, there is not enough information about needleless electrospinning. In this study, we focused on roller electrospinning and parameters. Parameters of roller electrospinning system can be divided into two groups such as dependent and independent. Independent parameters are the parameters which can be changed before or during spinning while dependent parameters are resultant parameters of independent ones. These parameters are explained in next section.

2   TECHNOLOGY AND PARAMETERS OF ROLLER ELECTROSPINNING

Roller electrospinning system is a highly productive method to produce nanofibers. In this method, there is a roller electrode which immersed in a solution tank (almost 1/3) and a motor connected to roller for rotation. Roller electrospinning system is a close system, there is only input for air and humidity and output for air suction On the top there is a collector (charged or grounded) and an conveyer material (generally nonwoven or paper) is passing through the collector as shown in Figure 1.

The parameters of roller electrospinning system were divided into two groups and tabulated in Table 1.
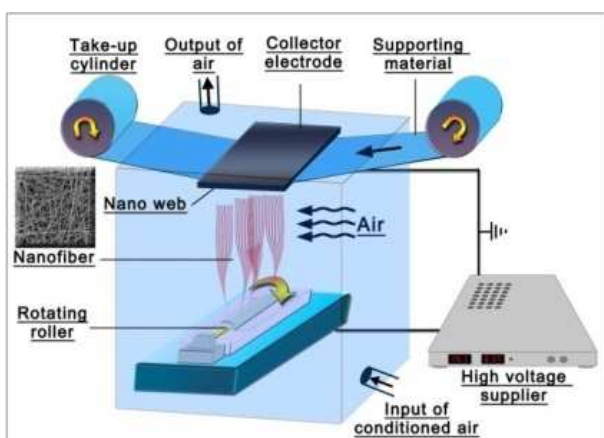
Figure 1 Schematic diagram of roller electrospinning system

Table 1 Parameters of roller electrospinning system

Independent Parameters
• Polymer solution properties (concentration, viscosity, composition, surface tension, conductivity, molecular weight)
• Applied voltage
• Distance between electrodes
• Velocity or rotating roller*
• Velocity of take-up fabric
• Geometry of electrode
• Geometry of collector
• Ambient conditions (temperature, relative humidity)
Dependent Parameters
• Number of cones, density of jets
• Life time of jets
• Spinning performance, spinning performance/per jet
• Total avr. current , current/jet*
• Thickness of polymer solution layer on the surface of the roller*
• Force acting on a jet*
• Spinning area*
• Distance between neighbouring jets*
• Jet length in stable zone
• Fiber diameter and distribution
• Non-fibrous area
• Launching time of jets

*The parameters introduced and defined or studied by the author

2.1 Independent Parameters
2.1.1 Polymer solution properties
Polymer jets must show some level of strength to create nanofibers during electrospinning. If the strength is too low, the jets break and create beads instead of fibers. With increasing the concentration of polymer solutions prepared using polymers with different molecular weight, the viscosity of polymer solutions was found to increase due to the densely entangled polymer chains. Electrospinning process operates due to external electric field, viscoelastic force due to the viscosity of the solution, surface tension force, conductivity, etc. Electric field between electrode and collector causes the solution to stretch. If the electrostatic field overcomes the surface tension, the nanofibers are formed. The stretching of the electrospun jet and the bending instability are mainly controlled by the Coulombic force between charges and the electric field. These forces arise due to the surface charge on the jet which can be varied by changing the conductivity of the solution.

Additives also affect the spinning performance and fiber diameter. It is common to use a salt in polymer solutions to increase their conductivity. In previous work we found that adding salt increase spinnability of polyburtyral nanofibers [6]. On the other side, Dao showed that adding salt to polyvinyl alcohol decreases the spinning performance [7]. The same results were observed in case of polyethylene oxide [8].

2.1.2 Applied voltage
Various voltages have significant effects on droplet size, fiber diameter and current transport. Increasing the voltage has been shown to increase jet diameter, as a result fiber diameter increased. In other investigations, increasing the voltage was shown to decrease the jet diameter, decrease the fiber diameter [9, 10].

The self-organization of liquid jet was analyzed by Lukas et al. [11]. In this analysis, it is supposed that electrohyrodynamics of a liquid surface can be analyzed with the capillary waves running on a one dimensional approximation of the liquid

surface, oriented along the horizontal axis, like x-axis, of Cartesian system of coordinates.

2.1.3 Distance between electrodes

The distance between electrodes is another phenomenon that controls the final fiber diameter and morphology. Sufficient time to dry out the solvent from polymer solution is necessary. If the distance between electrodes is too small, there is not enough time for drying, beaded and sticky fiber structures can be observed. On the contrary, if the distance is too big, the electric field between electrodes decrease and forming of fiber is difficult.

2.1.4 Ambient conditions

Electrospinning is affected by electric field. It means that any changes in the electrospinning environment will affect the electrospinning process. When humidity is high, it is likely that water condenses on the surface of the fiber. At a very low humidity, a volatile solvent may dry out very rapidly. The evaporation of the solvent may be very fast. As a result, the electrospinning process may only be carried out for a few minutes before the needle tip is clogged. Many works showed that ambient conditions (relative humidity, temperature) influence fiber diameter, morphology and spinning performance [12].

2.1.5 Velocity of rotating roller

The main function of the roller consists in feeding the polymer solution from a tank in the form of solution layer on the roller surface into the electrospinning process between the spinning and collector electrode.

2.1.6 Velocity of take-up fabric

During the roller electrospinning process, a supporting material (often a nonwoven fabric) is passing along the collector electrode to collect the fibers in the form of a more or less regular nanofiber layer on its surface. The speed of this fabric (in meters per minute) influences the area weight of nanofiber layer and also affects the quality of nanofibers membrane, namely its regularity and non-fibrous area.

2.1.7 Geometry of electrode

In the needleless electrospinning, many jets are formed simultaneously on the surface of the spinning electrode. Jets are generated on the free liquid surface by a self-organizing process. Because of this it is more difficult to control the spinning process when compared with the needle electrospinning process. The spinnerets in the needle electrospinning play essential role in determining the product quality and productivity.

2.1.8 Geometry and conductivity of collector electrode

The collector electrode in electrospinning is generally a conductive material. Collector can be directly connected to a high voltage supplier which gives the opposite charge than the spinning electrode has or it can be grounded. Fibers that are collected on the non-conducting material usually have a lower packing density compared to those collected on a conductive surface.

2.2 Dependent parameters

2.2.1 Number of cones

A number of Taylor's cones are simultaneously present on the spinning surface of the spinning roller electrode. Number of cones (N_c) depends strongly on independent electrospinning parameters.

2.2.2 Jet length

The distance between the tip of a Taylor cone and the splitting point of a jet is called length of jet. The long range repulsive electrostatic forces between ions of the same sign cause the disintegration of charged jet body. If electric forces are stronger than the capillary forces, the jet will split or will be formed by the whipping instability.

2.2.3 Spinning performance and spinning performance per jet

Spinning performance (SP) is one of the most important characteristics of nanofiber production process, influencing the production costs. Spinning performance strongly depends on all the independent parameters and influences the quality of nanofibers as well as that of nanofiber layers.

2.2.4 Fiber diameter and fiber diameter distribution

The fiber diameters are easily measured on the SEM microphotographs using software.

2.2.5 Non-fibrous area

The term non-fibrous area was created as a measure of nanofiber layer quality. This is a percentage of the area of a SEM microphotograph of nanofiber layer occupied by non-fibrous formations such as beads, foils and so on.

2.2.6 Life time of a jet

Life time of a jet can be defined as the period of time from the point that the jet appears on the spinning electrode to the point that the jet disappears. The solution properties, roller speed, electric field strength, number of cones and the thickness of layer on the roller surface are the main parameters that affect the life time of jet.

2.2.7 Measurement of current

The current is usually measured as the voltage drop across a resistor placed in series between the collector electrode and ground. The dependence of the jet current on independent process parameters, such as solution concentration and conductivity, feed rate, voltage, and so on.

2.2.8 Average current and current per jet

Under an electrostatic field, the polymer solution droplet becomes distorted by the induced electrical charge on the liquid surface, and a stable jet of polymer solution is then ejected from the cone. The break-up of the jet depends on the magnitude of the applied electric current. Measurement of current per one jet was suggested in previous work [13].

2.2.9 Parameters measured using camera records

These are spinning area and positions of jets, number of Taylor's cones per spinning area/distance between neighbouring jets.

2.2.10 Launching time of jet

Highly concentrated solutions have an intensive entanglement of polymer chains, therefore coulombic repulsion force will not be sufficient to start jetting. However, the surface area has to be increased to accommodate the charge build-up on the jet surface which occurs through the formation of fibers.

2.2.11 Force acting on a jet

Force acting on a jet was calculated in previous work [14]. In fact, the force F depends on electrical characteristics of the space between electrodes and on applied voltage.

3   CONCLUSION

In this work, we summarize the parameters of needleless electrospinning. Firstly, parameters grouped according to dependencies and secondly new parameters were introduced to literature. There are still many parameters waiting for investigation such as permittivity. Herein we tried to explain parameters for future works and for better productivity of nanofibers in fine diameter.

4   REFERENCES

1. Rajesh V., Dhirendra S.K.: Nanofibers and their applications in tissue engineering, Int J Nanomedicine 1(1), pp. 15-30, 2006
2. Xue J.J., He M., Liu H., Niu Y.Z., Crawford A., et al.: Drug loaded homogeneous electrospun PCL/gelatin hybrid nanofiber structures for anti-infective tissue regeneration membranes, Biomaterials 35(34), pp. 9395-9405, 2014
3. Heo D.N, Yang D.H., Lee J.B., Bae M.S., et al.: Burn-Wound Healing Effect of Gelatin/Polyurethane Nanofiber Scaffold Containing Silver-Sulfadiazine, Journal of Biomedical Nanotechnology 9(3), pp. 511-515, 2013
4. Niu H., Lin T.: Fiber Generators in Needleless Electrospinning, Journal of Nanomaterials, Volume 2012, Article ID 725950, 13 pages, 2012, http://dx.doi.org/10.1155/2012/725950
5. Jirsak O., Sanetrnik F., Lukas D., Kotek V., Martinova L., et al.: A Method of Nanofibers Production from a Polymer Solution Using Electrostatic Spinning and a Device for Carrying Out the Method, EP1673493, Czech Republic, 2005

6. Yener F., Jirsak O.: Improving Performance of Polyvinyl Butyral Electrospinning, 3th International Conference of Nanocon, Brno, Czech Republic, 2011

7. Dao T.A: The Role Of Rheological Properties Of Polymer Solutions In Needleless Electrostatic Spinning, Nonwoven. Phd. Thesis, Technical University of Liberec, Liberec, pp. 80, 2010

8. Mazari A.A.: Relationship Between Needle and Needle-less Electrospinning, MSc. Thesis, Technical University of Liberec, Liberec, pp. 66, 2011

9. Fong H., Chun I., Reneker D.H.: Beaded nanofibers formed during electrospinning, Polymer 40, pp. 4585-4592, 1999

10. Hohman M.M., Shin M., Rutledge G., Brenner M.P.: Electrospinning and electrically forced jets. II. Applications, Physics of Fluids 13, pp. 2221-2236, 2001

11. Lukas D., Sarkar A., Pokorny P: Self-organization of jets in electrospinning from free liquid surface: A generalized approach, Journal of Applied Physics 103(8), pp. 084309 1-7, 2008

12. Ramakrishna S., Fujihara K., Teo W.E., Lim T.C., Ma Z.: An Introduction to Electrospinning and Nanoflbers, World Scientific Publishing Co., 396 pages, 2005

13. Yener F., Yalcinkaya B., Jirsak O.: On the Measured Current in Needle- and Needleless Electrospinning, Journal of Nanoscience and Nanotechnology 13, pp. 4672-4679, 2013

14. Jirsak O., Frana K., Yener F.: Electrospinning studies: Jet forming Force. in: 19th International Conference of Strutex, Liberec, Czech Republic, pp. 97, 2012

DETECTION OF YARN LOCATIONS IN A WOVEN FABRIC IMAGE USING GRAY-LEVEL CO-OCCURRENCE MATRIX

Bekir Yildirim

Erciyes University, Engineering Faculty, Department of Textile Engineering, Kayseri, Turkey
bekiryildirim@erciyes.edu.tr; tel: +90 352 207 66 66, fax: +90 352 437 49 31

Abstract: *In this research, an algorithm is proposed for detecting yarn locations in a woven fabric image based on median filtering, wavelet decompositions and gray-level co-occurrence matrix (GLCM). In this approach woven fabric images are median filtered by row and column vector type kernels. Filtered images are decomposed by the wavelet transform. The matrix containing the horizontal and vertical sub-band coefficients are used as the source data for gray level co-occurence matrix. The approach is tested with real woven fabric images and experimental results show that this algorithm performs well on twill woven fabrics and colored yarns unlike using co-occurrence matrix (GLCM) method alone.*
Key words: *Image processing, woven fabric, wavelet transform, gray-level co-occurrence matrix.*

1 INTRODUCTION

Computer aided yarn location detection in a woven fabric surface image can serve as a basis of different applications, for example, to determine the number of yarns in a unit distance ie fabric density, to determine weave pattern recognition or to develop fabric fault detection methods. Unfortunately there is no generally accepted method has been developed so far due to the difficulty of the woven fabric surface characteristics to detect yarn locations in woven fabric images. Several researchers proposed computer assisted image analysis methods for woven fabric density measurement some of which might be also including yarn location detections. These methods can be classified into several approaches; co-occurence matrix approach [3, 5], spectral approaches based on Fourier Transform [5-7], the gray line profile method [2, 5]. Using second order statistics based on grey level coocurrence matrix to measure weaving density is only suitable for single-color plain weave fabrics [3].

In this paper, an algorithm based on Gray Level Co-occurrence Matrix for yarn location detection in a woven fabric surface image is proposed. Median filtering and using the wavelet decomposition, the horizontal and vertical structure of the woven fabric image can be extracted and emphasized, which will improve the accuracy of Gray Level Co-occurrence Matrix method. On the other hand, the computational cost is less. Experimental results show that the proposed algorithm can deal with colored yarns and twill weaves also.

2 THE PROPOSED ALGORITHM

2.1 Median filtering

Median filtering is a nonlinear digital filtering technique often used in image processing to reduce speckle noise and impulsive noise. Median filtering can be used for directional yarn enhancing in a woven fabric image. In order to enhance horizontal aligned yarns row vector [1xN] shape kernels and for enhancing vertical aligned yarns column vector [Nx1] shape kernels can be used. A twill woven fabric is filtered with row kernel median filter and a column kernel median filter shown in Figure 1. It can be seen that the row kernel median filtering enhances the horizontal yarns and column kernel enhances the vertical yarns in the woven fabric image.
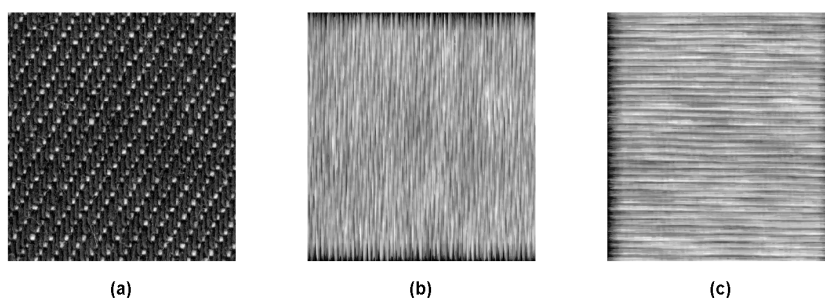
Figure 1 Median filtering for decomposing a) two colored yarn twill woven fabric, b) column kernel filtered, c) row kernel filtered
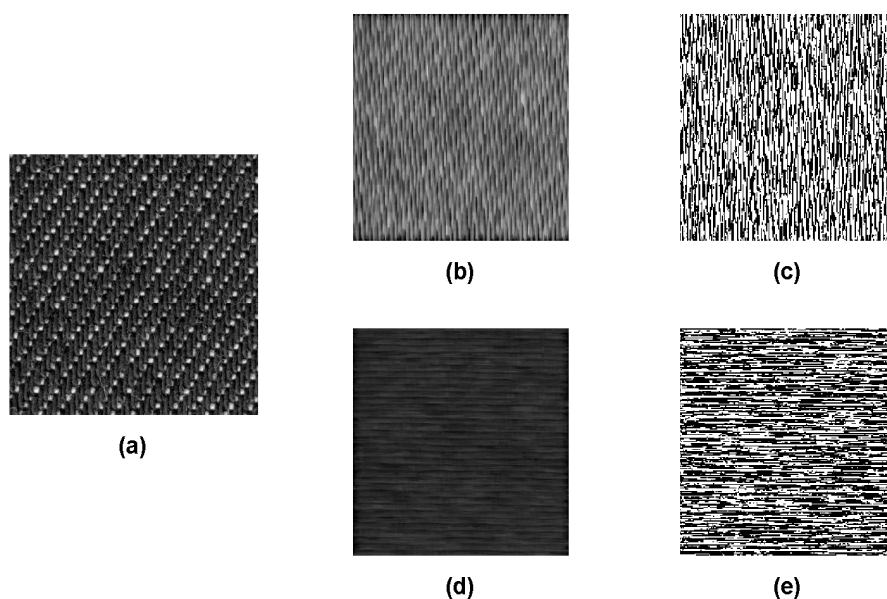
Figure 2 Example of wavelet transform of median filtered image (one level decomposition using haar wavelets) a) original woven fabric image, b) median filtered with kernel (41x1), c) vertical detail coefficients of wavelet decomposed image of b, d) median filtered with kernel (1x41), e) horizontal detail coefficients of wavelet decomposed image of d

2.2 Two-dimensional wavelet decomposition

In the algorithm, a two-dimensional discrete wavelet transform (2D-DWT) is used. The lowpass filters (L) smooth the image while the highpass filters (H) look for detailed information in the image. Figure 2 gives a woven fabric image and its first level decomposition result using the "haar" wavelet.

2.3 Gray Level Coocurrence Matrices (GLCM)

Gray level co-occurrence estimates image properties related to second-order statistics which considers the relationship among neighbouring pixels in an image. Mathematically, a co-occurrence matrix P is defined over an NxM image icon be defined as:

$$P(i,j) = \sum_{x=1}^{N}\sum_{y=1}^{M}\begin{cases} 1, & if \quad I(x,y) = i \, and \, I(x+\Delta x, y+\Delta y) = j \\ 0, & otherwise \end{cases}$$

where i and j are the image intensity values, x and y are the spatial positions in the image, $\Delta x, \Delta y$ are the offset. Although Haralick [1] described 14 statistic measurements that can be calculated from the co-occurrence matrix, in this study four of those, homogeneity,

contrast, correlation and energy are extracted in order to compare the effectiveness of the statistic measurements.

The proposed algorithm can be summarized as follows:

1. Input gray-scale image (Ig)
2. Median filter the input image with row kernel for horizontal yarn detection (Igrm) and column kernel filter for vertical yarn decomposition (Igcm)
3. Decompose Igrm with 2D-DWT and obtain Horizontal details coefficients matrix (Igrmh). Decompose Igcm with 2D-DWT and obtain Vertical details coefficients matrix (Igcmv).
4. GLCM of the sub-band (Igrmh) and of the sub-band (Igcmv)
5. Statistics of GLCM energy is computed for both directions so as to get vertical and horizontal yarn information

3   EXPERIMENTAL

To examine the performance of the proposed method, different real woven fabric samples are used. The woven fabric surface images are scanned using a HP flatbed scanner in true colors in resolution of 600 dpi with a size of 700×700 pixels and selected arbitrarily for investigation. The proposed algorithm is implemented in MATLAB (MathWorks 2008) and tested on a computer with 3.20 GHz processor and 2 GB RAM.

4   RESULTS AND DISCUSSION

The projection profile analysis is a common method for yarn location detection. Therefore, the comparison between the projection profile, the texture analysis with the original image and the proposed algorithm is shown in Figure 4. Twill woven fabric with two different colored yarns is used. Projection profile was so noisy to detect the yarn locations in this sample. Although glcm used alone missed some of the yarns due to the reasons explained as in reference [3], it can be analyzed that the proposed method has detected the yarns right.
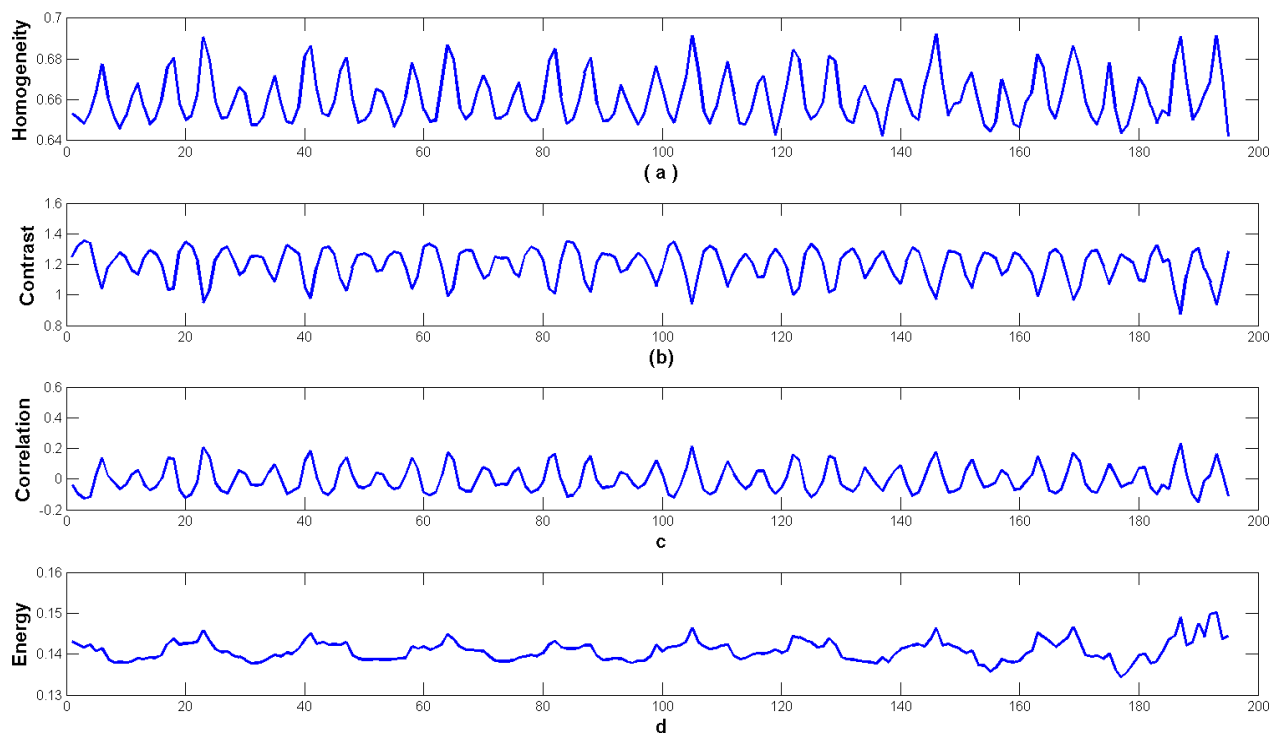
Figure 3 Example of extracted statistic measurements of vertical yarns of twill woven fabric image a) homogeneity, b) contrast, c) correlation, d) energy
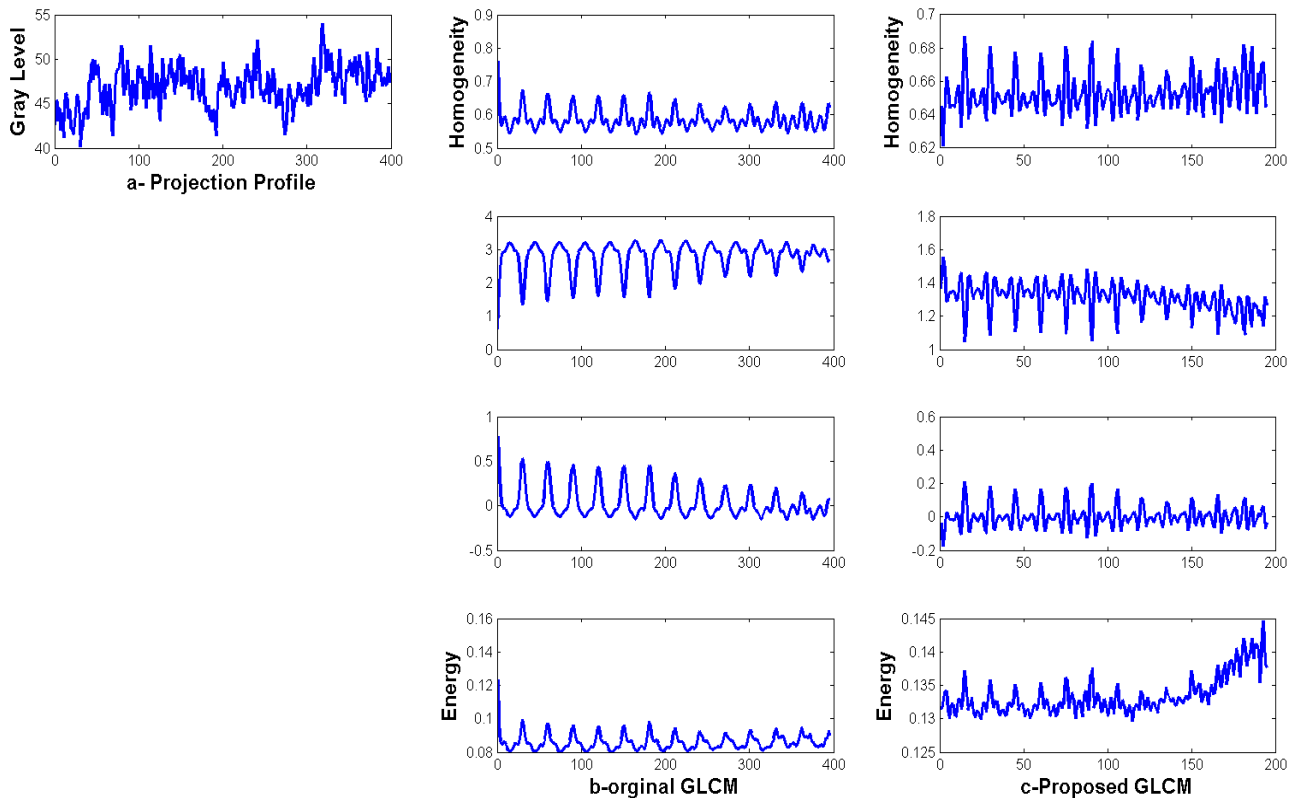
Figure 4 Example of extracted statistic measurements of vertical yarns of twill woven fabric image a-projection profile of the vertical yarns b- different statistic measurements of glcm of woven fabric c-different statistic measurements of glcm of woven fabric which is processed using the proposed algorithm

5 CONCLUSIONS

In this paper, an algorithm based on Gray Level Co-occurrence Matrix for yarn location detection in a woven fabric surface image is proposed. Median filtering and using the wavelet decomposition, the horizontal and vertical structure of the woven fabric image can be extracted and emphasized, which improve the accuracy of the method. The computational cost is less due to the down-sampling of wavelet transform. Experimental results show that the proposed algorithm can deal with colored yarns and twill weaves also unlike using the glcm method alone.

6 REFERENCES

1. Haralick R.M., Shanmugam K., Dinstein I.: Textural Features for Image Classification, IEEE Transactions on Systems, Man, and Cybernetics 3(6), pp. 610-621, 1973
2. Jeong Y.J,. Jang J.: Applying image analysis to automatic inspection of fabric density for woven fabrics, Fibers and Polymers 6, pp. 156 -161, 2005
3. Lin J.J.: Applying a co-occurrence matrix to automatic inspection of weaving density for woven fabrics, Textile Research Journal 72(6), pp. 486-490, 2002
4. Pan R., Gao W., Liu Kuo C.J., Shih C.Y., Lee J.Y.: Automatic recognition of fabric weave patterns by a fuzzy c-means clustering method, Textile Research Journal 74(2), pp. 107-111, 2004
5. Techniková L, Tunák M.: Weaving Density Evaluation with the Aid of Image Analysis, Fibres & Textiles in Eastern Europe 21(2), pp. 74-79, 2013
6. Tunak M., Linka A., Volf P.: Automatic Assessing and Monitoring of Weaving Density, Fibers and Polymers 10(6), pp. 830-836, 2009
7. Xu B.: Identifying Fabric Structures with Fast Fourier Transform Techniques, Textile Research Journal 66(8), pp. 496-506, 1996

NUMERICAL SIMULATION OF COUPLED FLUID FLOW AND HEAT TRANSFER OF FABRIC

Guocheng Zhu, Dana Kremenakova, Yan Wang and Jiri Militky

Department of Material Engineering, Technical University of Liberec
Studentská 1402/2, Liberec, Czech Republic
zgc100100@hotmail.com, tel.: 776109703

Abstract: Fluid flow and convective heat transfer of cold air over fabric was investigated numerically. The laminar model and the standard k-ε model were applied for Reynolds number 5637. The numerical calculation results from the standard k-ε model are a little higher since the Reynolds number is smaller than the critical value of turbulent flow. But the numerical calculation results from laminar model are in good agreement with well-known correlation results, which also illustrated that the numerical simulation would be an effective and reliable method for predicting the thermal property of textiles under convective heat transfer.
Key words: Numerical simulation, fluid flow, heat transfer, Nusselt number.

1   INTRODUCTION

Studies on convection through porous media have increased significantly during recent years. This is because the applications of porous media can range from filtration purposes to heat exchangers, energy storage units, ceramic processing, and packed bed chemical reactors, etc. Textile structures especially, being inherently porous in nature, have been put into use for many of these applications. The main problem faced in convective heat transfer was the calculation of heat transfer coefficients. On the other hand, various software programs can be put into use to find out the response of temperature of the clothing and the wearer to various climatic conditions.

In this work, the temperature distribution, heat flux distribution, heat transfer coefficients, and Nusselt number on fabric surface was investigated by numerical simulation and the results from simulation were compared with one well-known model in order to valid the simulation.

Nomenclature

H	Enthalpy, (J·kg^{-1})	Re_x	Local reynolds number, (1)
h_x	Local heat transfer coefficient (W·m^{-2}·K^{-1})	T_0	Air temperature at inlet, (K)
k	Heat capacity ratio, (1)	T_s	Temperature of solid, (K)
M_a	Mach number, (1)	T_f	Temperature of fluid, (K)
Nu_x	Local Nusselt number, (1)	T_{fabric}	Temperature of fabric, (K)
p	Pressure, (Pa)	T_{air}	Air temperature, (K)
p_t	Total pressure, (Pa)	u_0	Inlet velocity, (m·s^{-1})
p_b	Back pressure, (Pa)	U	Velocity vector, (m·s^{-1})
Δp	Pressure drop, (Pa)	x	Distance, (m)
Pr	Prandtl number, (1)	λ_s	Thermal conductivity of solid, (W·m^{-1}·K^{-1})
q_x	Heat flux, (W·m^{-2})	λ_f	Thermal conductivity of fluid, (W·m^{-1}·K^{-1})
R	Gas constant, (J·kg^{-1}·K^{-1})	λ_a	Thermal conductivity of air, (W·m^{-1}·K^{-1})
Re	Reynolds number, (1)	ρ	Density, (kg·m^{-3})
		μ	Dynamic viscosity, (Pa·s or kg·m^{-1}·s^{-1})

2 PHYSICAL MODEL, GOVERNING EQUATIONS AND NUMERICAL METHOD

The 3-D geometric model consists of polyester fabric and air flow, which is shown in Figure 1. The dimensions of polyester fabric are 15×15×0.36 mm in length (x direction), width (y direction) and height (z direction), and the dimensions of air flow are 15×15×5 mm in length, width and height. The grid of geometric model is shown in Figure 2, which includes 34373 cells and 39835 nodes. The minimum orthogonal quality of mesh was 0.999996 and the maximum aspect ratio was 8.71694, which means the mesh quality was very good. The density, heat capacity, and thermal conductivity of polyester fabric are 1416 kg/m^3, 1340 kJ/(kg·K), and 0.12 W/(m·K), respectively. And the ideal gas was applied for simulation since the density of air would be changed according to different pressure and temperature.
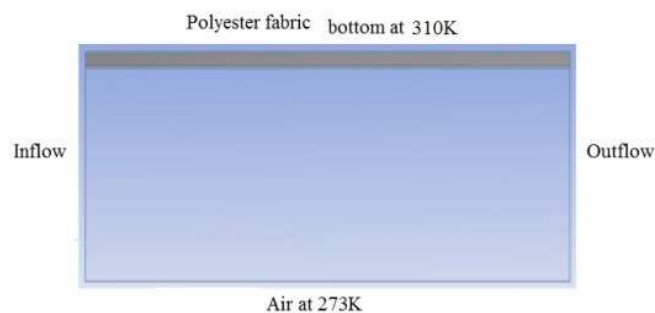
Figure1 Geometric model
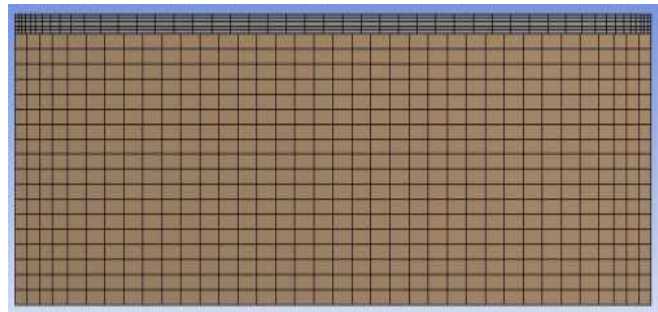
Figure 2 Grid of geometric model

The heat conduction equation for the solid part is:

$$\nabla \cdot \left(\lambda_s \nabla T_s \right) = 0 \tag{1}$$

The mass, momentum and energy equations for the fluid are:

$$\nabla \cdot \left(\rho U \right) = 0 \tag{2}$$

$$\nabla \cdot \left(\rho U U \right) = -\nabla p + \nabla \cdot \left(\mu \left(\nabla U - \frac{2}{3} \nabla \cdot U I \right) \right) \tag{3}$$

$$\nabla \cdot \left(\rho U H \right) = \nabla \cdot \left(\lambda_f \nabla T_f \right) \tag{4}$$

where *I* is the unit tensor.
The boundary conditions include the bottom temperature (310 K) of polyester fabric, the temperature (273 K) and the velocity (5 m/s) of air flow.
The transport equations of the standard k-ε model for turbulence kinetic energy *k* and its dissipation rate ε are [1]:

$$\frac{\partial}{\partial t}\left(\rho k \right) + \frac{\partial}{\partial x_i}\left(\rho k u_i \right) = \frac{\partial}{\partial x_j}\left[\left(\mu + \frac{\mu_t}{\sigma_k} \right) \frac{\partial k}{\partial x_j} \right] + G_k + G_b - \rho \varepsilon - Y_M + S_k \tag{5}$$

and

$$\frac{\partial}{\partial t}\left(\rho \varepsilon \right) + \frac{\partial}{\partial x_i}\left(\rho \varepsilon u_i \right) = \frac{\partial}{\partial x_j}\left[\left(\mu + \frac{\mu_t}{\sigma_\varepsilon} \right) \frac{\partial \varepsilon}{\partial x_j} \right] + C_{1\varepsilon}\frac{\varepsilon}{k}\left(G_k + C_{3\varepsilon}G_b \right) - C_{2\varepsilon}\rho\frac{\varepsilon^2}{k} + S_\varepsilon \tag{6}$$

3   RESULTS AND DISCUSSIONS

In order to obtain the heat transfer coefficient of fabric under heat convection, the temperature gradient and heat flux are needed according to equation:

$$h_x = \frac{q_x}{\left(T_{air} - T_{fabric}\right)} \tag{7}$$

The temperature distributions and heat flux distributions on the fabric surface in laminar and turbulent flow are given in Figure 3.

In a rough comparison, the maximum temperature on the fabric surface in laminar flow is slight higher than the maximum temperature of turbulent flow, and the heat flux range on the fabric surface in laminar flow is much larger than the result from the turbulent flow.
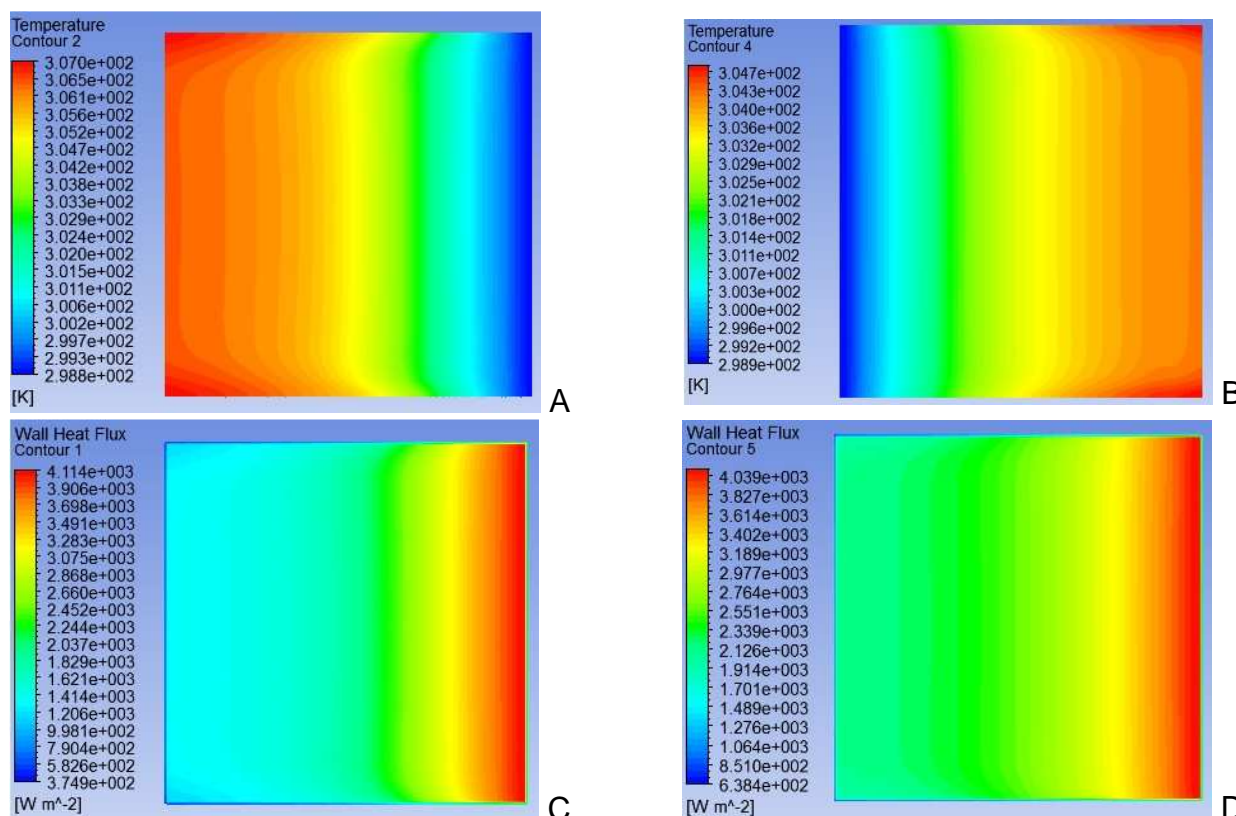
Figure 3 Temperature and heat flux distribution on the fabric surface in laminar and turbulent flow (A) temperature distribution in laminar flow; (B) temperature distribution in turbulent flow; (C) heat flux distribution in laminar flow; (D) heat flux distribution in turbulent flow
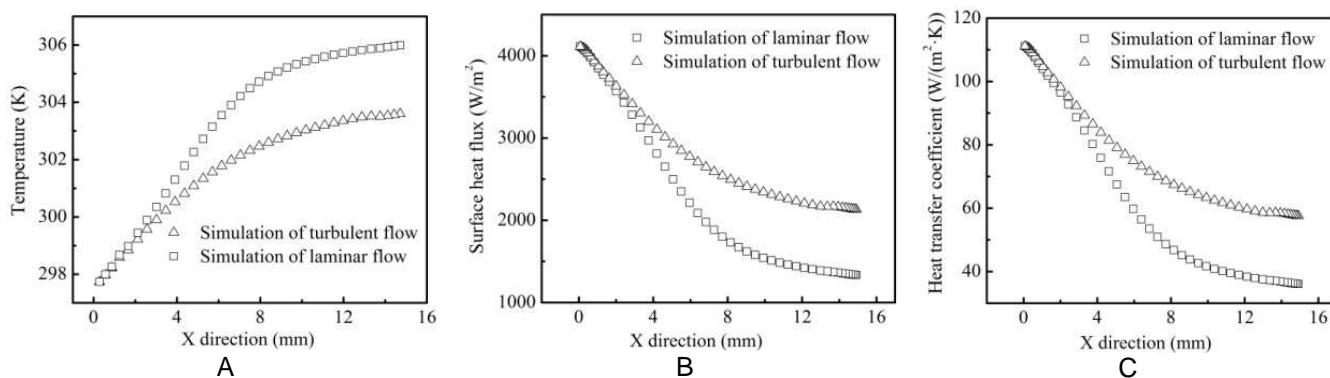
Figure 4 The temperature and heat flux distribution and heat transfer coefficient of fabric

In order to compare the results more clearly, the temperature and the heat flux distributions, and heat transfer coefficient in the middle of fabric surface are given in Figure 4. In the region of near-to-airflow inlet, the temperature, heat flux, and the heat transfer coefficient from laminar and turbulent flow are almost the same. But as the distance increase, the temperatures from laminar flow are higher than the temperatures from turbulent flow, which is due to the decrease of heat flux in laminar flow (Figure 4A and B). And according to equation (7), the heat transfer coefficients from laminar flow were lower than the results from turbulent flow.

In addition, the Nusselt number is always one important parameter to evaluate the heat transfer under convection. Nusselt number represents the enhancement of heat transfer through a fluid layer as a result of convection relative to conduction across the same fluid layer.

The larger the Nusselt number, the more effective the convection [2]. The equation for calculating Nusselt number is given:

$$Nu_x = h_x x / \lambda_a \qquad (8)$$

On the other hand, the Nusselt number is one function of Reynolds number (the ratio of inertial force to viscous force) and Prandtl number (the ratio of molecular diffusivity of momentum to molecular diffusivity of heat) based on plenty of experimental work, and the general expression for flat plate is [2]:

$$Nu_x = 0.332\, Re_x^{0.5}\, Pr^{1/3} \qquad (9)$$

The Nusselt numbers from simulation and from model are given in Figure 5. The Nusselt numbers increased as the increase of Reynolds number, and the results from laminar flow had a very good agreement with the results from model, which indicated the numerical simulation was suitable for predicting the thermal property of fabrics under heat convection. On the other hand, the Nusselt numbers from turbulent flow were a little higher than the results from model,

which is due to the lower Reynolds number used for turbulent flow in simulation.
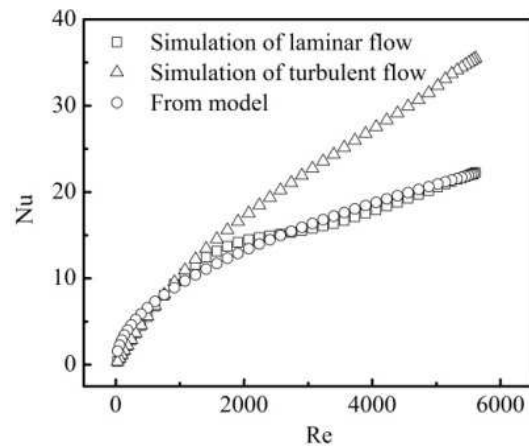
Figure 5 Comparison of Nusselt numbers from simulation and analytical model

4　CONCLUSIONS

Forced convective heat transfer for a horizontal fabric was numerically investigated. Based on this work, some conclusions can be draw:
1) with the increase in distance (far away from the airflow inlet), there is an increase on the fabric surface in temperature and a decrease on the fabric surface in heat flux and heat transfer coefficient;
2) as the increase of Reynolds number, the Nusselt number increased;
3) the numerical simulation results from laminar flow had a very good agreement with the results from analytical model;
4) numerical simulation could be an effective and reliable method for predicting the thermal property of fabrics under heat convection.

5　REFERENCES

1. FLUENT User's Guide, Release 6.1; Lebanon, 2001
2. Cengel Y.A.: Heat transfer, A practical approach. 2nd ed.; McGraw-Hill: New York, 2003

MODELLING OF TEXTILE STRUCTURES USING PRINCIPLES OF CLASSICAL MECHANICS

Josef Žák

VÚTS a.s., VVO TKA, Liberec, Czech republic
josef.zak@vuts.cz; tel. +420 485 302 219

Abstract: In our work we tried to find a simple and reliable method to determine mechanical properties of a woven fabric with the main respect to the processing of these fabrics on a weaving machine. Some interesting results emerged by that way concerning for example the design of fabrics. We were using primarily the means of classical mechanics and we tried to avoid as much as possible the use of computer resource demanding tools. Also we were concerned by the as large as possible applicability of results since our weaving machines are processing a wide spectrum of fabrics.
In this paper, the principles of our approach are presented with some numerical examples. Few practical experiments were carried out at this moment, so only limited comparison with the reality could be done.
Key words: Fabrics, energy based methods, textile structures modelling.

1   INTRODUCTION

By modelling textile structures such as a woven fabrics, double or triple twisted threads or knitted structures one soon realizes that a mathematical model is needed to describe their form or properties. There are several methods to do it, most of them using a geometric interpretation of the structure without taking into account the mechanic properties of the constituting yarns (Pierce's model). Some methods are using them, e.g. Oloffson for woven fabrics, but neither those latter ones do cover completely the characteristics of the structures. There exist some methods said modern, although the term trendy or popular should be more appropriate, that use the instruments of classic mechanics to determine the properties of textile structure. Here come mainly methods based on finite elements. Theirs drawbacks lie primarily in requirements on computational resources, secondly, the method necessarily requires a complete set of physical constants to enter in the computation - and to be determined by a cost demanding experiment - and thirdly, its versatility is - for a given input - only limited. A very interesting approach was used by

Kawabata, but his work too relies substantially on experimentally acquired data and in general is focused on another domain of use.

2   PRINCIPLES OF METHOD

Each mechanical system of deformable bodies in static conditions shall take such configuration whose total energy will be minimal. This energy consists of internal energy of deformation of the bodies and of the energy of external forces. The final configuration of the system will depend on the properties of the bodies and on the boundary conditions. The internal forces in the system must vanish and the principle of impenetrability of bodies must be respected. Given the above principles we have to find the final configuration of bodies. Once the deformed shape of bodies known we can determine the mechanical properties of system in its deformed state.

2.1   Description of model
In our work we focused on the modelling of one binding point of a fabric in plain weave. This singular binding point is part of an infinite fabric, in which it is repeated countless many

times. Thus no border effect is to be considered, we are searching the shape of a binding point in the middle of an infinite domain. In this case the individual bodies will be corresponding segments of weft and of warp. In other types of weave, e.g. twill, satin,…, or in any other textile structures, a similar repeat may be found and modelled.
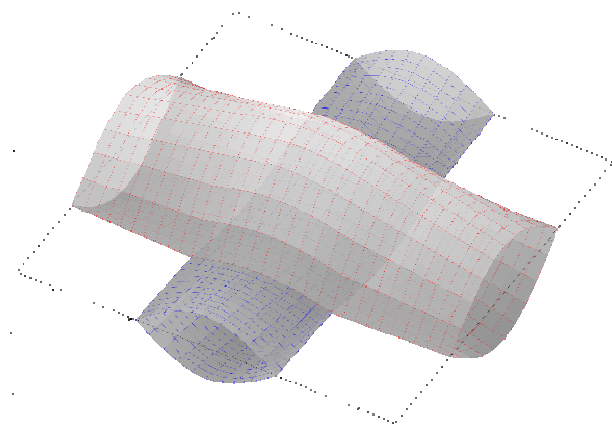
Figure 1 Model of singular binding point of plain weave

2.2   Boundary conditions

Boundary condition for the given configuration is as follows:

a) On the boundary planes of the binding point, i.e. planes of periodic repetition of weave (more precisely, planes of antisymmetry, but let's call them from here on 'planes of symmetry') the cross sections of threads, weft or warp, must be symmetric in respect to the plane of fabric, i.e. the horizontal plane. For the structure other than fabric in plain weave a similar condition must be established, which may not be necessarily of the same kind (symmetry etc.).

b) Dimensions of modelled domain, i.e. the distance between the planes of symmetry along the weft or warp, are equal to the lengths of repeat along the yarns. It is to say the reciprocal value of the sett of corresponding threads, and all these lengths are constant.

c) Condition of orthogonality of yarns must be respected, and this either in the current sense either in the mathematical sense of

word. Analogical geometrical conditions may be required in other textile structures.

2.3   Definition of deformable bodies

Now we have to define the behavior of a deformable body by using a geometric function. This shape function shall satisfy the former constraints and principles. Because we will use Lagrange's method of expression of functional of potential energy this function must also satisfy identically the boundary conditions. The function will depend on two independent geometric variables x, y, will be continuous and smooth. In order to determine the energy of deformation we have to choose a constitutive model of relation between deformation and stress. For our purposes we have opted for the simplest way, it is the elastic behavior of the material, without taking into account the effects of viscoplasticity of yarns. Anyway principles of virtual works use the linearized expression of actual value of material constants.

2.4   Lagrange's variation principle

To obtain the deformed shape of the system weft – warp we used the principle of virtual works. Lagrange's method consists in the minimization of the potential energy of the system by varying its shape, expressed in terms of shape function parameters.

2.5   Behaviors of yarns in a binding point of plain weave

In our work we tried to predict shape and mechanical properties of a fabric in plain weave. We focused on the fabric constituted of "normal" yarns, i.e. no monofils or effect yarns or similar were considered, simple spun yarns composed of great number of elementary filaments only were modelled. Then the following hypothesis may be raised: the total majority of mechanical energy in the deformed yarn in a binding point – or in any similar textile structure built of such yarns – is due to the elongation of elementary filaments. No deformation of cross section of filaments occurs that could be bound with a change of mechanical energy and all the filaments in the yarn are of the same

length, at least over the length of one pitch of twist. The elongation of filaments may be determined from the geometry of yarns, this latter being given by the interpolation functions. Another interesting behavior emerges: the deformation of such a yarn approaches the deformation of an ideal cable or chain with no stiffness in bending and mathematic apparatus of catenary may be used. In reality a yarn approaches this ideal with increasing number of filaments.

2.6 Choice of functions

With all mentioned premises and conditions in mind a choice of shape and interpolation functions may be done. In order to maintain the problem simply solvable we opted for the minimal required number of parameters, it is one per yarn and one "global" common to both yarns. Thus we will have to solve a general nonlinear system of three equations.

The proper choice of function may be arbitrary, though respecting the above mentioned conditions. For the reasons which lie out of the scope of this paper we have opted for combination of function *cosine* and linear function along the axis of yarn and *cosine* for the shape of its cross section. Such functions satisfy - beside the mandatory conditions - also the differential equation of a catenary through which the yarns may be modelled as shown in previous section.

2.7 Elastic properties of yarns

It is obvious that knowledge of elastic constants is necessary to calculate the mechanical energy. Those constants may be determined experimentally or be derived more or less analytically from the known properties of the material of yarn.

2.8 Mechanical energy in a binding point of plain weave

The mechanical energy in such conditions may be expressed as the sum of energy of elongation of filaments due to the elongation of yarn along its longitudinal axis and energy of elongation of filaments due to the deformation of shape of the cross section

of yarn. The calculation of both parts of mechanical energy takes us to the evaluation of length of yarn along its longitudinal axis and of length of its circumference, and this by means of function parameters defined above. Then by using Hook's law in our case (or any other constitutive model in general) we obtain an expression of energy as function of these parameters, which in turn became the optimization parameters to be found.

2.9 Mathematical background of solution

The solution of problem consists in searching such combination of values of function parameters for which the mechanical energy is minimal (minimization of energetic functional). This is done by means of solution of nonlinear system of equations by using e.g. Newton – Raphson's method. Another difficulty in our approach was the evaluation of length of function *cosine*. This was done by the Gauss integration, which means exact integration of a polynomial of an arbitrary degree, into which the function *cosine* could be developed.

3 RESULTS AND DISCUSSION

At the moment mainly numerical results were obtained. Few practical results are available because of difficulty of experiments. The evaluation of results was done basically by comparing the shape of calculated state with the real fabric.
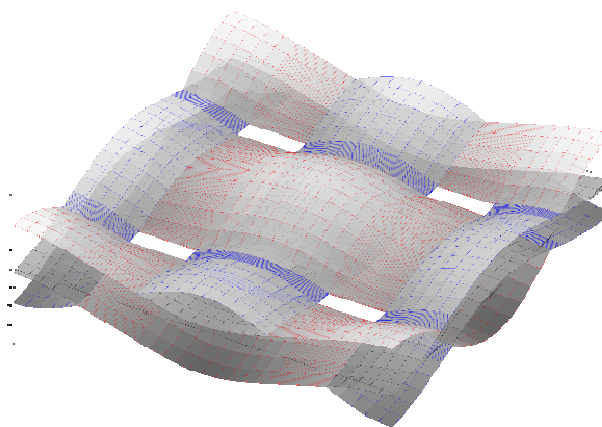
Figure 2 An example of a randomly chosen fabric model in plain weave
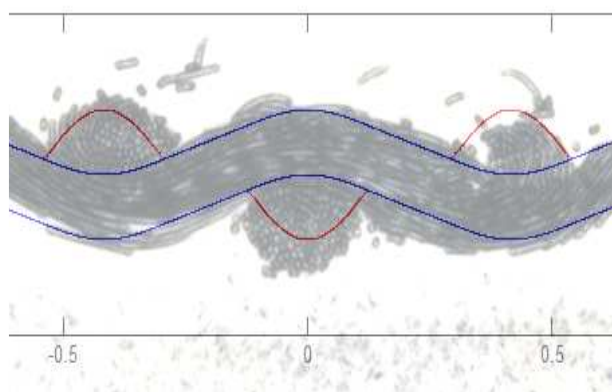
Figure 3 Comparison of the numerical simulation and the real fabric

4   CONCLUSIONS

In our quest for a presentation of a textile structure as a mechanical element we succeeded in the approach using physical principles that are analogic to those used in "classical" mechanics. The calculated shapes of yarns were used to estimate the stiffness of fabric as product of weaving action on the loom. As a byproduct some interesting results were found, e.g. for textile designers or similar branches. Anyway an important amount of mainly experimental work is to be carried out in future to validate this method.

5   REFERENCES

1. Bittnar Z., Šejnoha J.: Numerické metody mechaniky (1 ed.), Vydavatelství ČVUT (Praha), 1992
2. Haftka R.T., Gurdal Z.: Elements of Structural Optimization (3 ed.), Kluwer Academic Publishers (Boston), 1992
3. Rektorys K.: Variační metody v inženýrských problémech a v problémech matematické fyziky (1 ed.), SNTL (Praha), 1974

INSTRUCTIONS FOR AUTHORS

The journal ,,**Vlákna a textil**" (Fibres and Textiles) is the scientific and professional journal with a view to technology of fibres and textiles, with emphasis to chemical and natural fibres, processes of fibre spinning, finishing and dyeing, to fibrous and textile engineering and oriented polymer films. The original contributions and works of background researches, new physical-analytical methods and papers concerning the development of fibres, textiles and the marketing of these materials as well as review papers are published in the journal.

Manuscript
The text should be in ***single-column format***. The original research papers are required to be written in English language with summary. Main results and conclusion of contribution from Slovak and Czech Republic should be in Slovak or Czech language as well.
The other parts of the journal will be published in Slovak language; the advertisements will be published in a language according to the mutual agreement.
The first page of the manuscript has to contain:
The title of the article (16 pt bold, capital letters, centred)
The initials of the **first name** (s) and also **surnames** of all authors (12 pt, normal, centred)
The complete address of the working place of the authors, e-mail of first author (12 pt, italic, centred)
Abstract (10 pt, italic)
Key words (10 pt, italic)

The manuscript has to be written in A4 standard form, in **Arial**.
Do not number the pages and do not use footnotes. Do not use business letterhead.
Figures, tables, schemes and photos should be numbered by Arabic numerals and titled over the table and under the figure or picture. The total number of figures and tables should not be more than 10.
Photos and schemes have to be sufficiently contrastive and insert in text as pictures.
Mathematical formulae should be centred on line and numbered consecutively on the right margin.
Physical and technical properties have to be quantified in SI units, names and abbreviations of the chemical materials have to be stated according to the IUPAC standards.
References in the text have to be in square brackets and literature cited at the end of the text. References have to contain names of all authors.

1. Surname N., Surname N.: Name of paper or Chapter, In *Name of Book (in Italics)*, Publisher, Place of Publication, pp. xxx-yyy, YYYY
2. Surname N., Surname N.: Name of paper, *Name of Journal (in Italics)* Vol. (No.), pp. xxx-yyy, YYYY
3. Surname N., Surname, N.: Title of conference paper, *Proceedings of xxx xxx*, conference location, Month and Year, Publisher, City, Surname N. (Ed.), pp. xxx-yyy, YYYY
4. Surname N., Surname N.: Name of Paper, *Available from* http://www.exact-address-of-site, *Accessed:* YYYY-MM-DD

Authors are kindly requested to deliver the paper to be published by e-mail (in Word form).

Address of the Editor Office:

Marcela Hricová
FCHPT, STU in Bratislava
Radlinskeho 9
812 37 Bratislava,
Slovakia
e-mail: marcela.hricova@stuba.sk

"TRADITION AND HIGH-TECH DEVELOPMENT – KEYS TO THE TEXTILE MARKET"

24th IFATCC World Congress, June 13-16 2016, PARDUBICE (Czech Republic)

At the end of the nineteenth century the first attempts of textile chemists and colorists to join and work hand in hand in the fast growing textile industry of northeast Bohemia region began. These efforts were crowned with the foundation of the first Continental Textile Chemists and Colorists Society in 1908. In the same area production of dyestuffs has started and several small producers of textile auxiliary agents supported the tremendous development of the textile manufacturing.

The textile chemistry and coloration nowadays are becoming a new dimension – not only as the key to the fashion and comfort but also as a tool of the textile industry sustainability and last but not least as an extension of the new textile materials and fabrics into the new technical applications. Environmentally friendly, cost effective and energy efficient flexible technologies joining the tradition of chemistry with high-technologies, and boosted by new emerging disciplines, such as, to name a few biotech and nanotech, need to be communicated. Due to the significance of modern textile sector the forthcoming congress has obtained patronage of the Prime Minister of the Czech Republic.

Let´s come and acquaint ourselves with these trends, let´s unite with the business partners and friends from our branch and enjoy the hospitality of Pardubice region, the center of chemistry, horse racing and gingerbread. A kind invitation of the modern campus of the Pardubice University shall provide us with a good opportunity to engage youth to follow the tradition and to get together with the industrial representatives – breathing in the most recent innovation impulses of researchers.

Let´s make the 24th International IFATCC Congress a three-day living space for multidisciplinary professional communication and multinational partnering event.

MAIN TOPICS OF THE CONGRESS
Motto of the Congress:
"Tradition and high-tech development – keys to the textile market"

- Emerging technologies as a challenging tool for textile innovations
- Bio-based materials and technologies
- Renewable natural resources
- (Multi) functional textiles
- Nano-based materials and technologies
- Textile surface treatment
- Digital printing/digital jet processing
- Advanced dyes and dyeing methods
- Advanced fibers
- Ecology and environment/green textile technologies
- Testing, physical and chemical analysis of textiles and textile processes
- Regulatory issues and limitations

Deadline: Abstract Submission (oral/poster presentation) 15.10.2015

STCHK (Czech Society of Textile Chemists and Colorists) as the main Congress organizer is pleased to welcome your organization to sign a sponsor agreement for XXIV IFATCC International Congress, Pardubice (CZ). As in case of previous IFATCC Congresses this is a great opportunity for your organization to highlight your association with the centennial reputation of IFATCC as a global brand representing tradition and unfailing care about the transfer of innovations as key instruments of textile sustainability and the multidisciplinary approach encouragement. Sponsorship of Congress demonstrates your affiliation to the textile chemistry and processing branches.

You can see more about Congress at: http://ifatcc2016-pardubice.upce.cz/

Jan Marek   František Janak

IFATCC/STCHK President   Congress Organizing Committee Chairman

The 24th IFATCC World Congress
13.-16.6.2016 in Pardubice – Czech Republic

At the end of the nineteenth century the first attempts of textile chemists and colorists to join and work hand in hand in the fast growing textile industry of northeast Bohemia region began. These efforts were crowned with the foundation of the first Continental Textile Chemists and Colorists Society in 1908. In the same area production of dyestuffs has started and several small producers of textile auxiliary agents supported the tremendous development of the textile manufacturing.

The textile chemistry and coloration nowadays are becoming a new dimension - not only as the key to the fashion and comfort but also as a tool of the textile industry sustainability and last but not least as an extension of the new textile materials and fabrics into the new technical applications. Environmentally friendly, cost effective and energy efficient flexible technologies joining the tradition of chemistry with high-technologies, and boosted by new emerging disciplines, such as, to name a few biotech and nanotech, need to be communicated.

Let's come and acquaint with these trends, let's unite with the business partners and friends from our branch and enjoy the hospitality of Pardubice region, the center of chemistry, horse racing and gingerbread. A kind invitation of the modem campus of the Pardubice University shall provide us with a good opportunity to engage youth to follow the tradition and to get together with the industrial representatives - breathing in the most recent innovation impulses of researchers.

Let's make the 24th International IFATCC Congress a three-day living space for multidisciplinary professional communication and multinational partnering event. Call for papers is now open to get a wide space for your innovative presentations from both - research and industrial innovation spheres. See more about highlighted program topics and deadlines at http://ifatcc2016-pardubice.upce.cz

STCHK (Czech Society of Textile Chemists and Colorists) as the main Congress organizer is pleased to welcome your organization to sign a sponsor agreement for XXIV IFATCC International Congress, Pardubice (CZ). This is a great opportunity for your organization to highlight your association with the centennial reputation of IFATCC as a global brand representing tradition and unfailing care about the transfer of innovations as key instruments of textile sustainability and the multidisciplinary approach encouragement.
The 24th IFATCC Congress is organized under the patronage of Czech Prime Minister Mr. Bohuslav Sobotka.

Jan Marek
IFATCC/STCHK President
on behalf of the Scientific and Organizing committees